THE EUROPEAN
PHYSICAL JOURNAL C

Measurement of the top quark mass in the $t\bar{t} \to$ lepton+jets channel from $\sqrt{s} = 8$ TeV ATLAS data and combination with previous results

ATLAS Collaboration[*]

CERN, 1211 Geneva 23, Switzerland

Abstract The top quark mass is measured using a template method in the $t\bar{t} \to$ lepton + jets channel (lepton is e or μ) using ATLAS data recorded in 2012 at the LHC. The data were taken at a proton–proton centre-of-mass energy of $\sqrt{s} = 8$ TeV and correspond to an integrated luminosity of 20.2 fb^{-1}. The $t\bar{t} \to$ lepton + jets channel is characterized by the presence of a charged lepton, a neutrino and four jets, two of which originate from bottom quarks (b). Exploiting a three-dimensional template technique, the top quark mass is determined together with a global jet energy scale factor and a relative b-to-light-jet energy scale factor. The mass of the top quark is measured to be $m_{\text{top}} = 172.08 \pm 0.39$ (stat) ± 0.82 (syst) GeV. A combination with previous ATLAS m_{top} measurements gives $m_{\text{top}} = 172.69 \pm 0.25$ (stat) ± 0.41 (syst) GeV.

1 Introduction

The mass of the top quark m_{top} is an important parameter of the Standard Model (SM). Precise measurements of m_{top} provide crucial information for global fits of electroweak parameters [1–3] which help to assess the internal consistency of the SM and probe its extensions. In addition, the value of m_{top} affects the stability of the SM Higgs potential, which has cosmological implications [4–6].

Many measurements of m_{top} in each $t\bar{t}$ decay channel were performed by the Tevatron and LHC collaborations. The most precise measurements per experiment in the $t\bar{t} \to$ lepton + jets channel are $m_{\text{top}} = 172.85 \pm 0.71$ (stat) ± 0.84 (syst) GeV by CDF [7], $m_{\text{top}} = 174.98 \pm 0.58$ (stat) ± 0.49 (syst) GeV by D0 [8], $m_{\text{top}} = 172.33 \pm 0.75$ (stat) ± 1.03 (syst) GeV by ATLAS [9] and $m_{\text{top}} = 172.35 \pm 0.16$ (stat) ± 0.48 (syst) GeV by CMS [10]. Combinations are performed, by either the individual experiments, or by several Tevatron and LHC experiments [11]. In

these combinations, selections of measurements from all $t\bar{t}$ decay channels are used. The latest combinations per experiment are $m_{\text{top}} = 173.16 \pm 0.57$ (stat) ± 0.74 (syst) GeV by CDF [12], $m_{\text{top}} = 174.95 \pm 0.40$ (stat) ± 0.64 (syst) GeV by D0 [13], $m_{\text{top}} = 172.84 \pm 0.34$ (stat) ± 0.61 (syst) GeV by ATLAS [14] and $m_{\text{top}} = 172.44 \pm 0.13$ (stat) ± 0.47 (syst) GeV by CMS [10].

In this paper, an ATLAS measurement of m_{top} in the $t\bar{t} \to$ lepton + jets channel is presented. The result is obtained from pp collision data recorded in 2012 at a centre-of-mass energy of $\sqrt{s} = 8$ TeV with an integrated luminosity of about 20.2 fb^{-1}. The analysis exploits the decay $t\bar{t} \to W^+W^-b\bar{b} \to \ell\nu q\bar{q}'b\bar{b}$, which occurs when one W boson decays into a charged lepton (ℓ is e or μ including $\tau \to e, \mu$ decays) and a neutrino (ν), and the other into a pair of quarks. In the analysis presented here, m_{top} is obtained from the combined sample of events selected in the electron+jets and muon+jets final states. Single-top-quark events with the same reconstructed final states contain information about the top quark mass and are therefore included as signal events.

The measurement uses a template method, where simulated distributions are constructed for a chosen quantity sensitive to the physics parameter under study using a number of discrete values of that parameter. These templates are fitted to functions that interpolate between different input values of the physics parameter while fixing all other parameters of the functions. In the final step, an unbinned likelihood fit to the observed data distribution is used to obtain the value of the physics parameter that best describes the data. In this procedure, the experimental distributions are constructed such that fits to them yield unbiased estimators of the physics parameter used as input in the signal Monte Carlo (MC) samples. Consequently, the top quark mass determined in this way corresponds to the mass definition used in the MC simulation. Because of various steps in the event simulation, the mass measured in this way does not necessarily directly coincide with mass definitions within a given renormalization scheme,

[*] e-mail: atlas.publications@cern.ch

e.g. the top quark pole mass. Evaluating these differences is a topic of theoretical investigations [15–19].

The measurement exploits the three-dimensional template fit technique presented in Ref. [9]. To reduce the uncertainty in m_{top} stemming from the uncertainties in the jet energy scale (JES) and the additional b-jet energy scale (bJES), m_{top} is measured together with the jet energy scale factor (JSF) and the relative b-to-light-jet energy scale factor (bJSF). Given the larger data sample than used in Ref. [9], the analysis is optimized to reject combinatorial background arising from incorrect matching of the observed jets to the daughters arising from the top quark decays, thereby achieving a better balance of the statistical and systematic uncertainties and reducing the total uncertainty. Given this new measurement, an update of the ATLAS combination of m_{top} measurements is also presented.

This document is organized as follows. After a short description of the ATLAS detector in Sect. 2, the data and simulation samples are discussed in Sect. 3. Details of the event selection are given in Sect. 4, followed by the description of the reconstruction of the three observables used in the template fit in Sect. 5. The optimization of the event selection using a multivariate analysis approach is presented in Sect. 6. The template fits are introduced in Sect. 7. The evaluation of the systematic uncertainties and their statistical uncertainties are discussed in Sect. 8, and the measurement of m_{top} is given in Sect. 9. The combination of this measurement with previous ATLAS results is discussed in Sect. 10 and compared with measurements of other experiments. The summary and conclusions are given in Sect. 11. Additional information about the optimization of the event selection and on specific uncertainties in the new measurement of m_{top} in the $t\bar{t} \rightarrow$ lepton + jets channel are given in Appendix A, while Appendix B contains information about various combinations performed, together with comparisons with results from other experiments.

2 The ATLAS experiment

The ATLAS experiment [20] at the LHC is a multipurpose particle detector with a forward–backward symmetric cylindrical geometry and a near 4π coverage in the solid angle.[1] It consists of an inner tracking detector surrounded by a thin superconducting solenoid providing a 2 T axial mag-

netic field, electromagnetic and hadronic calorimeters, and a muon spectrometer. The inner tracking detector covers the pseudorapidity range $|\eta| < 2.5$. It consists of silicon pixel, silicon microstrip, and transition radiation tracking detectors. Lead/liquid-argon (LAr) sampling calorimeters provide electromagnetic (EM) energy measurements with high granularity. A hadronic (steel/scintillator-tile) calorimeter covers the central pseudorapidity range ($|\eta| < 1.7$). The endcap and forward regions are instrumented with LAr calorimeters for both the EM and hadronic energy measurements up to $|\eta| = 4.9$. The muon spectrometer surrounds the calorimeters and is based on three large air-core toroid superconducting magnets with eight coils each. Its bending power is 2.0 to 7.5 T m. It includes a system of precision tracking chambers and fast detectors for triggering.

A three-level trigger system was used to select events. The first-level trigger is implemented in hardware and used a subset of the detector information to reduce the accepted rate to at most 75 kHz. This is followed by two software-based trigger levels that together reduced the accepted event rate to 400 Hz on average depending on the data-taking conditions during 2012.

3 Data and simulation samples

The analysis is based on pp collision data recorded by the ATLAS detector in 2012 at a centre-of-mass energy of $\sqrt{s} = 8$ TeV. The integrated luminosity is 20.2 fb^{-1} with an uncertainty of 1.9% [21]. The modelling of top quark pair ($t\bar{t}$) and single-top-quark signal events, as well as most background processes, relies on MC simulations. For the simulation of $t\bar{t}$ and single-top-quark events, the POWHEG- BOX v1 [22–24] program was used. Within this framework, the simulations of the $t\bar{t}$ [25] and single-top-quark production in the s- and t-channels [26] and the Wt-channel [27] used matrix elements at next-to-leading order (NLO) in the strong coupling constant α_S with the NLO CT10 [28] parton distribution function (PDF) set and the h_{damp} parameter[2] set to infinity. Using m_{top} and the top quark transverse momentum p_T for the underlying leading-order Feynman diagram, the dynamic factorization and renormalization scales were set to $\sqrt{m_{top}^2 + p_T^2}$. The PYTHIA (v6.425) program [29] with the P2011C [30] set of tuned parameters (tune) and the corresponding CTEQ6L1 PDFs [31] provided the parton shower, hadronization and underlying-event modelling.

For m_{top} hypothesis testing, the $t\bar{t}$ and single-top-quark event samples were generated with five different assumed

---

[1] ATLAS uses a right-handed coordinate system with its origin at the nominal interaction point (IP) in the centre of the detector and the z-axis along the beam pipe. The x-axis points from the IP to the centre of the LHC ring, and the y-axis points upwards. Cylindrical coordinates (r, ϕ) are used in the transverse plane, ϕ being the azimuthal angle around the z-axis. The pseudorapidity is defined in terms of the polar angle θ as $\eta = -\ln\tan(\theta/2)$. Angular distance is measured in units of $\Delta R \equiv \sqrt{(\Delta\eta)^2 + (\Delta\phi)^2}$.

[2] The h_{damp} parameter controls the transverse momentum p_T of the first additional emission beyond the leading-order Feynman diagram in the parton shower and therefore regulates the high-p_T emission against which the $t\bar{t}$ system recoils.

values of m_{top} in the range from 167.5 to 177.5 GeV in steps of 2.5 GeV. The integrated luminosity of the simulated $t\bar{t}$ sample with $m_{top} = 172.5$ GeV is about 360 fb^{-1}. Each of these MC samples is normalized according to the best available cross-section calculations. For $m_{top} = 172.5$ GeV, the $t\bar{t}$ cross-section is $\sigma_{t\bar{t}} = 253^{+13}_{-15}$ pb, calculated at next-to-next-to-leading order (NNLO) with next-to-next-to-leading logarithmic soft gluon terms [32–36] with the Top++ 2.0 program [37]. The PDF- and α_S-induced uncertainties in this cross-section were calculated using the PDF4LHC prescription [38] with the MSTW2008 68% CL NNLO PDF [39,40], CT10 NNLO PDF [28,41] and NNPDF2.3 5f FFN PDF [42] and were added in quadrature with the uncertainties obtained from the variation of the factorization and renormalization scales by factors of 0.5 and 2.0. The cross-sections for single-top-quark production were calculated at NLO and are $\sigma_t = 87.8^{+3.4}_{-1.9}$ pb [43], $\sigma_{Wt} = 22.4 \pm 1.5$ pb [44] and $\sigma_s = 5.6 \pm 0.2$ pb [45] in the t-, the Wt- and the s-channels, respectively.

The ALPGEN (v2.13) program [46] interfaced to the PYTHIA6 program was used for the simulation of the production of $W^{\pm}$ or Z bosons in association with jets. The CTEQ6L1 PDFs and the corresponding AUET2 tune [47] were used for the matrix element and parton shower settings. The W+jets and Z+jets events containing heavy-flavour (HF) quarks ($Wb\bar{b}$+jets, $Zb\bar{b}$+jets, $Wc\bar{c}$+jets, $Zc\bar{c}$+jets, and Wc+jets) were generated separately using leading-order (LO) matrix elements with massive bottom and charm quarks. Double-counting of HF quarks in the matrix element and the parton shower evolution was avoided via a HF overlap-removal procedure that used the ΔR between the additional heavy quarks as the criterion. If the ΔR was smaller than 0.4, the parton shower prediction was taken, while for larger values, the matrix element prediction was used. The Z+jets sample is normalized to the inclusive NNLO calculation [48]. Due to the large uncertainties in the overall W+jets normalization and the flavour composition, both are estimated using data-driven techniques as described in Sect. 4.2. Diboson production processes (WW, WZ and ZZ) were simulated using the ALPGEN program with CTEQ6L1 PDFs interfaced to the HERWIG (v6.520) [49] and JIMMY (v4.31) [50] programs. The samples are normalized to their predicted cross-sections at NLO [51].

All samples were simulated taking into account the effects of multiple soft pp interactions (pile-up) that are present in the 2012 data. These interactions were modelled by overlaying simulated hits from events with exactly one inelastic collision per bunch crossing with hits from minimum-bias events produced with the PYTHIA (v8.160) program [52] using the A2 tune [53] and the MSTW2008 LO PDF. The number of additional interactions is Poisson-distributed around the mean number of inelastic pp interactions per bunch crossing μ. For a given simulated hard-scatter event, the value of μ depends on the instantaneous luminosity and the inelastic pp

cross-section, taken to be 73 mb [21]. Finally, the simulation sample is reweighted such as to match the pile-up observed in data.

A simulation [54] of the ATLAS detector response based on GEANT4 [55] was performed on the MC events. This simulation is referred to as full simulation. The events were then processed through the same reconstruction software as the data. A number of samples used to assess systematic uncertainties were produced bypassing the highly computing-intensive full GEANT4 simulation of the calorimeters. They were produced with a faster version of the simulation [56], which retained the full simulation of the tracking but used a parameterized calorimeter response based on resolution functions measured in full simulation samples. This simulation is referred to as fast simulation.

4 Object reconstruction, background estimation and event preselection

The reconstructed objects resulting from the top quark pair decay are electron and muon candidates, jets and missing transverse momentum (E_T^{miss}). In the simulated events, corrections are applied to these objects based on detailed data-to-simulation comparisons for many different processes, so as to match their performance in data.

4.1 Object reconstruction

Electron candidates [57] are required to have a transverse energy of $E_T > 25$ GeV and a pseudorapidity of the corresponding EM cluster of $|\eta_{cluster}| < 2.47$ with the transition region $1.37 < |\eta_{cluster}| < 1.52$ between the barrel and the endcap calorimeters excluded. Muon candidates [58] are required to have transverse momentum $p_T > 25$ GeV and $|\eta| < 2.5$. To reduce the contamination by leptons from HF decays inside jets or from photon conversions, referred to collectively as non-prompt (NP) leptons, strict isolation criteria are applied to the amount of activity in the vicinity of the lepton candidate [57–59].

Jets are built from topological clusters of calorimeter cells [60] with the anti-k_t jet clustering algorithm [61] using a radius parameter of $R = 0.4$. The clusters and jets are calibrated using the local cluster weighting (LCW) and the global sequential calibration (GSC) algorithms, respectively [62–64]. The subtraction of the contributions from pile-up is performed via the jet area method [65]. Jets are calibrated using an energy- and η-dependent simulation-based scheme with in situ corrections based on data [63]. Jets originating from pile-up interactions are identified via their jet vertex fraction (JVF), which is the p_T fraction of associated tracks stemming from the primary vertex. The requirement JVF > 0.5 is applied solely to jets with $p_T < 50$ GeV

and $|\eta| < 2.4$ [65]. Finally, jets are required to satisfy $p_T > 25$ GeV and $|\eta| < 2.5$.

Muons reconstructed within a $\Delta R = 0.4$ cone around the axis of a jet with $p_T > 25$ GeV are excluded from the analysis. In addition, the closest jet within a $\Delta R = 0.2$ cone around an electron candidate is removed, and then electrons within a $\Delta R = 0.4$ cone around any of the remaining jets are discarded.

The identification of jets containing reconstructed b-hadrons, called b-tagging, is used for event reconstruction and background suppression. In the following, irrespective of their origin, jets tagged by the b-tagging algorithm are referred to as b-tagged jets, whereas those not tagged are referred to as untagged jets. Similarly, whether they are tagged or not, jets containing b-hadrons in simulation are referred to as b-jets and those containing only lighter-flavour hadrons from u, d, c, s-quarks, or originating from gluons, are collectively referred to as light-jets. The working point of the neural-network-based MV1 b-tagging algorithm [66] corresponds to an average b-tagging efficiency of 70% for b-jets in simulated $t\bar{t}$ events and rejection factors of 5 for jets containing a c-hadron and 140 for jets containing only lighter-flavour hadrons. To match the b-tagging performance in the data, p_T- and η-dependent scale factors, obtained from dijet and $t\bar{t} \rightarrow$ dilepton events, are applied to MC jets depending on their generated quark flavour, as described in Refs. [66–68].

The missing transverse momentum E_T^{miss} is the absolute value of the vector $\overrightarrow{E_T}^{miss}$ calculated from the negative vectorial sum of all transverse momenta. The vectorial sum takes into account all energy deposits in the calorimeters projected onto the transverse plane. The clusters are corrected using the calibrations that belong to the associated physics object. Muons are included in the calculation of the E_T^{miss} using their momentum reconstructed in the inner tracking detectors [69].

4.2 Background estimation

The contribution of events falsely reconstructed as $t\bar{t} \rightarrow$ lepton + jets events due to the presence of objects misidentified as leptons (fake leptons) and NP leptons originating from HF decays, is estimated from data using the matrix-method [70]. The technique employed uses η- and p_T-dependent efficiencies for NP/fake-leptons and prompt-leptons. They are measured in a background-enhanced control region with low E_T^{miss} and from events with dilepton masses around the Z boson peak [71], respectively. For the W+jets background, the overall normalization is estimated from data. The estimate is based on the charge-asymmetry method [72], relying on the fact that at the LHC more W^+ than W^- bosons are produced. In addition, a data-driven estimate of the $Wb\bar{b}$, $Wc\bar{c}$, Wc and W+light-jet fractions is

performed in events with exactly two jets and at least one b-tagged jet. Further details are given in Ref. [73]. The Z+jets and diboson background processes are normalized to their predicted cross-sections as described in Sect. 3.

4.3 Event preselection

Triggering of events is based solely on the presence of a single electron or muon, and no information from the hadronic final state is used. A logical *OR* of two triggers is used for each of the $t\bar{t} \rightarrow$ electron + jets and $t\bar{t} \rightarrow$ muon + jets channels. The triggers with the lower thresholds of 24 GeV for electrons or muons select isolated leptons. The triggers with the higher thresholds of 60 GeV for electrons and 36 GeV for muons do not include an isolation requirement. The further selection requirements closely follow those in Ref. [9] and are

- Events are required to have at least one primary vertex with at least five associated tracks. Each track needs to have a minimum p_T of 0.4 GeV. For events with more than one primary vertex, the one with the largest $\sum p_T^2$ is chosen as the vertex from the hard scattering.
- The event must contain exactly one reconstructed charged lepton, with $E_T > 25$ GeV for electrons and $p_T > 25$ GeV for muons, that matches the charged lepton that fired the corresponding lepton trigger.
- In the $t\bar{t} \rightarrow$ muon + jets channel, $E_T^{miss} > 20$ GeV and $E_T^{miss} + m_T^W > 60$ GeV are required.[3]
- In the $t\bar{t} \rightarrow$ electron + jets channel, more stringent requirements on E_T^{miss} and m_T^W are applied because of the higher level of NP/fake-lepton background. The requirements are $E_T^{miss} > 30$ GeV and $m_T^W > 30$ GeV.
- The presence of at least four jets with $p_T > 25$ GeV and $|\eta| < 2.5$ is required.
- The presence of exactly two b-tagged jets is required.

The resulting event sample is statistically independent of the ones used for the measurement of m_{top} in the $t\bar{t} \rightarrow$ dilepton and $t\bar{t} \rightarrow$ all jets channels at $\sqrt{s} = 8$ TeV [14,74]. The observed number of events in the data after this preselection and the expected numbers of signal and background events corresponding to the same integrated luminosity as the data are given in Table 1. For all predictions, the uncertainties are estimated as the sum in quadrature of the statistical uncertainty, the uncertainty in the integrated luminosity and all systematic uncertainties assigned to the measurement of m_{top} listed in Sect. 8, except for the PDF and pile-up uncertainties, which are small. The normalization uncertainties listed

---

[3] Here m_T^W is the transverse mass of the W boson, defined as $\sqrt{2 p_{T,\ell} E_T^{miss} \left(1 - \cos \phi(\ell, \overrightarrow{E_T}^{miss})\right)}$, where $\overrightarrow{E_T}^{miss}$ provides an estimate of the transverse momentum of the neutrino.

Table 1 The observed numbers of events in data after the event preselection and the BDT selection (see Sect. 6). In addition, the expected numbers of signal events for $m_{top} = 172.5$ GeV and background events corresponding to the same integrated luminosity as the data are given. The uncertainties in the predicted number of events take into account the statistical and systematic sources explained in Sect. 4.3. Two significant digits are used for the uncertainties in the predicted events

Selection	Preselection	BDT selection
Data	96105	38054
$t\bar{t}$ signal	85000 ± 10000	36100 ± 5500
Single-top-quark signal	4220 ± 360	883 ± 85
NP/fake leptons (data-driven)	700 ± 700	9.2 ± 9.2
W+jets (data-driven)	2800 ± 700	300 ± 100
Z+jets	430 ± 230	58 ± 33
$WW/WZ/ZZ$	63 ± 32	7.0 ± 5.2
Signal+background	93000 ± 10000	37300 ± 5500
Expected background fraction	0.043 ± 0.012	0.010 ± 0.003
Data/(signal+background)	1.03 ± 0.12	1.02 ± 0.15

below are included for the predictions shown in this section, but due to their small effect on the measured top quark mass they are not included in the final measurement.

For the signal, the 5.7% uncertainty in the $t\bar{t}$ cross-section introduced in Sect. 3 and a 6.0% uncertainty in the single-top-quark cross-section are used. The latter uncertainty is obtained from the cross-section uncertainties given in Sect. 3 and the fractions of the various single-top-quark production processes after the selection requirements. The background uncertainties contain uncertainties of 48% in the normalization of the diboson and Z+jets production processes. These uncertainties are calculated using Berends–Giele scaling [75]. Assuming a top quark mass of $m_{top} = 172.5$ GeV, the predicted number of events is consistent within uncertainties with the number observed in the data.

5 Reconstruction of the three observables

As in Ref. [9], a full kinematic reconstruction of the event is done with a likelihood fit using the KLFITTER package [76,77]. The KLFITTER algorithm relates the measured kinematics of the reconstructed objects to the leading-order representation of the $t\bar{t}$ system decay using $t\bar{t} \rightarrow \ell\nu b_{lep} q_1 q_2 b_{had}$. In this procedure, the measured jets correspond to the quark decay products of the W boson, q_1 and q_2, and to the b-quarks, b_{lep} and b_{had}, produced in the semi-leptonic and hadronic top quark decays, respectively.

The event likelihood is the product of Breit–Wigner (BW) distributions for the W bosons and top quarks and transfer functions (TFs) for the energies of the reconstructed objects that are input to KLFITTER. The W boson BW distributions use the world combined values of the W boson mass and decay width from Ref. [3]. A common mass parameter

m_{top}^{reco} is used for the BW distributions describing the semi-leptonically and hadronically decaying top quarks and is fitted event-by-event. The top quark width varies with m_{top}^{reco} according to the SM prediction [3]. The TFs are derived from the POWHEG+PYTHIA $t\bar{t}$ signal MC simulation sample at an input mass of $m_{top} = 172.5$ GeV. They represent the experimental resolutions in terms of the probability that the observed energy at reconstruction level is produced by a given parton-level object for the leading-order decay topology and in the fit constrain the variations of the reconstructed objects.

The input objects to the event likelihood are the reconstructed charged lepton, the missing transverse momentum and up to six jets. These are the two b-tagged jets and the four untagged jets with the highest p_T. The x- and y-components of the missing transverse momentum are starting values for the neutrino transverse-momentum components, and its longitudinal component $p_{\nu,z}$ is a free parameter in the kinematic likelihood fit. Its starting value is computed from the $W \rightarrow \ell\nu$ mass constraint. If there are no real solutions for $p_{\nu,z}$, a starting value of zero is used. If there are two real solutions, the one giving the largest likelihood value is taken.

Maximizing the event-by-event likelihood as a function of m_{top}^{reco} establishes the best assignment of reconstructed jets to partons from the $t\bar{t} \rightarrow$ lepton + jets decay. The maximization is performed by testing all possibilities for assigning b-tagged jets to b-quark positions and untagged jets to light-quark positions. With the above settings of the reconstruction algorithm, compared with the settings[4] used in Ref. [9], a larger fraction of correct assignments of reconstructed jets to partons from the $t\bar{t} \rightarrow$ lepton + jets decay is achieved. The performance of the reconstruction algorithm is discussed in Sect. 6.

The value of m_{top}^{reco} obtained from the kinematic likelihood fit is used as the observable primarily sensitive to the underlying m_{top}. The invariant mass of the hadronically decaying W boson m_W^{reco}, which is sensitive to the JES, is calculated from the assigned jets of the chosen permutation. Finally, an observable called R_{bq}^{reco}, designed to be sensitive to the bJES, is computed as the scalar sum of the transverse momenta of the two b-tagged jets divided by the scalar sum of the transverse momenta of the two jets associated with the hadronic W boson decay:

$$R_{bq}^{reco} = \frac{p_T^{b_{had}} + p_T^{b_{lep}}}{p_T^{q_1} + p_T^{q_2}}.$$

---

[4] In Ref. [9] only four input jets were used. In addition, b-tagging efficiencies and rejection factors were used to favour permutations for which a b-tagged jet is assigned to a b-quark position and penalise those where a b-tagged jet is assigned to a light-quark position. However, the latter permutations were still accepted whenever they resulted in the largest likelihood.

The values of m_W^{reco} and R_{bq}^{reco} are computed from the jet four-vectors as given by the jet reconstruction instead of using the values obtained in the kinematic likelihood fit. This ensures the maximum sensitivity to the jet calibration for light-jets and b-jets.

Some distributions of the observed event kinematics after the event preselection and for the best permutation are shown in Fig. 1. Given the good description of the observed number of events by the prediction shown in Sect. 4.3 and that the measurement of m_{top} is mostly sensitive to the shape of the distributions, the comparison of the data with the predictions is based solely on the distributions normalized to the number of events observed in data. The systematic uncertainty assigned to each bin is calculated from the sum in quadrature of all systematic uncertainties discussed in Sect. 4.3. Within uncertainties, the predictions agree with the observed distributions in Fig. 1, which shows the transverse momentum of the lepton, the average transverse momentum of the jets, the transverse momentum of the hadronically decaying top quark $p_{\text{T,had}}$, the transverse momentum of the $t\bar{t}$ system, the logarithm of the event likelihood of the best permutation and the distance ΔR of the two untagged jets q_1 and q_2 assigned to the hadronically decaying W boson. The distributions of transverse momenta predicted by the simulation, e.g. the $p_{\text{T,had}}$ distribution shown in Fig. 1c, show a slightly different trend than observed in data, with the data being softer. This difference is fully covered by the uncertainties. This trend was also observed in Ref. [14] for the $p_{\text{T},\ell b}$ distribution in the $t\bar{t} \rightarrow$ dilepton channel and in the measurement of the differential $t\bar{t}$ cross-section in the lepton+jets channel [78].

In anticipation of the template parameterization described in Sect. 7, the following restrictions on the three observables are applied: $125 \leq m_{\text{top}}^{\text{reco}} \leq 200$ GeV, $55 \leq m_W^{\text{reco}} \leq 110$ GeV, and $0.3 \leq R_{bq}^{\text{reco}} \leq 3$. Since in this analysis only the best permutation is considered, events that do not pass these requirements are rejected. This removes events in the tails of the three distributions, which are typically poorly reconstructed with small likelihood values and do not contain significant information about m_{top}. The resulting templates have simpler shapes, which are easier to model analytically with fewer parameters. The preselection with these additional requirements is referred to as the *standard selection* to distinguish it from the boosted decision tree (BDT) optimization for the smallest total uncertainty in m_{top}, discussed in the next section.

6 Multivariate analysis and BDT event selection

For the measurement of m_{top}, the event selection is refined enriching the fraction of events with correct assignments of reconstruction-level objects to their generator-level counter-parts which should be better measured and therefore lead to smaller uncertainties. The optimization of the selection is based on the multivariate BDT algorithm implemented in the TMVA package [79]. The reconstruction-level objects are matched to the closest parton-level object within a ΔR of 0.1 for electrons and muons and 0.3 for jets. A matched object is defined as a reconstruction-level object that falls within the relevant ΔR of any parton-level object of that type, and a correct match means that this generator-level object is the one it originated from. Due to acceptance losses and reconstruction inefficiencies, not all reconstruction-level objects can successfully be matched to their parton-level counterparts. If any object cannot be unambiguously matched, the corresponding event is referred to as *unmatched*. The efficiency for correctly matched events ϵ_{cm} is the fraction of correctly matched events among all the matched events, and the selection purity π_{cm} is the fraction of correctly matched events among all selected events, regardless of whether they could be matched or not.

The BDT algorithm is exploited to enrich the event sample in events that have correct jet-to-parton matching by reducing the remainder, i.e. the sum of incorrectly matched and unmatched events. Using the preselection, the BDT algorithm is trained on the simulated $t\bar{t}$ signal sample with $m_{\text{top}} = 172.5$ GeV. Many variables were studied and only those with a separation[5] larger than 0.1% are used in the training. The 13 variables chosen for the final training are given in Table 2. For all input variables to the BDT algorithm, good agreement between the MC predictions and the data is found, as shown in Fig. 1e, f for the examples of the likelihood of the chosen permutation and the opening angle ΔR of the two untagged jets associated with the W boson decay. These two variables also have the largest separation for the correctly matched events and the remainder. The corresponding distributions for the two event classes are shown in Fig. 2a, b. These figures show a clear separation of the correctly matched events and the remainder. Half the simulation sample is used to train the algorithm and the other half to assess its performance. The significant difference between the distributions of the output value r_{BDT} of the BDT classifier between the two classes of events in Fig. 2c shows their efficient separation by the BDT algorithm. In addition, reasonable agreement is found for the r_{BDT} distributions in the statistically independent test and training samples. The r_{BDT} distributions in simulation and data in Fig. 2d agree within the experimental uncertainties. The above findings justify the application of the BDT approach to the data.

The full m_{top} analysis detailed in Sect. 8 is performed, except for the evaluation of the small method and pile-up uncertainties described in Sect. 8, for several minimum

---

[5] The chosen definition of the separation is given in Eq. (1) of the TMVA manual [79].

(a) Transverse momentum of the lepton

(b) Average transverse momentum of jets

(c) Transverse momentum of the hadronically decaying top quark

(d) Transverse momentum of the $t\bar{t}$ system

(e) Logarithm of the event likelihood

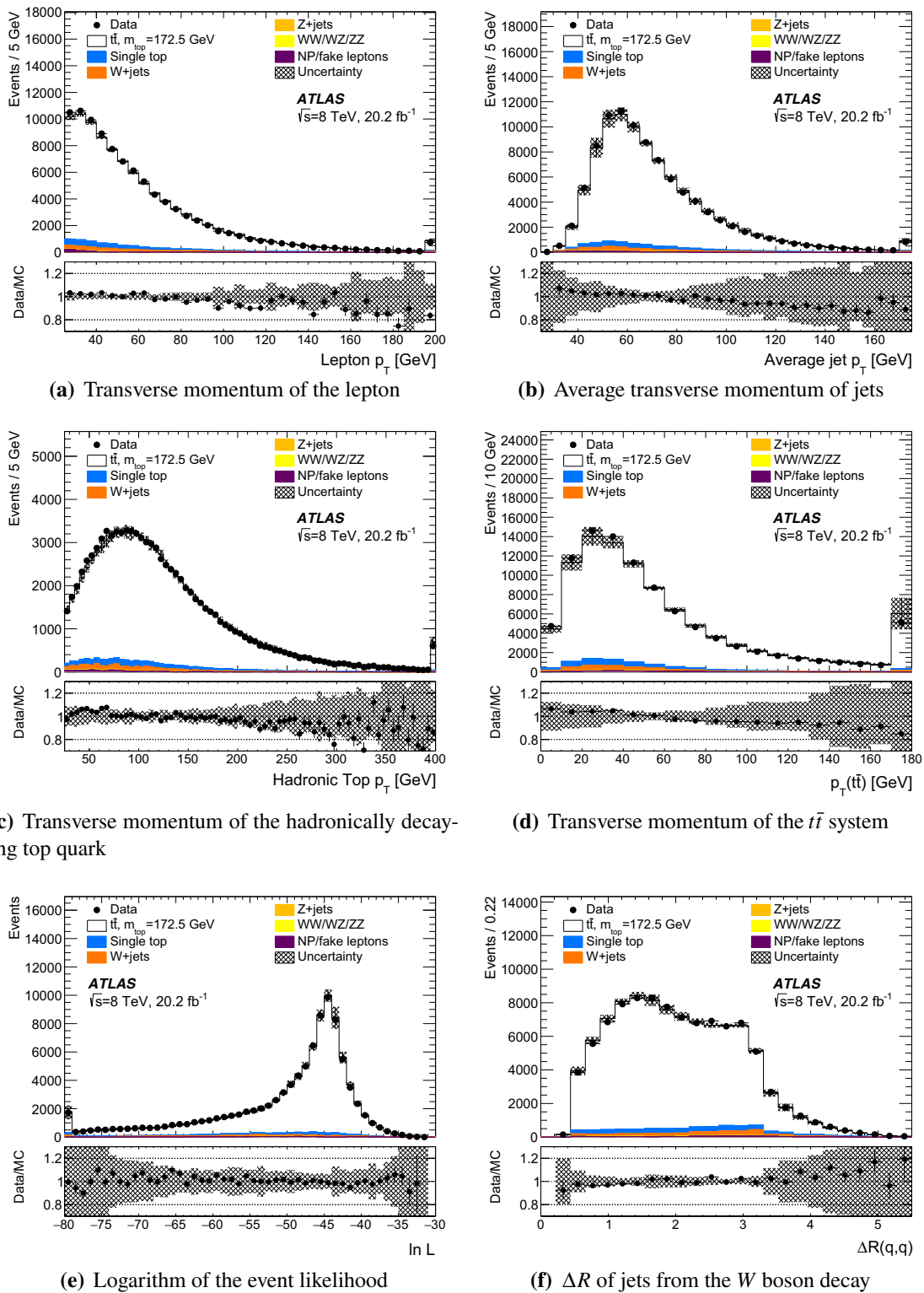

(f) ΔR of jets from the W boson decay

Fig. 1 Distributions for the events passing the preselection. The data are shown together with the signal-plus-background prediction, normalized to the number of events observed in the data. The hatched area is the uncertainty in the prediction as described in the text. The rightmost bin contains all entries with values above the lower edge of this bin, similarly the leftmost bin contains all entries with values below the upper edge of this bin. **a** shows the transverse momentum of the lepton, **b** shows the average transverse momentum of the jets, **c** shows the transverse momentum of the hadronically decaying top quark, **d** shows the transverse momentum of the $t\bar{t}$ system, **e** shows the logarithm of the event likelihood of the best permutation and **f** shows the distance ΔR of the two untagged jets q_1 and q_2 from the hadronically decaying W boson

Table 2 The input variables to the BDT algorithm sorted by their separation

Separation (%)	Description
31	Logarithm of the event likelihood of the best permutation, $\ln L$
13	ΔR of the two untagged jets q_1 and q_2 from the hadronically decaying W boson, $\Delta R(q, q)$
5.0	p_{T} of the hadronically decaying W boson
4.3	p_{T} of the hadronically decaying top quark
4.2	Relative event probability of the best permutation
2.0	p_{T} of the reconstructed $t\bar{t}$ system
1.7	p_{T} of the semi-leptonically decaying top quark
1.2	Transverse mass of the leptonically decaying W boson
0.3	p_{T} of the leptonically decaying W boson
0.3	Number of jets
0.2	ΔR of the reconstructed b-tagged jets
0.2	Missing transverse momentum
0.1	p_{T} of the lepton

requirements on r_{BDT} in the range of $[-0.10, 0.05]$ in steps of 0.05 to find the point with smallest total uncertainty. The total uncertainty in m_{top} together with the various classes of uncertainty sources as a function of r_{BDT} evaluated in the BDT optimization are shown in Fig. 3. The minimum requirement $r_{\mathrm{BDT}} = -0.05$ provides the smallest total uncertainty in m_{top}. The resulting numbers of events for this BDT selection are given in Table 1. Compared with the preselection, ϵ_{cm} is increased from 0.71 to 0.82, albeit at the expense of a significant reduction in the number of selected events. The purity π_{cm} is increased from 0.28 to 0.41. In addition, the intrinsic resolution in m_{top} of the remaining event sample is improved, i.e. the statistical uncertainty in m_{top} in Fig. 3 is almost constant as a function of r_{BDT}; in particular, it does not scale with the square root of the number of events retained. For the signal sample with $m_{\mathrm{top}} = 172.5\,\mathrm{GeV}$, the template fit functions for the standard selection and the BDT selection, together with their ratios, are shown in Fig. 12 in Appendix A. The shape of the signal modelling uncertainty derives from a sum of contributions with different shapes. The curves from the signal Monte Carlo generator and colour reconnection uncertainties decrease, the one from the underlying event uncertainty is flat, the one from the initial- and final-state QCD radiation has a valley similar to the sum of all contributions, and finally the one from the hadronization uncertainty rises.

Some distributions of the observed event kinematics after the BDT selection are shown in Fig. 4. Good agreement between the MC predictions and the data is found, as seen for the preselection in Fig. 1. The examples shown are the observed W boson transverse mass for the semi-leptonically decaying top quark in Fig. 4a and the three observables of

the m_{top} analysis (within the ranges of the template fit) in Fig. 4b–d. The sharp edge observed at 30 GeV in Fig. 4a originates from the different selection requirements for the W boson transverse mass in the electron+jets and muon+jets final states.

7 Template fit

This analysis uses a three-dimensional template fit technique which determines m_{top} together with the jet energy scale factors JSF and bJSF. The aim of the multi-dimensional fit to the data is to measure m_{top} and, at the same time, to absorb the mean differences between the jet energy scales observed in data and MC simulated events into jet energy scale factors. By using JSF and bJSF, most of the uncertainties in m_{top} induced by JES and bJES uncertainties are transformed into additional statistical components caused by the higher dimensionality of the fit. This method reduces the total uncertainty in m_{top} only for sufficiently large data samples. In this case, the sum in quadrature of the additional statistical uncertainty in m_{top} due to the JSF (or bJSF) fit and the residual JES-induced (or bJES-induced) systematic uncertainty is smaller than the original JES-induced (or bJES-induced) uncertainty in m_{top}. This situation was already realized for the $\sqrt{s} = 7$ TeV data analysis [9] and is even more advantageous for the much larger data sample of the $\sqrt{s} = 8$ TeV data analysis. Since JSF and bJSF are global factors, they do not completely absorb the JES and bJES uncertainties which have p_{T}- and η-dependent components.

For simultaneously determining m_{top}, JSF and bJSF, templates are constructed from the MC samples. Templates of $m_{\mathrm{top}}^{\mathrm{reco}}$ are constructed with several input m_{top} values used in the range 167.5–177.5 GeV and for the sample at $m_{\mathrm{top}} = 172.5$ GeV also with independent input values for JSF and bJSF in the range 0.96–1.04 in steps of 0.02. Statistically independent MC samples are used for different input values of m_{top}. The templates with different values of JSF and bJSF are constructed by scaling the energies of the jets appropriately. In this procedure, JSF is applied to all jets, while bJSF is solely applied to b-jets according to the generated quark flavour. The scaling is performed after the various correction steps of the jet calibration but before the event selection. This procedure results in different events passing the BDT selection from one energy scale variation to another. However, many events are in all samples, resulting in a large statistical correlation of the samples with different jet scale factors. Similarly, templates of m_W^{reco} and R_{bq}^{reco} are constructed with the above listed input values of m_{top}, JSF and bJSF.
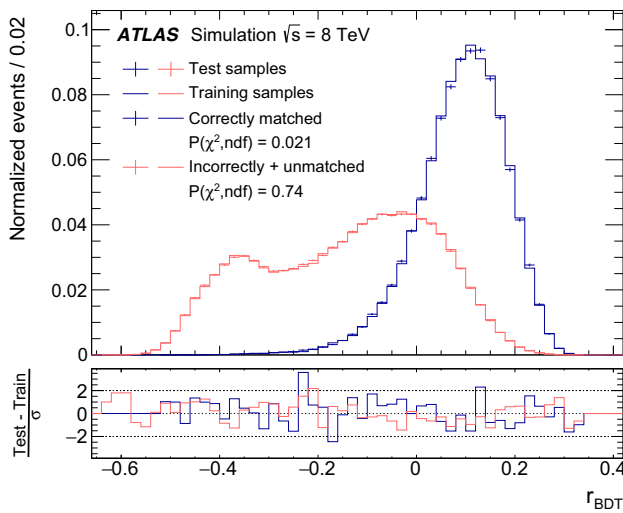
Independent signal templates are derived for the three observables for all m_{top}-dependent samples, consisting of the $t\bar{t}$ signal events and single-top-quark production events. This procedure is adopted because single-top-quark produc-
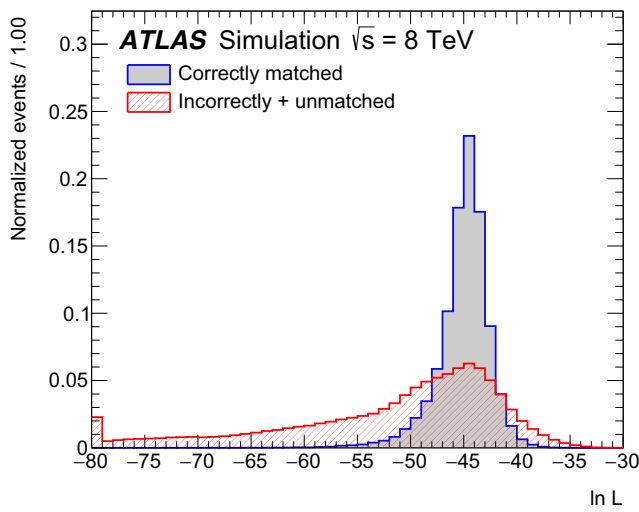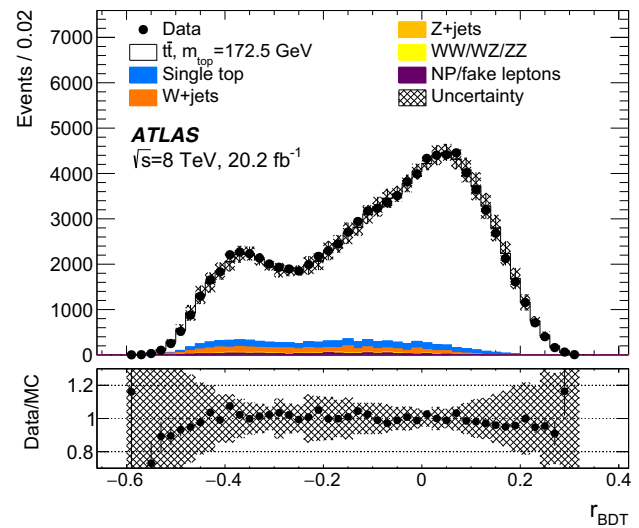
(a) Logarithm of the event likelihood
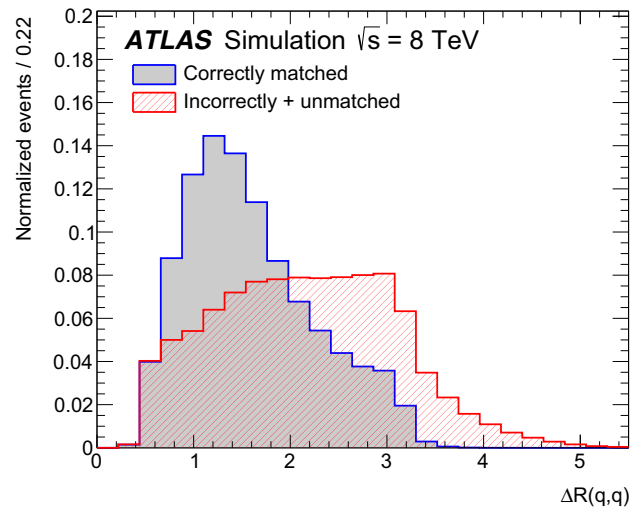
(b) ΔR of jets from the W boson decay

(c) BDT test and training samples

(d) Data-to-simulation comparison for r_{BDT}

Fig. 2 Input and results of the BDT training on $t\bar{t}$ signal events for the preselection. **a** shows the logarithm of the event likelihood of the best permutation ($\ln L$) for the correctly matched events and the remainder. Similarly, **b** shows the distribution of the ΔR between the two untagged jets assigned to the W boson decay. **c** shows the distribution of the BDT output (r_{BDT}) for the two classes of events for both the training (histograms) and test samples (points with statistical uncertainties). The compatibility in terms of the χ^2 probability is also listed. The distri-butions peaking at around $r_{\mathrm{BDT}} = 0.1$ are for the correctly matched events, the ones to the left are for incorrectly or unmatched events. The ratio figure shows the difference between the number of events in the training and test samples divided by the statistical uncertainty in this difference. Finally, **d** shows the comparison of the r_{BDT} distributions observed in data and MC simulation. The hatched area includes the uncertainties as detailed in the text. The uncertainty bars correspond to the statistical uncertainties in the data

tion carries information about the top quark mass, and in this way, m_{top}-independent background templates can be used. The signal templates are simultaneously fitted to the sum of a Gaussian and two Landau functions for $m_{\mathrm{top}}^{\mathrm{reco}}$, to the sum of two Gaussian functions for m_W^{reco} and to the sum of two Gaussian and one Landau function for R_{bq}^{reco}. This set of functions leads to an unbiased estimate of m_{top}, but is not unique. For the background, the $m_{\mathrm{top}}^{\mathrm{reco}}$ distribution is fitted to a Landau

function, while both the m_W^{reco} and the R_{bq}^{reco} distributions are fitted to the sum of two Gaussian functions.

In Fig. 5a–c, the sensitivity of $m_{\mathrm{top}}^{\mathrm{reco}}$ to the fit parameters m_{top}, JSF and bJSF is shown by the superposition of the signal templates and their fits for three input values per varied parameter. In a similar way, the sensitivity of m_W^{reco} to JSF is shown in Fig. 5d. The dependences of m_W^{reco} on the input values of m_{top} and bJSF are negligible and are not shown.
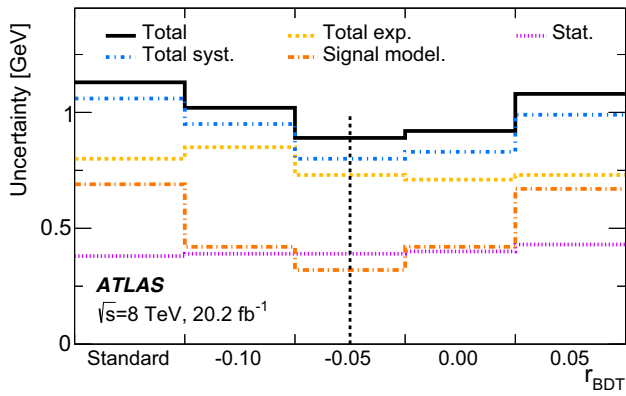
Fig. 3 Various classes of m_{top} uncertainties as a function of the minimum requirement on the BDT output r_{BDT} and for the standard selection. The total uncertainty (solid line) is the sum in quadrature of the statistical (dotted line) and total systematic uncertainty (short dash-dotted line). The total systematic uncertainty consists of the total experimental (dashed line) and total signal-modelling uncertainty (long dash-dotted line). The uncertainties in the background estimate are included in the total experimental uncertainty. The minimum requirement on r_{BDT} defining the BDT selection is indicated by the vertical black dashed line. All uncertainties are included except for the method and the pile-up uncertainties

Consequently, to increase the size of the simulation sample, the fit is performed on the sum of the m_W^{reco} distributions of the samples with different input top quark masses. Finally, the sensitivity of R_{bq}^{reco} to the input values of m_{top} and bJSF is shown in Fig. 5e, f. The dependence of R_{bq}^{reco} on JSF (not shown) is much weaker than the dependence on bJSF.

For the signal, the parameters of the fitting functions for m_{top}^{reco} depend linearly on m_{top}, JSF and bJSF. The parameters of the fitting functions for m_W^{reco} depend linearly on JSF. Finally, the parameters of the fitting functions for R_{bq}^{reco} depend linearly on m_{top}, JSF and bJSF. For the background, the dependences of the parameters of the fitting functions are identical to those for the signal, except that they do not depend on m_{top} and that those for R_{bq}^{reco} do not depend on JSF.

Signal and background probability density functions P_{top}^{sig} and P_{top}^{bkg} for the m_{top}^{reco}, m_W^{reco} and R_{bq}^{reco} distributions are used in an unbinned likelihood fit to the data for all events, $i = 1, \ldots N$. The likelihood function maximized is

$$L_{shape}^{\ell+jets}(m_{top}, JSF, bJSF, f_{bkg})$$
$$= \prod_{i=1}^{N} P_{top}(m_{top}^{reco,i} \mid m_{top}, JSF, bJSF, f_{bkg})$$
$$\times P_W(m_W^{reco,i} \mid JSF, f_{bkg})$$
$$\times P_{R_{bq}}(R_{bq}^{reco,i} \mid m_{top}, JSF, bJSF, f_{bkg}), \qquad (1)$$

with

$$P_{top}(m_{top}^{reco,i} \mid m_{top}, JSF, bJSF, f_{bkg})$$
$$= (1 - f_{bkg}) \cdot P_{top}^{sig}(m_{top}^{reco,i} \mid m_{top}, JSF, bJSF)$$
$$+ f_{bkg} \cdot P_{top}^{bkg}(m_{top}^{reco,i} \mid JSF, bJSF),$$
$$P_W(m_W^{reco,i} \mid JSF, f_{bkg})$$
$$= (1 - f_{bkg}) \cdot P_W^{sig}(m_W^{reco,i} \mid JSF)$$
$$+ f_{bkg} \cdot P_W^{bkg}(m_W^{reco,i} \mid JSF), \quad \text{and}$$
$$P_{R_{bq}}(R_{bq}^{reco,i} \mid m_{top}, JSF, bJSF, f_{bkg})$$
$$= (1 - f_{bkg}) \cdot P_{R_{bq}}^{sig}(R_{bq}^{reco,i} \mid m_{top}, JSF, bJSF)$$
$$+ f_{bkg} \cdot P_{R_{bq}}^{bkg}(R_{bq}^{reco,i} \mid bJSF)$$

where the fraction of background events is denoted by f_{bkg}. The parameters determined by the fit are m_{top}, JSF and bJSF, while f_{bkg} is fixed to its expectation shown in Table 1. It was verified that the correlations between m_{top}^{reco}, m_W^{reco} and R_{bq}^{reco} of $\rho(m_{top}^{reco}, m_W^{reco}) = 0.05$, $\rho(m_{top}^{reco}, R_{bq}^{reco}) = 0.18$, and $\rho(m_W^{reco}, R_{bq}^{reco}) = -0.13$, are small enough that formulating the likelihood in Eq. (1) as a product of three one-dimensional likelihoods does not bias the result.

Pseudo-experiments are used to verify the internal consistency of the fitting procedure and to obtain the expected statistical uncertainty for the data. For each set of parameter values, 500 pseudo-experiments are performed, each corresponding to the integrated luminosity of the data. To retain the correlation of the three observables for the three-dimensional fit, individual events are used. Because this exceeds the number of available MC events, results are corrected for oversampling [80]. The results of pseudo-experiments for different input values of m_{top} are obtained from statistically independent samples, while the results for different JSF and bJSF are obtained from statistically correlated samples as explained above. For each fitted quantity and each variation of input parameters, the residual, i.e. the difference between the input value and the value obtained by the fit, is compatible with zero. The three expected statistical uncertainties are

$$\sigma_{stat}(m_{top}) = 0.389 \quad \pm 0.004 \text{ GeV},$$
$$\sigma_{stat}(JSF) = 0.00115 \pm 0.00001, \quad \text{and}$$
$$\sigma_{stat}(bJSF) = 0.0046 \quad \pm 0.0001,$$

where the values quoted are the mean and RMS of the distribution of the statistical uncertainties in the fitted quantities from pseudo-experiments. The widths of the pull distributions are below unity for m_{top} and the two jet scale factors, which results in an overestimation of the uncertainty in m_{top} of up to 7%. Since this leads to a conservative estimate of the uncertainty in m_{top}, no attempts to mitigate this feature are made.

(a) *W* boson transverse mass

(b) Reconstructed top quark mass

(c) Reconstructed *W* boson mass

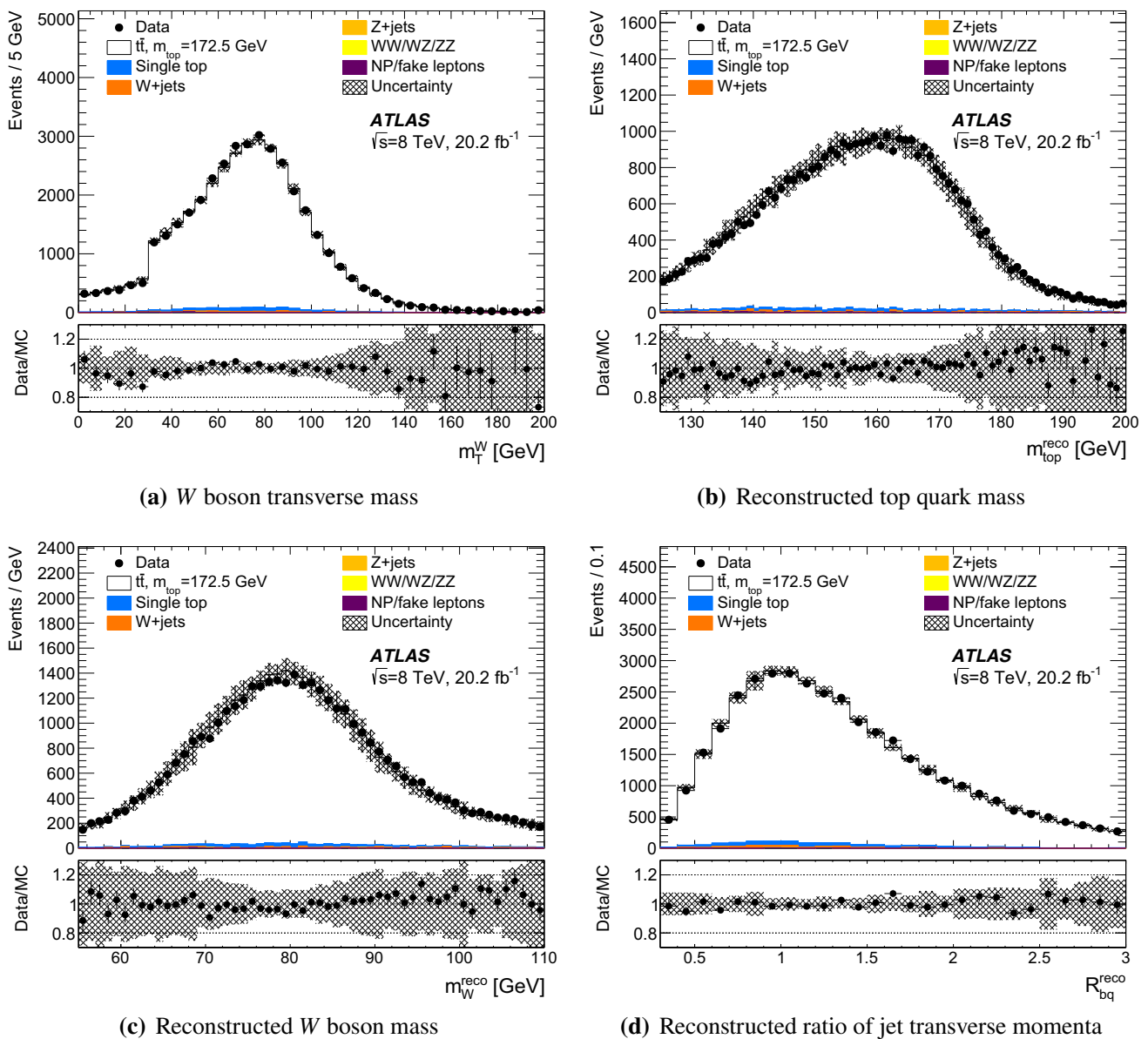**(d)** Reconstructed ratio of jet transverse momenta

Fig. 4 Distributions for the events passing the BDT selection. The data are shown, together with the signal-plus-background prediction normalized to the number of events observed in the data. The hatched area is the uncertainty in the prediction described in the text. The rightmost bin contains all entries with values above the lower edge of this bin, similarly the leftmost bin contains all entries with values below the upper edge of this bin. **a** shows the *W* boson transverse mass for the semi-leptonic top quark decay. The remaining figures show the three observables used for the determination of m_{top}, where **b** shows the reconstructed top quark mass m_{top}^{reco}, **c** shows the reconstructed invariant mass of the *W* boson m_W^{reco} and **d** shows the reconstructed ratio of jet transverse momenta R_{bq}^{reco}. The three distributions are shown within the ranges of the template fit

8 Uncertainties affecting the m$_{top}$ determination

This section focuses on the treatment of uncertainty sources of a systematic nature. The same systematic uncertainty sources as in Ref. [9] are investigated. If possible, the corresponding uncertainty in m_{top} is evaluated by varying the respective quantities by $\pm 1\sigma$ from their default values, constructing the corresponding event sample and measuring the average m_{top} change relative to the result from the nomi-

nal MC sample with 500 pseudo-experiments each, drawn from the full MC sample. In the absence of a $\pm 1\sigma$ variation, e.g. for the evaluation of the uncertainty induced by the choice of signal MC generator, the full observed difference is assigned as a symmetric systematic uncertainty and further treated as a variation equivalent to a $\pm 1\sigma$ variation. Wherever a $\pm 1\sigma$ variation can be performed, half the observed difference between the $+1\sigma$ and -1σ variation in m_{top} is assigned as an uncertainty if the m_{top} values obtained from

(a) m_{top}^{reco} with three input m_{top}

(b) m_{top}^{reco} with three input JSF

(c) m_{top}^{reco} with three input bJSF

(d) m_W^{reco} with three input JSF

(e) R_{bq}^{reco} with three input m_{top}

(f) R_{bq}^{reco} with three input bJSF
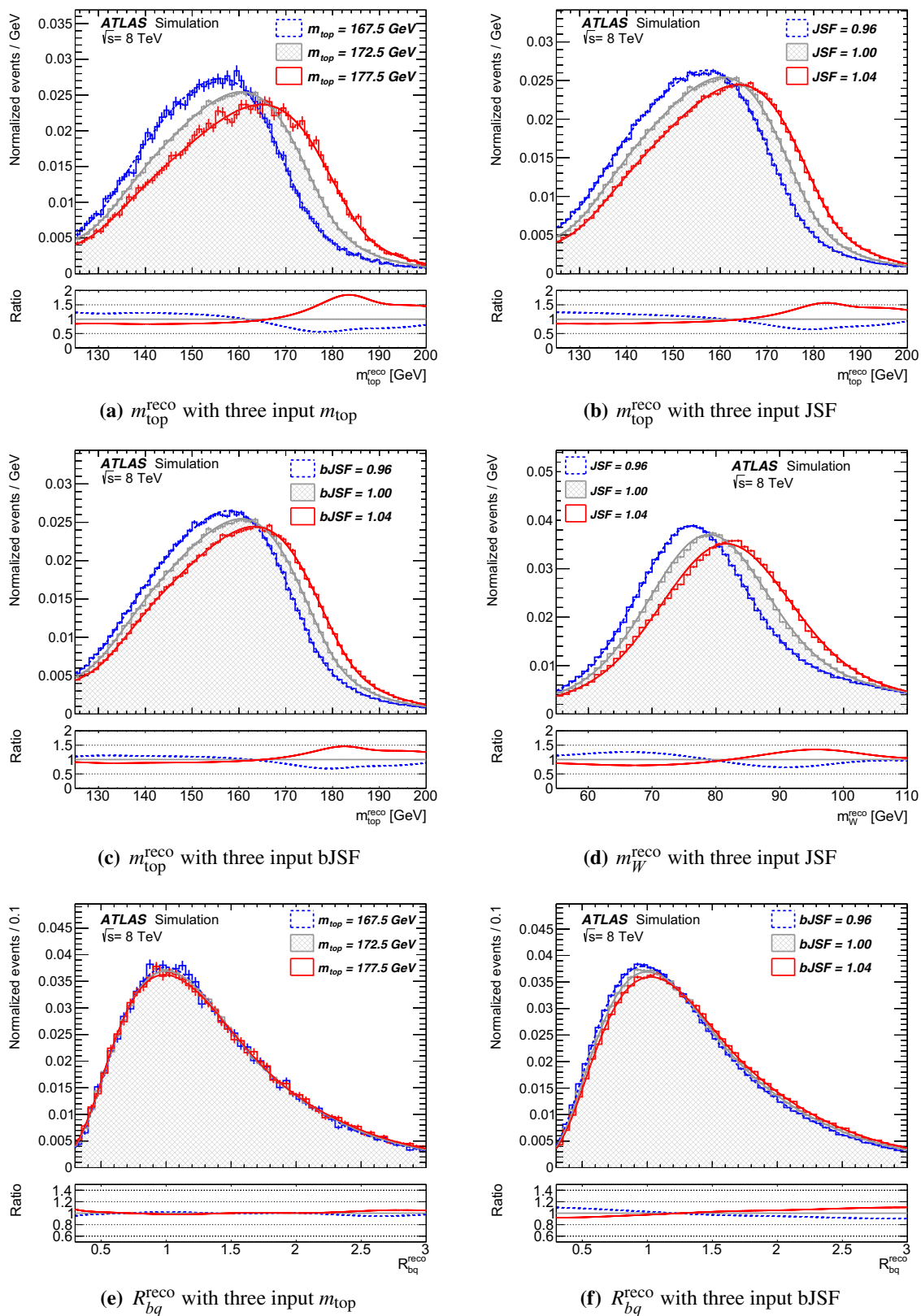
Fig. 5 Template parameterizations for signal events, composed of $t\bar{t}$ and single-top-quark production events. **a–c** show the sensitivity of m_{top}^{reco} to m_{top}, JSF and bJSF, **d** shows the sensitivity of m_W^{reco} to JSF and **e, f** show the sensitivity of R_{bq}^{reco} to m_{top} and bJSF. Each template is overlaid with the corresponding probability density function from the combined fit to all templates described in the text. The ratios shown are calculated relative to the probability density function of the central sample with $m_{top} = 172.5$ GeV, JSF = 1 and bJSF = 1

Table 3 Systematic uncertainties in m_{top}. The measured values of m_{top} are given together with the statistical and systematic uncertainties in GeV for the standard and the BDT event selections. For comparison, the result in the $t\bar{t} \rightarrow$ lepton + jets channel at $\sqrt{s} = 7$ TeV from Ref. [9] is also listed. For each systematic uncertainty listed, the first value corresponds to the uncertainty in m_{top}, and the second to the statistical precision in this uncertainty. An integer value of zero means that the corresponding uncertainty is negligible and therefore not evaluated. Statistical uncertainties quoted as 0.00 are smaller than 0.005. The statistical uncertainty in the total systematic uncertainty is calculated from uncertainty propagation. The last line refers to the sum in quadrature of the statistical and systematic uncertainties

| Event selection | $\sqrt{s} = 7$ TeV | $\sqrt{s} = 8$ TeV | |
	Standard	Standard	BDT
m_{top} result [GeV]	172.33	171.90	172.08
Statistics	0.75	0.38	0.39
– *Stat. comp.* (m_{top})	0.23	0.12	0.11
– *Stat. comp.* (JSF)	0.25	0.11	0.11
– *Stat. comp.* (bJSF)	0.67	0.34	0.35
Method	0.11 ± 0.10	0.04 ± 0.11	0.13 ± 0.11
Signal Monte Carlo generator	0.22 ± 0.21	0.50 ± 0.17	0.16 ± 0.17
Hadronization	0.18 ± 0.12	0.05 ± 0.10	0.15 ± 0.10
Initial- and final-state QCD radiation	0.32 ± 0.06	0.28 ± 0.11	0.08 ± 0.11
Underlying event	0.15 ± 0.07	0.08 ± 0.15	0.08 ± 0.15
Colour reconnection	0.11 ± 0.07	0.37 ± 0.15	0.19 ± 0.15
Parton distribution function	0.25 ± 0.00	0.08 ± 0.00	0.09 ± 0.00
Background normalization	0.10 ± 0.00	0.04 ± 0.00	0.08 ± 0.00
W+jets shape	0.29 ± 0.00	0.05 ± 0.00	0.11 ± 0.00
Fake leptons shape	0.05 ± 0.00	0	0
Jet energy scale	0.58 ± 0.11	0.63 ± 0.02	0.54 ± 0.02
Relative b-to-light-jet energy scale	0.06 ± 0.03	0.05 ± 0.01	0.03 ± 0.01
Jet energy resolution	0.22 ± 0.11	0.23 ± 0.03	0.20 ± 0.04
Jet reconstruction efficiency	0.12 ± 0.00	0.04 ± 0.01	0.02 ± 0.01
Jet vertex fraction	0.01 ± 0.00	0.13 ± 0.01	0.09 ± 0.01
b-tagging	0.50 ± 0.00	0.37 ± 0.00	0.38 ± 0.00
Leptons	0.04 ± 0.00	0.16 ± 0.01	0.16 ± 0.01
Missing transverse momentum	0.15 ± 0.04	0.08 ± 0.01	0.05 ± 0.01
Pile-up	0.02 ± 0.01	0.14 ± 0.01	0.15 ± 0.01
Total systematic uncertainty	1.04 ± 0.08	1.07 ± 0.10	0.82 ± 0.06
Total	1.28 ± 0.08	1.13 ± 0.10	0.91 ± 0.06

the variations lie on opposite sides of the nominal result. If they lie on the same side, the maximum observed difference is taken as a symmetric systematic uncertainty. Since the systematic uncertainties are derived from simulation or data samples with limited numbers of events, all systematic uncertainties have a corresponding statistical uncertainty, which is calculated taking into account the statistical correlation of the considered samples, as explained in Sect. 8.5. The statistical uncertainty in the total systematic uncertainty is dominated by the limited sizes of the simulation samples. The resulting systematic uncertainties are given in Table 3 independent of their statistical significance. Further information is given in Tables 8, 9, 10, 11 and 12 in Appendix A. This approach follows the suggestion in Ref. [81] and relies on the fact that, given a large enough number of considered uncertainty sources, statistical fluctuations average out.[6] The uncertainty sources are designed to be uncorrelated with each other, and

thus the total uncertainty is taken as the sum in quadrature of uncertainties from all sources. The individual uncertainties are compared in Table 3 for three cases: the standard selection for the $\sqrt{s} = 7$ TeV [9] and 8 TeV data and the BDT selection for $\sqrt{s} = 8$ TeV data. Many uncertainties in m_{top} obtained with the standard selection at the two centre-of-mass energies agree within their statistical uncertainties such that the resulting total systematic uncertainties are almost identical. Consequently, repeating the $\sqrt{s} = 7$ TeV analysis on $\sqrt{s} = 8$ TeV data would have only improved the statistical precision. The picture changes when comparing the uncertainties in $\sqrt{s} = 8$ TeV data for the standard selection and the BDT selection. In general, the experimental uncertainties change only slightly, with the largest reduction observed for the JES uncertainty. In contrast, a large improvement comes from the reduced uncertainties in the modelling of the $t\bar{t}$ signal processes as shown in Table 3. This, together with the improved intrinsic resolution in m_{top}, more than compensates for the small loss in precision caused by the increased statistical uncertainty. The individual sources of systematic

---

[6] In the limit of many small systematic uncertainties with large statistical uncertainties, this procedure on average leads to an overestimate of the total systematic uncertainty.

uncertainties and the evaluation of their effect on m_{top} are described in the following.

8.1 Statistics and method calibration

Uncertainties related to statistical effects and the method calibration are discussed here.

Statistical: The quoted statistical uncertainty consists of three parts: a purely statistical component in m_{top} and the contributions stemming from the simultaneous determination of JSF and bJSF. The purely statistical component in m_{top} is obtained from a one-dimensional template method exploiting only the $m_{\text{top}}^{\text{reco}}$ observable, while fixing the values of JSF and bJSF to the results of the three-dimensional analysis. The contribution to the statistical uncertainty in the fitted parameters due to the simultaneous fit of m_{top} and JSF is estimated as the difference in quadrature between the statistical uncertainty in a two-dimensional fit to $m_{\text{top}}^{\text{reco}}$ and m_W^{reco} while fixing the value of bJSF and the one-dimensional fit to the data described above. Analogously, the contribution of the statistical uncertainty due to the simultaneous fit of m_{top} together with JSF and bJSF is defined as the difference in quadrature between the statistical uncertainties obtained in the three-dimensional and the two-dimensional fits to the data. This separation allows a comparison of the statistical sensitivities of the m_{top} estimator used in this analysis, to those of analyses exploiting a different number of observables in the fit. In addition, the sensitivity of the estimators to the global jet energy scale factors can be compared directly. These uncertainties are treated as uncorrelated uncertainties in m_{top} combinations. Together with the systematic uncertainty in the residual jet energy scale uncertainties discussed below, they directly replace the uncertainty in m_{top} from the jet energy scale variations present without the in situ determination.

Method: The residual difference between fitted and generated m_{top} when analysing a template from a MC sample reflects the potential bias of the method. Consequently, the largest observed fitted m_{top} residual and the largest observed statistical uncertainty in this quantity, in any of the five signal samples with different assumed values of m_{top}, is assigned as the method calibration uncertainty and its corresponding statistical uncertainty, respectively. This also covers effects from limited numbers of simulated events in the templates and potential deficiencies in the template parameterizations.

8.2 Modelling of signal processes

The modelling of $t\bar{t} \rightarrow$ lepton + jets events incorporates a number of processes that have to be accurately described, resulting in systematic effects, ranging from the $t\bar{t}$ production to the hadronization of the showered objects.

Thanks to the restrictive event-selection requirements, the contribution of non-$t\bar{t}$ processes, comprising the single-top-quark process and the various background processes, is very low. The systematic uncertainty in m_{top} from the uncertainty in the single-top-quark normalization is estimated from the corresponding uncertainty in the theoretical cross-section given in Sect. 3. The resulting systematic uncertainty is small compared with the systematic uncertainty in the $t\bar{t}$ production and is consequently neglected. For the modelling of the signal processes, the consequence of including single-top-quark variations in the uncertainty evaluation was investigated for various uncertainty sources and found to be negligible. Therefore, the single-top-quark variations are not included in the determination of the signal event uncertainties.

Signal Monte Carlo generator: The full observed difference in fitted m_{top} between the event samples produced with the POWHEG- BOX and MC@NLO [82,83] programs is quoted as a systematic uncertainty. For the renormalization and factorization scales the POWHEG- BOX sample uses the function given in Sect. 3, while the MC@NLO sample uses $\mu_{\text{R,F}} = \sqrt{m_{\text{top}}^2 + 0.5(p_{\text{T},t}^2 + p_{\text{T},\bar{t}}^2)}$. Both samples are generated with a top quark mass of $m_{\text{top}} = 172.5$ GeV with the CT10 PDFs in the matrix-element calculation and use the HERWIG and JIMMY programs with the ATLAS AUET2 tune [47].

Hadronization: To cover the choice of parton shower and hadronization models, samples produced with the POWHEG-BOX program are showered with either the PYTHIA6 program using the P2011C tune or the HERWIG and JIMMY programs using the ATLAS AUET2 tune. This includes different approaches in shower modelling, such as using a p_{T}-ordered parton showering in the PYTHIA program or angular-ordered parton showering in the HERWIG program, the different parton shower matching scales, as well as fragmentation functions and hadronization models, such as choosing the Lund string model [84,85] implemented in the PYTHIA program or the cluster fragmentation model [86] used in the HERWIG program. The full observed difference between the samples is quoted as a systematic uncertainty.

As shown in Fig. 1, the distributions of transverse momenta in data are slightly softer than those in the POWHEG+PYTHIA MC simulation samples. Similarly to what was observed in the $t\bar{t} \rightarrow$ dilepton channel for the $p_{\text{T},\ell b}$ distribution, in the $t\bar{t} \rightarrow$ lepton + jets channel the POWHEG+HERWIG sample is much closer to the data for several distributions of transverse momenta. The $p_{\text{T,had}}$ distribution is much better described by the POWHEG+HERWIG sample as was also observed in Ref. [78]. In addition, but to a lesser extent, the MC@NLO sample used to assess the signal Monte Carlo generator uncertainty and the samples to assess the initial- and final-state QCD radiation uncertainty

discussed next also lead to a softer distribution in simulation. Given this, the observed difference in the $p_{T,had}$ distribution is covered by a combination of the signal-modelling uncertainties given in Table 3.

Despite the fact that the JES and bJES are estimated independently using dijet and other non-$t\bar{t}$ samples [63], some double-counting of hadronization-uncertainty-induced uncertainties in the JES and m_{top} cannot be excluded. This was investigated closely for the ATLAS top quark mass measurement in the $t\bar{t} \rightarrow$ lepton + jets channel at $\sqrt{s} = 7$ TeV. The results in Ref. [87] revealed that the amount of double-counting of JES and hadronization effects for the $t\bar{t} \rightarrow$ lepton + jets channel is small.

Initial- and final-state QCD radiation (ISR/FSR): ISR/FSR leads to a higher jet multiplicity and different jet energies than the hard process, which affects the distributions of the three observables. The uncertainties due to ISR/FSR modelling are estimated with samples generated with the POWHEG- BOX program interfaced to the PYTHIA6 program for which the parameters of the generation are varied to span the ranges compatible with the results of measurements of $t\bar{t}$ production in association with jets [88–90]. This uncertainty is evaluated by comparing two dedicated samples that differ in several parameters, namely the QCD scale Λ_{QCD}, the transverse momentum scale for space-like parton-shower evolution Q^2_{max}, the h_{damp} parameter [91] and the P2012 RADLO and RADHI tunes [30]. In Ref. [90], it was shown that a number of final-state distributions are better accounted for by the POWHEG+PYTHIA samples with $h_{damp} = m_{top}$. Therefore, these samples are used for evaluating this uncertainty, taking half the observed difference between the up variation and the down variation sample. Because the parameterizations for the template fit to data are obtained from POWHEG+PYTHIA samples using $h_{damp} = \infty$, it was verified that, considering the method uncertainty quoted in Table 3, applying the same functions to the $h_{damp} = m_{top}$ samples leads to a result compatible with the input top quark mass.

Underlying event: To reduce statistical fluctuations in the evaluation of this systematic uncertainty, the difference in underlying-event modelling is assessed by comparing a pair of POWHEG- BOX samples based on the same partonic events generated with the CT10 PDFs. A sample with the P2012 tune is compared with a sample with the P2012 MPIHI tune [30], with both tunes using the same CTEQ6L1 PDFs [92] for parton showering and hadronization. The Perugia 2012 MPIHI tune provides more semi-hard multiple parton interactions and is used for this comparison with identical colour reconnection parameters in both tunes. The full observed difference is assigned as a systematic uncertainty.

Colour reconnection: This systematic uncertainty is estimated using a pair of samples with the same partonic events as for the underlying-event uncertainty evaluation but with

the P2012 tune and the P2012 LOCR tune [30] for parton showering and hadronization. The full observed difference is assigned as a systematic uncertainty.

Parton distribution function (PDF): The PDF systematic uncertainty is the sum in quadrature of three contributions. These are the sum in quadrature of the differences in fitted m_{top} for the 26 eigenvector variations of the CT10 PDF and two differences in m_{top} obtained from reweighting the central CT10 PDF set to the MSTW2008 PDF [39] and the NNPDF2.3 PDF [42].

8.3 Modelling of background processes

Uncertainties in the modelling of the background processes are taken into account by variations of the corresponding normalizations and shapes of the distributions.

Background normalization: The normalizations are varied for the data-driven background estimates according to their uncertainties. For the negligible contribution from diboson production, no normalization uncertainty is evaluated.

Background shape: For the W+jets background, the shape uncertainty is evaluated from the variation of the heavy-flavour fractions. The corresponding uncertainty is small. Given the very small contribution from Z+jets, diboson and NP/fake-lepton backgrounds, no shape uncertainty is evaluated for these background sources.

8.4 Detector modelling

The level of understanding of the detector response and of the particle interactions therein is reflected in numerous systematic uncertainties.

Jet energy scale (JES): The JES is measured with a relative precision of about 1% to 4%, typically falling with increasing jet p_T and rising with increasing jet $|\eta|$ [93,94]. The total JES uncertainty consists of more than 60 subcomponents originating from the various steps in the jet calibration. The number of these nuisance parameters is reduced with a matrix diagonalization of the full JES covariance matrix including all nuisance parameters for a given category of the JES uncertainty components.

The analyses of $\sqrt{s} = 7$ TeV and $\sqrt{s} = 8$ TeV data make use of the EM+JES and LCW+GSC [93] jet calibrations, respectively. The two calibrations feature different sets of nuisance parameters, and the LCW+GSC calibration generally has smaller uncertainties than the EM+JES calibration. While the pile-up correction for the jet calibration for $\sqrt{s} = 7$ TeV data only depends on the number of primary vertices (n_{vtx}) and the mean number of interactions per bunch crossing (μ), a pile-up subtraction method based on jet area is introduced for the $\sqrt{s} = 8$ TeV data. Terms to account

for uncertainties in the pile-up estimation are added. They depend on the jet p_T and the local transverse momentum density. In addition, the punch-through uncertainty, i.e. an uncertainty for jets that penetrate through to the muon spectrometer, is added. The final reduced number of nuisance parameters for the $\sqrt{s} = 8$ TeV analysis is 25. The JES-uncertainty-induced uncertainty in m_{top} is the dominant systematic uncertainty for all results shown in Table 3. When only a one-dimensional fit to m_{top}^{reco} or a two-dimensional fit to m_{top}^{reco} and m_W^{reco} is done, this uncertainty is 0.99 GeV or 0.74 GeV, respectively.

Relative b-to-light-jet energy scale (bJES): The bJES uncertainty is an additional uncertainty for the remaining differences between b-jets and light-jets after the global JES is applied, and therefore the corresponding uncertainty is uncorrelated with the JES uncertainty. An additional uncertainty of 0.2% to 1.2% is assigned to b-jets, with the lowest uncertainty for b-jets with high transverse momenta [63]. Due to the determination of bJSF, the bJES uncertainty leads to a very small contribution to the uncertainty in m_{top} in Table 3. However, performing only a two-dimensional fit to m_{top}^{reco} and m_W^{reco} would result in an uncertainty of 0.47 GeV from this source.

Jet energy resolution (JER): The JER uncertainty is determined following an eigenvector decomposition strategy similar to the JES systematic uncertainties [93,94]. The 11 components take into account various effects evaluated from simulation-to-data comparisons including calorimeter noise terms in the forward region. The corresponding uncertainty in m_{top} is the sum in quadrature of the components of the eigenvector decomposition.

Jet reconstruction efficiency (JRE): This uncertainty is evaluated by randomly removing 0.23% of the jets with $p_T < 30$ GeV from the simulated events prior to the event selection to reflect the precision with which the data-to-simulation JRE ratio is known [62]. The fitted m_{top} difference between the varied sample and the nominal sample is taken as a systematic uncertainty.

Jet vertex fraction (JVF): When summing the scalar p_T of all tracks in a jet, the JVF is the fraction contributed by tracks originating at the primary vertex. The uncertainty in m_{top} is evaluated by varying the requirement on the JVF within its uncertainty [65].

b-tagging: Mismodelling of the b-tagging efficiency and mistag rate is accounted for by the application of jet-specific scale factors to simulated events [66]. These scale factors depend on jet p_T, jet η and the underlying quark flavour. The ones used in this analysis are derived from dijet and $t\bar{t} \rightarrow$ dilepton [66] events. They are the same as those used for the measurement of m_{top} in the $t\bar{t} \rightarrow$ dilepton channel [14].

Similarly to the JES uncertainties, the b-tagging uncertainties are estimated by using an eigenvector approach, based on the b-tagging calibration analysis [66–68]. They include the uncertainties in the b-tagging, c/τ-tagging and mistagging scale factors. This uncertainty in m_{top} is derived by varying the scale factors within their uncertainties and adding the resulting fitted differences in quadrature. In this procedure, uncertainties that are considered both in the b-tagging calibration and as separate sources in the m_{top} analysis are taken into account simultaneously by applying the corresponding varied b-tagging scale factors together with the varied sample when assessing the corresponding uncertainty in m_{top}. The final uncertainty is the sum in quadrature of these independent components. Compared with the result from $\sqrt{s} = 7$ TeV data, this uncertainty is reduced by about one third for both the standard and BDT event selections in accordance with the improvements made in the calibrations of the b-tagging algorithm [66,67].

Leptons: The lepton uncertainties are related to the electron energy or muon momentum scale and resolution, as well as trigger, isolation and identification efficiencies. These are measured very precisely in high-purity $J/\psi \rightarrow \ell^+\ell^-$ and $Z \rightarrow \ell^+\ell^-$ data [57,58,95]. For each component, the corresponding uncertainty is propagated to the analysis by variation of the respective quantity. The changes are propagated to the E_T^{miss} as well.

Missing transverse momentum: The remaining contribution to the missing-transverse-momentum uncertainty stems from the uncertainties in calorimeter-cell energies associated with low-p_T jets (7 GeV $< p_T < 20$ GeV) without any corresponding reconstructed physics object or from pile-up interactions. They are accounted for as described in Ref. [69]. The corresponding uncertainty in m_{top} is small.

Pile-up: Besides the component treated in the JES uncertainty, the residual dependence of the fitted m_{top} on the amount of pile-up activity and a possible mismodelling of pile-up in MC simulation is determined. For this, the m_{top} dependence in bins of n_{vtx} and μ is determined for data and MC simulated events. Within the statistical uncertainties, the slopes of the linear dependences of m_{top} observed in data and predicted by the MC simulation are compatible. The same is true for JSF and bJSF. The final effect on the measurement is assessed by a convolution of the linear dependence with the respective n_{vtx} and μ distributions observed for data and MC simulated events. The maximum of the n_{vtx} and μ effects is assigned as an uncertainty due to pile-up. The pile-up conditions differ between the $\sqrt{s} = 7$ and 8 TeV data. For the BDT selection of $\sqrt{s} = 8$ TeV data used here, the average of the mean number of inelastic pp interactions per bunch crossing is $\langle \mu \rangle = 20.3$ and the average number of reconstructed primary vertices is about $n_{vtx} = 9.4$, to be compared

with $\langle\mu\rangle = 8.8$ and $n_{\text{vtx}} = 7.0$ for $\sqrt{s} = 7$ TeV data [65]. The corresponding uncertainty is somewhat larger than for $\sqrt{s} = 7$ TeV data but still small.

8.5 Statistical precision of systematic uncertainties

The systematic uncertainties quoted in Table 3 carry statistical uncertainties themselves. In view of a combination with other measurements, the statistical precision σ from a comparison of two samples (1 and 2) is determined for each uncertainty source based on the statistical correlation ρ_{12} of the underlying samples using $\sigma^2 = \sigma_1^2 + \sigma_2^2 - 2\rho_{12}\sigma_1\sigma_2$. The statistical correlation is expressed as a function of the fraction of shared events of both samples $\rho_{12} = \sqrt{N_{12}/N_1 \cdot N_{12}/N_2} = N_{12}/\sqrt{N_1 \cdot N_2}$, with N_1 and N_2 being the unweighted numbers of events in the two samples and N_{12} being the unweighted number of events present in both samples. The size of the MC sample at $m_{\text{top}} = 172.5$ GeV results in a statistical precision in m_{top} of about 0.1 GeV. Most estimations are based on the same sample with only a change in a single parameter, such as lepton energy scale uncertainties. This leads to a high correlation of the central m_{top} values and a correspondingly low statistical uncertainty in their difference. Others, which do not share the same generated events or exhibit other significant differences, have a lower correlation, and the corresponding statistical uncertainty is higher, such as in the case of the signal-modelling uncertainty. The statistical uncertainty in the total systematic uncertainty is calculated from the individual statistical uncertainties by the propagation of uncertainties.

9 Results

For the BDT selection, the likelihood fit to the data results in

$$m_{\text{top}} = 172.08 \pm 0.39 \text{ (stat) GeV},$$
$$\text{JSF} = 1.005 \ \pm 0.001 \text{ (stat)}, \quad \text{and}$$
$$\text{bJSF} = 1.008 \ \pm 0.005 \text{ (stat)}.$$

The statistical uncertainties are taken from the parabolic approximation of the likelihood profiles. The expected statistical uncertainties, calculated in Sect. 7, are compatible with those. The correlation matrices of the three variables with $i = 0$, 1 and 2 corresponding to m_{top}, JSF and bJSF are

$$\rho_{\text{stat}} = \begin{pmatrix} 1 & -0.27 & -0.92 \\ -0.27 & 1 & -0.02 \\ -0.92 & -0.02 & 1 \end{pmatrix} \quad \text{and}$$

$$\rho_{\text{tot}} = \begin{pmatrix} 1 & -0.30 & -0.39 \\ -0.30 & 1 & -0.42 \\ -0.39 & -0.42 & 1 \end{pmatrix}.$$

The upper matrix corresponds to the correlations for statistical uncertainties only, while the lower matrix is obtained by additionally taking into account all systematic uncertainties.

Figure 6 shows the $m_{\text{top}}^{\text{reco}}$, m_W^{reco} and R_{bq}^{reco} distributions in the data with statistical uncertainties together with the corresponding fitted probability density functions for the background alone and for the sum of signal and background. The uncertainty band attached to the fit to data is obtained in the following way. At each point in $m_{\text{top}}^{\text{reco}}$, m_W^{reco} and R_{bq}^{reco}, the band contains 68% of all fit function values obtained by randomly varying m_{top}, JSF and bJSF within their total uncertainties and taking into account their correlations. The waist in the uncertainty band is caused by the usage of normalized probability density functions. The band visualises the variations of the three template fit functions caused by all the uncertainties in m_{top} listed in Table 3. The total uncertainty in all three fitted parameters is dominated by their systematic uncertainty. Therefore, the band shown is much wider than the band that would be obtained by fitting to the distributions with statistical uncertainties only.

The measured value of m_{top} in the $t\bar{t} \rightarrow \text{lepton} + \text{jets}$ channel at $\sqrt{s} = 8$ TeV is

$$m_{\text{top}} = 172.08 \pm 0.39 \text{ (stat)} \pm 0.82 \text{ (syst) GeV}$$

with a total uncertainty of 0.91 GeV. The statistical precision of the systematic uncertainty is 0.06 GeV. This result corresponds to a 19% improvement on the result obtained using the standard selection on the same data. Compared with the result in the $t\bar{t} \rightarrow \text{lepton} + \text{jets}$ channel at $\sqrt{s} = 7$ TeV, the improvement is 29%. On top of the smaller statistical uncertainty, the increased precision is mainly driven by smaller theory modelling uncertainties achieved by the BDT selection. The larger number of events in the $\sqrt{s} = 8$ TeV dataset is effectively traded for lower systematic uncertainties, resulting in a significant gain in total precision. The new ATLAS result in the $t\bar{t} \rightarrow \text{lepton} + \text{jets}$ channel is more precise than the result from the CDF experiment, but less precise than the CMS and D0 results, measured in the same channel, as shown in Fig. 14b in Appendix B.

10 Combination with previous ATLAS results

This section presents the combination of the six m_{top} results of the ATLAS analyses in the $t\bar{t} \rightarrow \text{dilepton}$, $t\bar{t} \rightarrow \text{lepton} + \text{jets}$ and $t\bar{t} \rightarrow \text{all jets}$ channels at centre-of-mass energies of $\sqrt{s} = 7$ and 8 TeV. The treatment of the results that are input to the combinations are described, followed by a detailed explanation of the evaluation of the estimator correlations for the various sources of systematic uncertainty. The compatibilities of the measured m_{top} values are investigated using a pairwise χ^2 for all pairs of measurements

(a) Reconstructed top quark mass

(b) Reconstructed$W$ boson mass

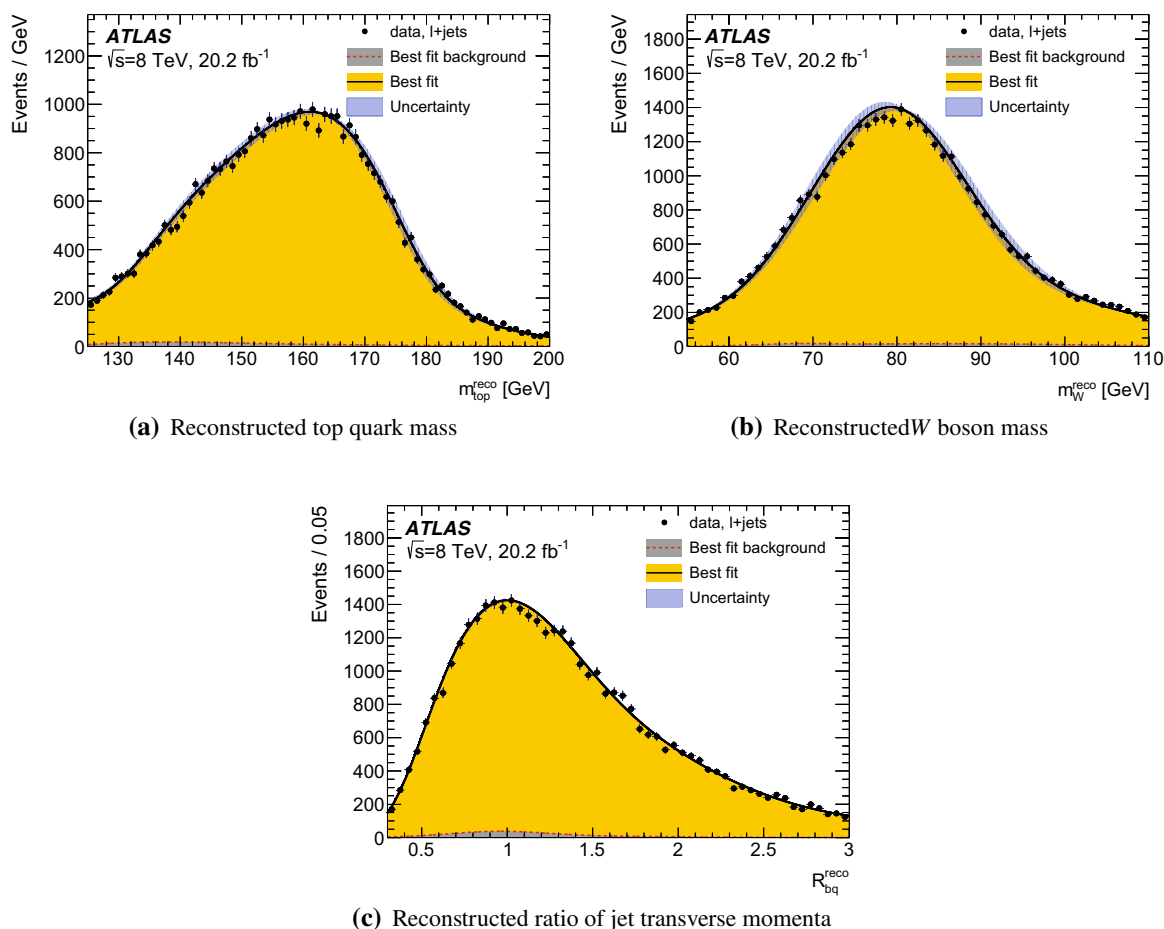**(c)** Reconstructed ratio of jet transverse momenta

Fig. 6 Results of the likelihood fit to the data. The figures show the data distributions of the three observables with statistical uncertainties together with the fitted probability density function for the background alone (barely visible at the bottom of the figure) and for the sum of signal and background. The uncertainty band corresponds to the one standard deviation total uncertainty in the fit function. It is based on the total uncertainty in the three fitted parameters as explained in the text. **a** shows the distribution of the reconstructed top quark mass m_{top}^{reco}, **b** shows the distribution of the reconstructed W boson mass m_W^{reco} and **c** shows the reconstructed ratio of jet transverse momenta R_{bq}^{reco}

and by evaluating the compatibility of selected combinations. Finally, the six results are combined, displaying the effect of individual results on the combined result.

10.1 Inputs to the combination and categorization of uncertainties

The measured values of the individual analyses and their statistical and systematic uncertainties are given in Table 4. For each result, the evaluated systematic uncertainties are shown together with their statistical uncertainties. The statistical uncertainties in the total systematic uncertainties and the total uncertainties are obtained from the propagation of uncertainties.[7]

For the combinations to follow, the combined uncertainties for the previous results, namely $t\bar{t} \to$ dilepton and $t\bar{t} \to$ lepton + jets at $\sqrt{s} = 7$ TeV from Ref. [9], $t\bar{t} \to$ all jets at $\sqrt{s} = 7$ TeV from Ref. [96], $t\bar{t} \to$ dilepton at $\sqrt{s} = 8$ TeV from Ref. [14] and $t\bar{t} \to$ all jets at $\sqrt{s} = 8$ TeV from Ref. [74], were all re-evaluated. In all cases, the numbers agree to within 0.01 GeV with the original publications, which in any case is the rounding precision due to the precision of some of the inputs. On top of this, the results listed in Table 4 differ in some aspects from the original publications as explained below.

The combination follows the approach developed for the combination of $\sqrt{s} = 7$ TeV analyses in Ref. [9], including the evaluation of the correlations given in Sect. 10.2 below. The treatment of uncertainty categories for the $t\bar{t} \to$ dilepton and $t\bar{t} \to$ lepton + jets measurements at $\sqrt{s} = 7$ TeV exactly follows Ref. [9]. The uncertainty categorizations for the $t\bar{t} \to$ all jets measurements at $\sqrt{s} = 7$ and 8 TeV from Refs. [74,96] closely follow this categorization but have

---

[7] For the previous results in the $t\bar{t} \to$ dilepton and $t\bar{t} \to$ lepton + jets channels, the values quoted for the statistical uncertainties in the total systematic uncertainties differ from the ones in the original publications, where just the sum in quadrature of the statistical uncertainties in the individual systematic uncertainties was used.

Table 4 The six measured values of m_{top} ($i = 0 \ldots, 5$) and their statistical and systematic uncertainty sources k, numbered as given in the first column. For the individual measurements, the systematic uncertainty in m_{top} and its associated statistical uncertainty are given for each source of uncertainty. The last line refers to the sum in quadrature of the statistical and systematic uncertainties. The statistical uncertainties in the total systematic uncertainties and in the total uncertainties are calculated from the propagation of uncertainties. Systematic uncertainties listed as 0 are not evaluated, while an empty cell indicates an uncertainty not applicable to the corresponding measurement. Statistical uncertainties quoted as 0.00 are smaller than 0.005

k		$\sqrt{s} = 7$ TeV			$\sqrt{s} = 8$ TeV		
		$m_{\text{top}}^{\text{dilepton}}$ [GeV]	$m_{\text{top}}^{\ell+\text{jets}}$ [GeV]	$m_{\text{top}}^{\text{all jets}}$ [GeV]	$m_{\text{top}}^{\text{dilepton}}$ [GeV]	$m_{\text{top}}^{\ell+\text{jets}}$ [GeV]	$m_{\text{top}}^{\text{all jets}}$ [GeV]
0	Results ($i = 0 \ldots, 5$)	173.79	172.33	175.06	172.99	172.08	173.72
	Statistics	0.54	0.75	1.35	0.41	0.39	0.55
	– *Stat. comp.* (m_{top})		0.23			0.11	
	– *Stat. comp.* (JSF)		0.25			0.11	
	– *Stat. comp.* (bJSF)		0.67			0.35	
1	Method	0.09 ± 0.07	0.11 ± 0.10	0.42 ± 0.01	0.05 ± 0.07	0.13 ± 0.11	0.11
2	Signal Monte Carlo generator	0.26 ± 0.16	0.22 ± 0.21	0.30 ± 0.30	0.09 ± 0.15	0.16 ± 0.17	0.18 ± 0.21
3	Hadronization	0.53 ± 0.09	0.18 ± 0.12	0.50 ± 0.15	0.22 ± 0.09	0.15 ± 0.10	0.64 ± 0.15
4	Initial- and final-state QCD radiation	0.47 ± 0.05	0.32 ± 0.06	0.22 ± 0.11	0.23 ± 0.07	0.08 ± 0.11	0.10 ± 0.28
5	Underlying event	0.05 ± 0.05	0.15 ± 0.07	0.08 ± 0.10	0.10 ± 0.14	0.08 ± 0.15	0.12 ± 0.16
6	Colour reconnection	0.14 ± 0.05	0.11 ± 0.07	0.22 ± 0.10	0.03 ± 0.14	0.19 ± 0.15	0.12 ± 0.16
7	Parton distribution function	0.10 ± 0.00	0.25 ± 0.00	0.09 ± 0.00	0.05 ± 0.00	0.09 ± 0.00	0.09 ± 0.00
8	Background normalization	0.04 ± 0.00	0.10 ± 0.00		0.03 ± 0.00	0.08 ± 0.00	
9	W/Z+jets shape	0.00 ± 0.00	0.29 ± 0.00		0	0.11 ± 0.00	
10	Fake leptons shape	0.01 ± 0.00	0.05 ± 0.00		0.07 ± 0.00	0	
11	Data-driven all-jets background			0.35 ± 0.21			0.17
12	Jet energy scale	0.76 ± 0.09	0.58 ± 0.11	0.50 ± 0.05	0.54 ± 0.04	0.54 ± 0.02	0.60 ± 0.03
13	Relative b-to-light-jet energy scale	0.68 ± 0.02	0.06 ± 0.03	0.62 ± 0.05	0.30 ± 0.01	0.03 ± 0.01	0.34 ± 0.02
14	Jet energy resolution	0.19 ± 0.04	0.22 ± 0.11	0.01 ± 0.08	0.09 ± 0.05	0.20 ± 0.04	0.10 ± 0.04
15	Jet reconstruction efficiency	0.07 ± 0.00	0.12 ± 0.00	0.01 ± 0.01	0.01 ± 0.00	0.02 ± 0.01	0
16	Jet vertex fraction	0.00 ± 0.00	0.01 ± 0.00	0.01 ± 0.01	0.02 ± 0.00	0.09 ± 0.01	0.03 ± 0.01
17	b-tagging	0.07 ± 0.00	0.50 ± 0.00	0.16 ± 0.00	0.04 ± 0.02	0.38 ± 0.00	0.10 ± 0.00
18	Leptons	0.13 ± 0.00	0.04 ± 0.00	0	0.14 ± 0.01	0.16 ± 0.01	0.01 ± 0.00
19	Missing transverse momentum	0.04 ± 0.03	0.15 ± 0.04	0.02 ± 0.05	0.01 ± 0.01	0.05 ± 0.01	0.01 ± 0.01
20	Pile-up	0.01 ± 0.00	0.02 ± 0.01	0.02 ± 0.00	0.05 ± 0.01	0.15 ± 0.01	0.01 ± 0.00
21	All-jets trigger			0.01 ± 0.01			0.01 ± 0.00
22	Fast vs. full simulation			0.24 ± 0.18			0.08 ± 0.01
	Total systematic uncertainty	1.31 ± 0.07	1.04 ± 0.08	1.21 ± 0.13	0.74 ± 0.05	0.82 ± 0.06	1.02 ± 0.11
	Total	1.42 ± 0.07	1.28 ± 0.08	1.82 ± 0.13	0.85 ± 0.05	0.91 ± 0.06	1.16 ± 0.11

some extra, analysis-specific sources of uncertainty, as shown in Table 4. In addition, the $t\bar{t} \rightarrow$ all jets result at $\sqrt{s} = 8$ TeV from Ref. [74] is based on a different treatment of the PDF-uncertainty-induced uncertainty in m_{top}. To allow the evaluation of the estimator correlations also for this uncertainty in m_{top}, for this combination, the respective uncertainty is newly evaluated according to the prescription given in Sect. 8.

For the $t\bar{t} \rightarrow$ all jets result at $\sqrt{s} = 7$ TeV the statistical precisions in the systematic uncertainties were not evaluated in Ref. [9] but were calculated for this combination. For the $t\bar{t} \rightarrow$ all jets result at $\sqrt{s} = 8$ TeV in Ref. [74], for some of the sources, the statistical uncertainty in the systematic uncertainty was not evaluated, such that the quoted statistical uncertainty in the total systematic uncertainty is a lower limit.

For the mapping of uncertainty categories for data taken at different centre-of-mass energies, the choice of Ref. [14] is employed. The most complex cases are the uncertainties involving eigenvector decompositions, such as the JES and b-tagging scale factor uncertainties, and the uncertainty categories that do not apply to all input measurements. The JES-uncertainty-induced uncertainty in m_{top} is obtained from a number of JES subcomponents. Some JES subcomponents have an equivalent at the other centre-of-mass energy and others do not. As in Ref. [14], the JES subcomponents without an equivalent at the other centre-of-mass energy are treated as independent, resulting in vanishing estimator correlations for that part of the covariance matrix. For the remaining subcomponents, the estimator correlations are partly positive and partly negative. As an example, for the flavour part of the JES-uncertainty-induced uncertainty in m_{top}, the two most precise results, the $t\bar{t} \rightarrow$ dilepton and $t\bar{t} \rightarrow$ lepton + jets measurements at $\sqrt{s} = 8$ TeV, are negatively correlated. Consequently, for this pair, the resulting estimator correlation for the total JES-induced uncertainty in m_{top} is also negative. At the quoted precision, the two assumptions about the equivalence of the JES subcomponents between the datasets at the two centre-of-mass energies, i.e. the weak and strong correlation scenarios described in Table 10 in Appendix A, leave the combined value and uncertainty unchanged.

Following Ref. [14], the $\sqrt{s} = 7$ and 8 TeV measurements are treated as uncorrelated for the nuisance parameters of the b-tagging, c/τ-tagging, mistagging and JER uncertainties. In Ref. [14] it was shown that a correlated treatment of the flavour-tagging nuisance parameters results in an insignificant change in the combination. For the statistical, method calibration, MC-based background shape at $\sqrt{s} = 7$ and 8 TeV, and the pile-up uncertainties in m_{top}, the measurements are assumed to be uncorrelated. Details of the evaluation of the correlations for all remaining systematic uncertainties are discussed below.

10.2 Mathematical framework and evaluation of estimator correlations

All combinations are performed using the best linear unbiased estimate (BLUE) method [97,98] in a C++ implementation described in Ref. [99]. The BLUE method uses a linear combination of the inputs to combine measurements. The coefficients (BLUE weights) are determined via the minimization of the variance of the combined result. They can be used to construct measures for the importance of a given single measurement in the combination [98]. For any combination, the measured values x_i, the list of uncertainties σ_{ik} and the correlations ρ_{ijk} of the estimators (i, j) for each source of uncertainty (k) have to be provided. For all uncertainties, a Gaussian probability distribution function is assumed. For the uncertainties in m_{top} for which the measurements are correlated, when using $\pm 1\sigma$ variations of a systematic effect, e.g. when changing the bJES by $\pm 1\sigma$, there are two possibilities. When simultaneously applying a variation for a systematic uncertainty, e.g. $+1\sigma$ for the bJES, to a pair (i, j) of measurements, e.g. the $t\bar{t} \rightarrow$ lepton + jets and $t\bar{t} \rightarrow$ dilepton measurements at $\sqrt{s} = 8$ TeV, both analyses can result in a larger or smaller m_{top} value than the one obtained for the nominal case (full correlation, $\rho_{ijk} = +1$), or one analysis can result in a larger and the other in a smaller value (full anti-correlation, $\rho_{ijk} = -1$). Consequently, an uncertainty from a source only consisting of a single variation, such as the bJES-uncertainty-induced uncertainty or the uncertainty related to the choice of MC generator for signal events, results in a correlation of $\rho_{ijk} = \pm 1$. The estimator correlations for composite uncertainties are evaluated by calculating the correlation from the subcomponents. As an example, for the $t\bar{t} \rightarrow$ lepton + jets result at $\sqrt{s} = 8$ TeV, the subcomponents of the JES uncertainty are shown in Table 10 in Appendix A. For any pair of measurements (i, j), this evaluation is done by adding the covariance terms of the subcomponents k with $\rho_{ijk} = \pm 1$ and dividing by the total uncertainties for that source. The resulting estimator correlation is

$$\rho_{ij} = \frac{\sum_{k=1}^{N_{\text{comp}}} \rho_{ijk}\sigma_{ik}\sigma_{jk}}{\sigma_i \sigma_j}.$$

The quantity $\sigma_i^2 = \sum_{k=1}^{N_{\text{comp}}} \sigma_{ik}^2$ is the sum of the single subcomponent variances in analysis i. This procedure is applied to all uncertainty sources that consist of more than one subcomponent to reduce the large list of uncertainty subcomponents per estimator of $\mathcal{O}(100)$ to a suitable number of uncertainty sources, i.e. to those given in Table 4. Since the full
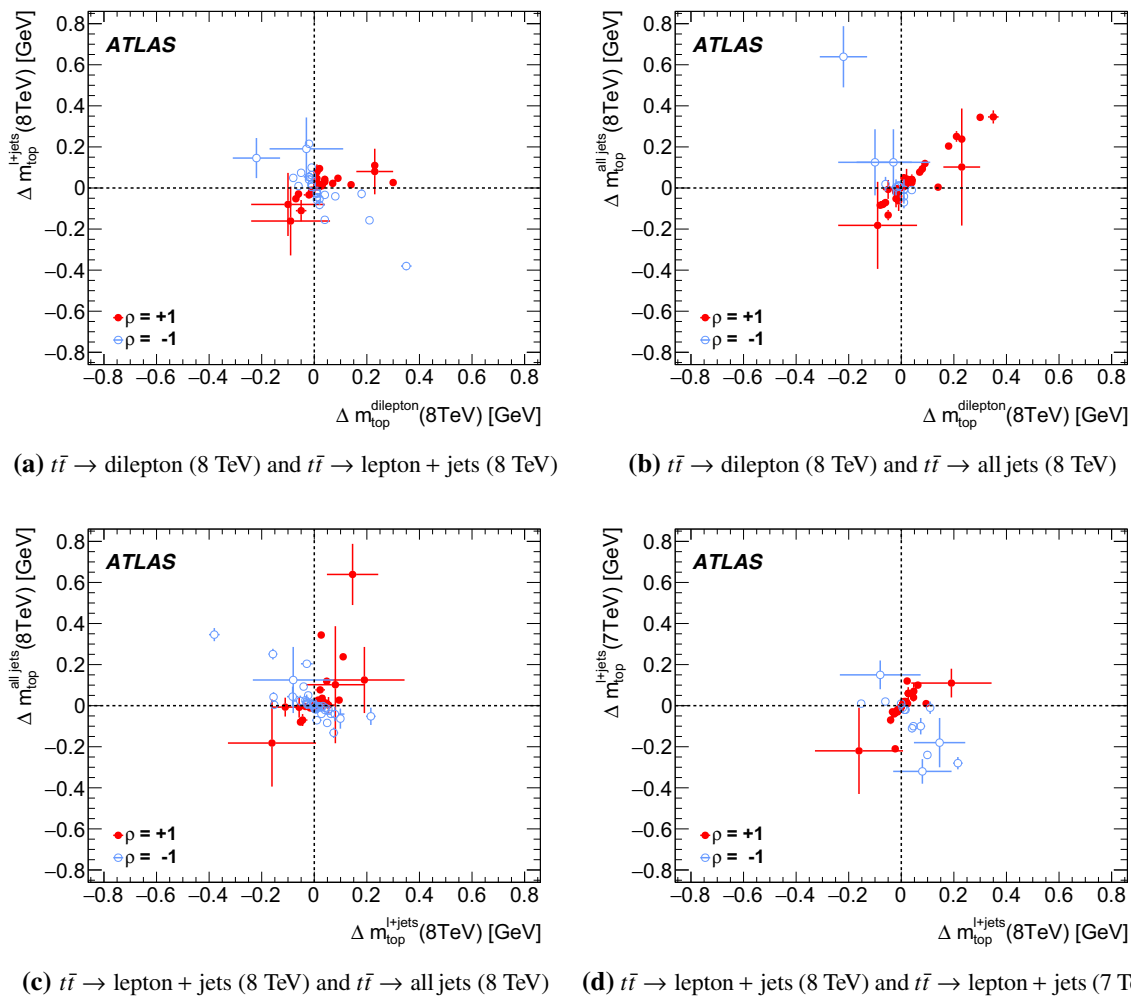
(a) $t\bar{t} \to$ dilepton (8 TeV) and $t\bar{t} \to$ lepton + jets (8 TeV)

(b) $t\bar{t} \to$ dilepton (8 TeV) and $t\bar{t} \to$ all jets (8 TeV)

(c) $t\bar{t} \to$ lepton + jets (8 TeV) and $t\bar{t} \to$ all jets (8 TeV)

(d) $t\bar{t} \to$ lepton + jets (8 TeV) and $t\bar{t} \to$ lepton + jets (7 TeV)

Fig. 7 The pairwise shifts in m_{top} when simultaneously varying a pair of measurements for a systematic uncertainty or a subcomponent of a systematic uncertainty. **a**, **b** show the correlations of the $t\bar{t} \to$ dilepton measurement at $\sqrt{s} = 8$ TeV with the two other measurements at the same centre-of-mass energy for all sources of uncertainty for which the estimators are correlated. **c** shows the correlations of the present measurement with the $t\bar{t} \to$ all jets measurement at $\sqrt{s} = 8$ TeV, while **d** shows the correlations of the present measurement with the $t\bar{t} \to$ lepton + jets measurement at $\sqrt{s} = 7$ TeV. The crosses indicate the statistical uncertainty in the systematic uncertainties. The solid points indicate the fully correlated cases, and the open points indicate the anti-correlated ones

covariance matrix is independent of how the subsets are chosen, this does not affect the combination.

For the three analyses, the evaluated shifts in m_{top} per uncertainty subcomponent are referred to as $\Delta m_{\text{top}}^{\text{dilepton}}$, $\Delta m_{\text{top}}^{\ell+\text{jets}}$ and $\Delta m_{\text{top}}^{\text{all jets}}$. They are shown in Fig. 7 for the various uncertainty subcomponents in selected pairs of analyses. The pairs using the results from $\sqrt{s} = 8$ TeV data are shown in Fig. 7a–c, while Fig. 7d is for the two analyses in the $t\bar{t} \to$ lepton + jets channel at the two centre-of-mass energies. Each point represents the observed shifts for a systematic uncertainty or a subcomponent of a systematic uncertainty together with a cross, indicating the corresponding statistical precision in the systematic uncertainty in

the two results. The solid points indicate the fully correlated cases, and the open points indicate the anti-correlated ones.[8]

For many significant sources of uncertainty in Fig. 7a, the $t\bar{t} \to$ lepton + jets and $t\bar{t} \to$ dilepton measurements are anti-correlated. As shown in Ref. [9], this is caused by the the in situ determination of the JSF and bJSF in the three-dimensional $t\bar{t} \to$ lepton + jets analysis. In contrast, for most sources of uncertainty, a positive estimator correlation is observed for the $t\bar{t} \to$ dilepton and $t\bar{t} \to$ all jets measurements at $\sqrt{s} = 8$ TeV, shown in Fig. 7b. The prominent

---

[8] In the course of including more results into the combination of Ref. [14], the definitions of the variations were homogenized while leaving the estimator correlations unchanged. As a consequence, for the corresponding figures some of the points now are located in the respective other quadrant, e.g. for the $t\bar{t} \to$ dilepton result at $\sqrt{s} = 8$ TeV.

Table 5 The pairwise correlations ρ_{ijk} of the six measurements $i, j = 0, \ldots, 5$ of m_{top} for each source of systematic uncertainty $k = 0, \ldots, 22$, along with the total estimator correlations and the compatibility of the measurements using χ^2_{ij} from Eq. (2). The indices i and j are 0 for $t\bar{t} \rightarrow$ dilepton at $\sqrt{s} = 7$ TeV, 1 for $t\bar{t} \rightarrow$ lepton + jets at $\sqrt{s} = 7$ TeV, 2 for $t\bar{t} \rightarrow$ all jets at $\sqrt{s} = 7$ TeV, 3 for $t\bar{t} \rightarrow$ dilepton at $\sqrt{s} = 8$ TeV, 4 for $t\bar{t} \rightarrow$ lepton + jets at $\sqrt{s} = 8$ TeV, and 5

for $t\bar{t} \rightarrow$ all jets at $\sqrt{s} = 8$ TeV. The correspondence of the indices $k = 0, \ldots, 22$ and the sources of systematic uncertainty are given in Table 4. Correlations that are assigned, or cannot be evaluated because one uncertainty in the covariance term is zero at the quoted precision, are given as integer values, while evaluated correlations are shown as real values

k	$m_{top}^{dilepton}$ 7 TeV $i = 0$					$m_{top}^{\ell+jets}$ 7 TeV $i = 1$				$m_{top}^{all\,jets}$ 7 TeV $i = 2$			$m_{top}^{dilepton}$ 8 TeV $i = 3$		$m_{top}^{\ell+jets}$ 8 TeV $i = 4$
	ρ_{01}	ρ_{02}	ρ_{03}	ρ_{04}	ρ_{05}	ρ_{12}	ρ_{13}	ρ_{14}	ρ_{15}	ρ_{23}	ρ_{24}	ρ_{25}	ρ_{34}	ρ_{35}	ρ_{45}
0	0	0	0	0	0	0	0	0	0	0	0	0	0	0	0
1	0	0	0	0	0	0	0	0	0	0	0	0	0	0	0
2	1.00	−1.00	1.00	1.00	1.00	−1.00	1.00	1.00	1.00	−1.00	−1.00	−1.00	1.00	1.00	1.00
3	1.00	1.00	1.00	−1.00	−1.00	1.00	1.00	−1.00	−1.00	1.00	−1.00	−1.00	−1.00	−1.00	1.00
4	−1.00	1.00	1.00	1.00	1.00	−1.00	−1.00	−1.00	−1.00	1.00	1.00	1.00	1.00	1.00	1.00
5	−1.00	1.00	1.00	1.00	−1.00	−1.00	−1.00	−1.00	1.00	1.00	1.00	−1.00	1.00	−1.00	−1.00
6	−1.00	1.00	1.00	−1.00	−1.00	−1.00	−1.00	1.00	1.00	1.00	−1.00	−1.00	−1.00	−1.00	1.00
7	0.53	0.22	−0.02	0.72	−0.61	−0.36	−0.32	0.72	−0.81	0.41	−0.05	0.27	−0.48	0.40	−0.76
8	1.00	0	0.31	−0.77	0	0	0.31	−0.74	0	0	0	0	−0.06	0	0
9	0	0	0	0	0	0	0	0	0	0	0	0	0	0	0
10	0.20	0	0	0	0	0	0.27	0	0	0	0	0	0	0	0
11	0	0	0	0	0	0	0	0	0	0	0	1	0	0	0
12	−0.24	0.86	0.36	0.18	0.36	0.10	0.04	−0.29	0.13	0.41	0.09	0.42	−0.54	0.98	−0.57
13	1.00	1.00	1.00	1.00	1.00	1.00	1.00	1.00	1.00	1.00	1.00	1.00	1.00	1.00	1.00
14	−1.00	1.00	0	0	0	−1.00	0	0	0	0	0	0	0.22	−0.07	−0.17
15	1.00	1.00	1.00	1.00	0	1.00	1.00	1.00	0	1.00	1.00	0	1.00	0	0
16	−1.00	1.00	−1.00	−1.00	−1.00	−1.00	1.00	1.00	1.00	−1.00	−1.00	−1.00	1.00	1.00	1.00
17	−0.80	−0.03	0	0	0	0	0	0	0	0	0	0	−0.23	1	1
18	−0.35	0	0.93	−0.08	0.42	0	−0.51	−0.17	0.02	0	0	0	0.11	0.28	−0.36
19	0.00	−0.26	−0.26	−0.12	0.04	0.84	0.26	0.22	0.16	0	0	0	0.97	0.86	0.96
20	0	0	0	0	0	0	0	0	0	0	0	0	0	0	0
21	0	0	0	0	0	0	0	0	0	0	0	1.00	0	0	0
22	0	0	0	0	0	0	0	0	0	0	0	0	0	0	0
Total	−0.07	0.42	0.52	0.06	0.08	−0.01	−0.00	−0.07	−0.02	0.29	−0.06	−0.01	−0.19	0.32	0.00
χ^2_{ij}	0.55	0.51	0.44	1.09	0.00	1.50	0.18	0.02	0.64	1.37	2.06	0.39	0.45	0.37	1.25

exception is the hadronization-uncertainty-induced uncertainty in m_{top}, i.e. the single largest uncertainty in the $t\bar{t} \rightarrow$ all jets measurement at $\sqrt{s} = 8$ TeV, for which the two measurements are anti-correlated. On the contrary, the $t\bar{t} \rightarrow$ lepton + jets and $t\bar{t} \rightarrow$ all jets measurements at $\sqrt{s} = 8$ TeV, shown in Fig. 7c, are positively correlated for this uncertainty. Finally, the $t\bar{t} \rightarrow$ lepton + jets measurements at the two centre-of-mass energies in Fig. 7d show a rather low correlation. The correlations per source of uncertainty and the total estimator correlations are summarized in Table 5.

The improvement in the combination obtained by the use of evaluated correlations compared with using estimator correlations assigned solely by physics assessments (here referred to as assigned correlations) is quantified using an

example. Using the choices of assigned correlations from Ref. [11] for the ATLAS results in the $t\bar{t} \rightarrow$ dilepton and $t\bar{t} \rightarrow$ lepton + jets channels at $\sqrt{s} = 7$ TeV listed in Table 4 gives a combined value of $m_{top} = 172.91 \pm 0.50\,(\text{stat}) \pm 1.05\,(\text{syst})$ GeV compared with $m_{top} = 172.99 \pm 0.48\,(\text{stat}) \pm 0.78\,(\text{syst})$ GeV. The significant improvement in the precision of the combination demonstrates the particular importance of evaluating the correlations.

For the combinations presented in this paper, most estimator correlations could be evaluated. The most prominent exception is for the b-tagging uncertainty, where the $t\bar{t} \rightarrow$ all jets measurement at $\sqrt{s} = 8$ TeV is based on a different b-tagging algorithm and calibration than the $t\bar{t} \rightarrow$ dilepton and $t\bar{t} \rightarrow$ lepton + jets measurements at $\sqrt{s} = 8$ TeV. It

was verified that assignments of the estimator correlations of $\rho_{i5k} \in [-1, 1]$, with $i = 3, 4$ and $k = 17$, yield insignificant differences in the full combination. Estimator correlations of $\rho_{i5} = 1$ are assigned for this case, as this choice gives the largest uncertainty in the combination. A similar situation arises for the data-driven all-jets background uncertainty in the two $t\bar{t} \to$ all jets measurements, where the method used for the background estimate is similar but not identical for the two measurements. Consequently, the conservative ad hoc assignment of $\rho_{25k} = 1$ was also made for this source $k = 11$.

10.3 Compatibility of the inputs and selected combinations

Before any combination is performed, the compatibility of the input results is verified. For each pair of results, their compatibility is expressed by the ratio of the squared difference between the pair of measured values and the uncertainty in this difference [98] as

$$\chi^2_{ij} = \frac{(x_i - x_j)^2}{\sigma_i^2 + \sigma_j^2 - 2\rho_{ij}\sigma_i\sigma_j}. \tag{2}$$

The corresponding values are given in Table 5. Analysing the χ^2_{ij} values reveals good χ^2 probabilities, with the smallest χ^2 probability being $P(\chi^2, 1) = 15\%$. The largest sum of χ^2_{ij} values by far is observed for the $t\bar{t} \to$ all jets result at $\sqrt{s} = 7$ TeV.

The dependences of the combined values and their uncertainties on the total correlation for pairwise combinations of results are analysed. The dependences for pairs of the three results from $\sqrt{s} = 8$ TeV data are shown in Fig. 8. The largest information gain is achieved by combining the $t\bar{t} \to$ dilepton and $t\bar{t} \to$ lepton + jets results at $\sqrt{s} = 8$ TeV, shown in Fig. 8a, b, which are anti-correlated, i.e. $\rho = -0.19$.

Based on Tables 4 and 5, selected combinations are analysed, yielding the results given in Table 6 and shown in Fig. 9. The BLUE weights and the pulls[9] of the results are given in Table 7.

To investigate the difference in precision of combined results obtained from $\sqrt{s} = 7$ and 8 TeV results, two independent combinations of the three results per centre-of-mass energy are performed. For each decay channel, the results at $\sqrt{s} = 8$ TeV are significantly more precise than those at $\sqrt{s} = 7$ TeV. In addition, the two most precise results per centre-of-mass energy are significantly less correlated at $\sqrt{s} = 8$ TeV than at $\sqrt{s} = 7$ TeV. Consequently, the size of the uncertainty of the combined result at $\sqrt{s} = 8$ TeV ($m_{\text{top}}^{8\text{TeV}}$)

---

[9] Using the individual results $x_i \pm \sigma_i$ and the combined result $x \pm \sigma_x$, the pull of result i is calculated as $(x_i - x)/\sqrt{\sigma_i^2 - \sigma_x^2}$ and should be Gaussian distributed with mean zero and width unity. The pull is a measure of the likeliness of the x_i measured in data.

is 39% smaller than the one obtained from the results at $\sqrt{s} = 7$ TeV ($m_{\text{top}}^{7\text{TeV}}$). As shown in Fig. 13a, b in Appendix B, for both centre-of-mass energies, the combination is dominated by the results in the $t\bar{t} \to$ dilepton and $t\bar{t} \to$ lepton + jets channels.

To investigate whether the measured m_{top} depends on the $t\bar{t}$ decay mode, a combination of the six results is performed in which the results in the three $t\bar{t}$ decay channels are treated as determining potentially different masses, namely $m_{\text{top}}^{\text{dilepton}}$, $m_{\text{top}}^{\ell+\text{jets}}$ and $m_{\text{top}}^{\text{all jets}}$. In such a combination, results obtained in one decay channel influence the combined result in another decay channel by means of their estimator correlation. Therefore, for each observable, e.g. $m_{\text{top}}^{\text{dilepton}}$, by construction the sum of weights of the results in the corresponding decay channel equals unity, while for each of the other decay channels the sum of weights of the results equals zero [100]. The combination yields compatible results for the three masses listed in Table 6. Consequently, the data do not show any sign of a decay-channel-dependent m_{top}. The correlation matrix of the three observables 0, 1 and 2 corresponding to $m_{\text{top}}^{\text{dilepton}}$, $m_{\text{top}}^{\ell+\text{jets}}$ and $m_{\text{top}}^{\text{all jets}}$ is

$$\rho_{m_{\text{top}}} = \begin{pmatrix} 1 & -0.14 & 0.43 \\ -0.14 & 1 & -0.05 \\ 0.43 & -0.05 & 1 \end{pmatrix},$$

and the smallest χ^2 probability of any pair of combined results for determining the same m_{top} is $P(\chi^2, 1) = 11\%$. As shown in Fig. 13c–e in Appendix B, for the combination of the three observables, the results based on $\sqrt{s} = 7$ TeV data lead to significant improvements on their more precise counterparts obtained from $\sqrt{s} = 8$ TeV data, apart from the $t\bar{t} \to$ dilepton channel.

Given that no dependence of m_{top} on the centre-of-mass energy or the $t\bar{t}$ decay channel is expected, the above examples of combinations are merely additional investigations of the compatibility of the input results. The compatibility combinations are summarized in Fig. 9 and listed in Table 6. For all combinations, the values quoted in Fig. 9 are the combined value, the statistical uncertainty, the systematic uncertainty, the total uncertainty and the statistical uncertainty in the total uncertainty.
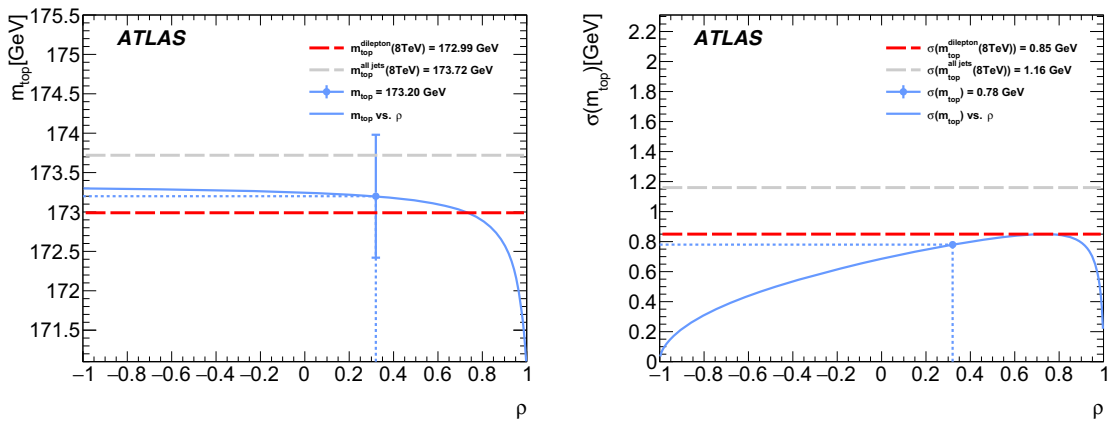
10.4 The combined result of m_{top}

The use of the statistical uncertainties in the systematic uncertainties has two main advantages. Firstly, it allows a determination of the uncertainties in the evaluation of the total correlations of the estimators, avoiding the need to perform ad hoc variations. Secondly, it enables the monitoring of the evolution of the combined result in relation to the precision in its uncertainty while including results, thereby evaluating
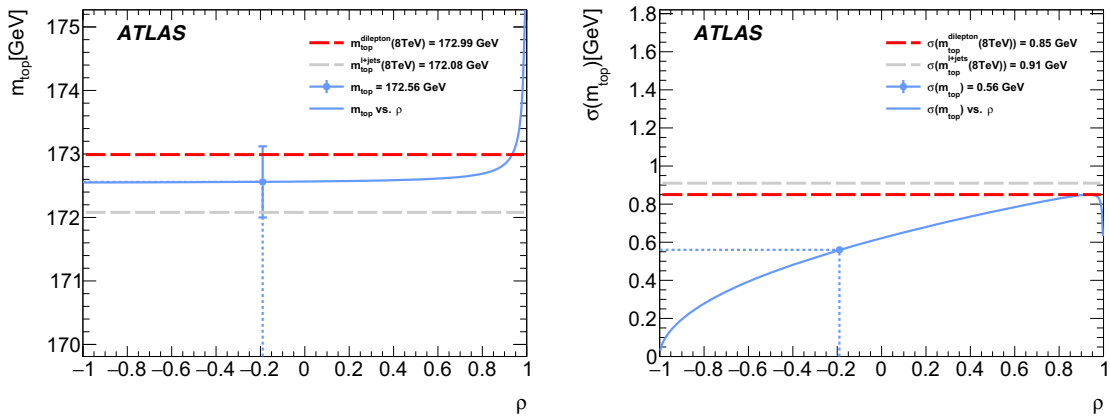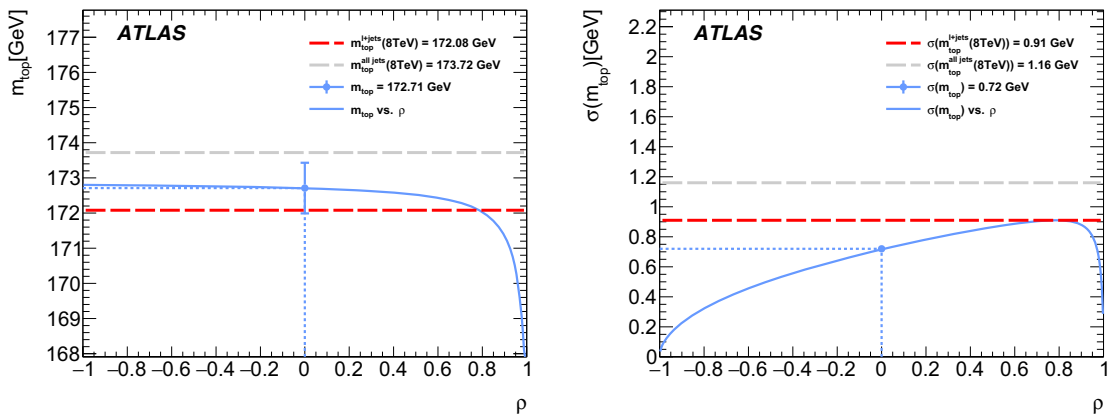
(a) $t\bar{t} \rightarrow$ dilepton (8 TeV) and $t\bar{t} \rightarrow$ lepton + jets (8 TeV)

(b) $t\bar{t} \rightarrow$ dilepton (8 TeV) and $t\bar{t} \rightarrow$ lepton + jets (8 TeV)

(c) $t\bar{t} \rightarrow$ dilepton (8 TeV) and $t\bar{t} \rightarrow$ all jets (8 TeV)

(d) $t\bar{t} \rightarrow$ dilepton (8 TeV) and $t\bar{t} \rightarrow$ all jets (8 TeV)

(e) $t\bar{t} \rightarrow$ lepton + jets (8 TeV) and $t\bar{t} \rightarrow$ all jets (8 TeV)

(f) $t\bar{t} \rightarrow$ lepton + jets (8 TeV) and $t\bar{t} \rightarrow$ all jets (8 TeV)

Fig. 8 The combined values (left) and uncertainties (right) of the combination of pairs of individual results at $\sqrt{s} = 8$ TeV, shown as functions of the total correlation ρ (solid lines). The combination of the $t\bar{t} \rightarrow$ dilepton and $t\bar{t} \rightarrow$ lepton + jets results is shown in the top row. The middle row is for the combination of the $t\bar{t} \rightarrow$ dilepton and

$t\bar{t} \rightarrow$ all jets results. Finally, the combination of the $t\bar{t} \rightarrow$ lepton + jets and $t\bar{t} \rightarrow$ all jets results is shown in the bottom row. For comparison, the corresponding values for the input results are also shown (dashed lines)

Table 6 The results for selected combinations based on the six results at $\sqrt{s}$ = 7 and 8 TeV. The left two columns of results show the combination of the three results at $\sqrt{s}$ = 7 TeV (m_{top}^{7TeV}) or at $\sqrt{s}$ = 8 TeV (m_{top}^{8TeV}), both combinations neglecting the results at the respective other centre-of-mass energy. The middle three columns show the combination of the six results as if pairs of measurements would determine a decay-specific top quark mass, namely $m_{top}^{dilepton}$, $m_{top}^{\ell+jets}$ and $m_{top}^{alljets}$. Finally, shown on the right is the combination of the three most important results in the combination denoted by $m_{top}^{(3)}$ and the combination of all results, i.e. the ATLAS result for m_{top} shown in Fig. 10. For each combination, the uncertainty is given for each source of uncertainty. Uncertainties quoted as 0.00 are smaller than 0.005, while empty cells indicate uncertainties that do not apply to the respective combination. Finally, the total systematic uncertainty and the sum in quadrature of the statistical and systematic uncertainties are given. Both are quoted including the precision at which the respective uncertainty is known

|	m_{top}^{7TeV} [GeV]	m_{top}^{8TeV} [GeV]	$m_{top}^{dilepton}$ [GeV]	$m_{top}^{\ell+jets}$ [GeV]	$m_{top}^{alljets}$ [GeV]	$m_{top}^{(3)}$ [GeV]	m_{top} [GeV]
Results	173.20	172.68	172.98	172.13	174.08	172.13	174.08
Statistics	0.46	0.26	0.39	0.37	0.56	0.27	0.25
Method	0.08	0.06	0.05	0.10	0.14	0.06	0.06
Signal Monte Carlo generator	0.17	0.13	0.12	0.15	0.03	0.14	0.12
Hadronization	0.35	0.04	0.18	0.03	0.32	0.07	0.00
Initial- and final-state QCD radiation	0.03	0.15	0.26	0.07	0.13	0.07	0.07
Underlying event	0.05	0.07	0.10	0.01	0.06	0.05	0.03
Colour reconnection	0.02	0.08	0.02	0.16	0.02	0.08	0.08
Parton distribution function	0.15	0.03	0.05	0.13	0.08	0.07	0.05
Background normalization	0.07	0.04	0.03	0.04	0.00	0.03	0.02
W/Z+jets shape	0.15	0.05	0.01	0.12	0.00	0.07	0.06
Fake leptons shape	0.03	0.03	0.07	0.02	0.00	0.03	0.03
Data-driven all-jets background	0.04	0.02	0.01	0.01	0.22		0.03
Jet energy scale	0.40	0.27	0.53	0.34	0.51	0.21	0.22
Relative b-to-light-jet energy scale	0.35	0.19	0.32	0.01	0.41	0.15	0.17
Jet energy resolution	0.04	0.10	0.09	0.16	0.07	0.10	0.09
Jet reconstruction efficiency	0.09	0.01	0.01	0.05	0.00	0.03	0.03
Jet vertex fraction	0.00	0.05	0.02	0.07	0.02	0.05	0.05
b-tagging	0.24	0.18	0.05	0.30	0.09	0.17	0.17
Leptons	0.04	0.10	0.14	0.11	0.01	0.09	0.08
Missing transverse momentum	0.08	0.03	0.01	0.07	0.01	0.04	0.04
Pile-up	0.01	0.07	0.05	0.10	0.01	0.06	0.06
All-jets trigger	0.00	0.01	0.00	0.00	0.06		0.01
Fast vs. full simulation	0.03		0.01	0.01	0.07		0.01
Total systematic uncertainty	0.76 ± 0.04	0.48 ± 0.04	0.74 ± 0.04	0.61 ± 0.04	0.80 ± 0.05	0.42 ± 0.04	0.41 ± 0.03
Total	0.89 ± 0.04	0.54 ± 0.04	0.84 ± 0.04	0.71 ± 0.04	0.98 ± 0.05	0.50 ± 0.04	0.48 ± 0.03
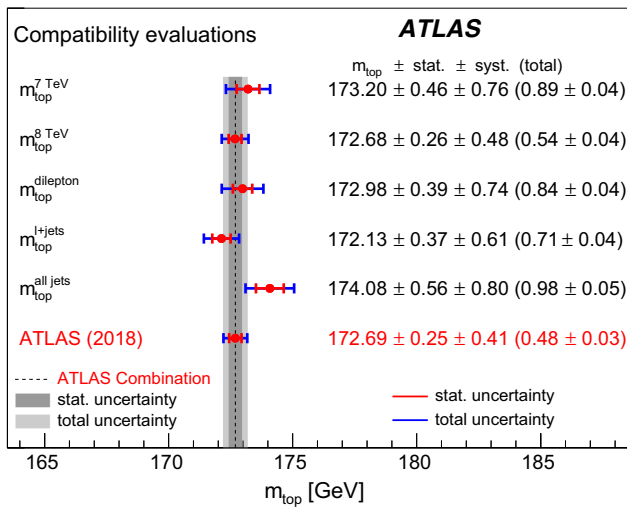
Fig. 9 The compatibility combinations performed for the six ATLAS results of m_{top}. The figure shows the combined results listed in Table 6, which are obtained from data taken at different centre-of-mass energies and for the three decay channels, in comparison to the new ATLAS result. The values quoted are the combined value, the statistical uncertainty, the systematic uncertainty, the total uncertainty and the uncertainty in the total uncertainty. The results are compared with the new ATLAS combination listed in the last line and shown as the grey vertical bands

their influence on the combination. The significance of the individual results in the combination is shown in Fig. 10. The individual results are shown in Fig. 10a. Their combination is displayed in Fig. 10b where, following Ref. [98], starting from the most precise result, i.e. the $t\bar{t} \rightarrow$ dilepton measurement at $\sqrt{s} = 8$ TeV, results are added to the combination one at a time according to their importance, and the combined result is reported. Each following line of this figure shows the combined result when adding the result listed to the input of the combination, indicated by the '+' in front of the name of

the added estimate. The last line in Fig. 10b shows the new ATLAS combined value of m_{top}.

The inclusion of the $t\bar{t} \rightarrow$ lepton + jets result at $\sqrt{s} = 8$ TeV leads to the result quoted in the second line, which improves the combined uncertainty by much more than the statistical precision in the uncertainty of the most precise result. The same is found when adding the $t\bar{t} \rightarrow$ lepton + jets result at $\sqrt{s} = 7$ TeV and comparing with the statistical uncertainty in the previous combination, albeit at a much reduced significance. The corresponding result obtained from these three results, denoted by $m_{\text{top}}^{(3)}$, is also listed in Table 6.

The improvement in the combination by applying the BDT selection to the $t\bar{t} \rightarrow$ lepton + jets analysis at $\sqrt{s} = 8$ TeV is sizeable. This is seen from repeating the combination of $m_{\text{top}}^{(3)}$ but using the result from the standard selection from Table 3. With this, the correlation of the $\sqrt{s} = 8$ TeV $t\bar{t} \rightarrow$ lepton + jets result with the $\sqrt{s} = 8$ TeV $t\bar{t} \rightarrow$ dilepton result changes from -0.19 to -0.02. The resulting uncertainty in the combination is 0.59 ± 0.05 GeV, i.e. the combination is 18% less precise than $m_{\text{top}}^{(3)}$ obtained using the result from the BDT selection. Adding the remaining results reduces the quoted combined uncertainty by 0.02 GeV, which is smaller than the statistical precision in the uncertainty of the previously achieved result of $m_{\text{top}}^{(3)}$.

The changes in statistical uncertainties in the combined value and its uncertainty due to variations of the input systematic uncertainties within their uncertainties are evaluated for two cases, namely for $m_{\text{top}}^{(3)}$ and for the combination of all results. Following Ref. [14], the distributions of the combined values and uncertainties are calculated from 500 combinations, where for each combination, the sizes of the uncertainties as well as the correlations are newly evaluated. Due to the re-evaluation of the correlation, the resulting distributions

Table 7 The BLUE weights and the pulls of the results for the combinations reported in Table 6. The upper part refers to the independent combinations of the three results per centre-of-mass energy resulting in uncorrelated results $m_{\text{top}}^{7\text{TeV}}$ and $m_{\text{top}}^{8\text{TeV}}$. The middle part is for the combination of the three observables from pairs of results per $t\bar{t}$ decay channel, resulting in correlated results $m_{\text{top}}^{\text{dilepton}}$, $m_{\text{top}}^{\ell+\text{jets}}$ and $m_{\text{top}}^{\text{all jets}}$. The lower part refers to the combination of the three most important results $m_{\text{top}}^{(3)}$ and of all results m_{top}

		$\sqrt{s} = 7$ TeV			$\sqrt{s} = 8$ TeV		
		$m_{\text{top}}^{\text{dilepton}}$	$m_{\text{top}}^{\ell+\text{jets}}$	$m_{\text{top}}^{\text{all jets}}$	$m_{\text{top}}^{\text{dilepton}}$	$m_{\text{top}}^{\ell+\text{jets}}$	$m_{\text{top}}^{\text{all jets}}$
$m_{\text{top}}^{7\text{TeV}}$	Weight	0.36	0.51	0.13			
	Pull	0.54	-0.95	1.18			
$m_{\text{top}}^{8\text{TeV}}$	Weight				0.45	0.44	0.12
	Pull				0.48	-0.82	1.02
$m_{\text{top}}^{\text{dilepton}}$	Weight	0.08	-0.04	-0.04	0.92	0.04	0.04
$m_{\text{top}}^{\ell+\text{jets}}$	Weight	-0.09	0.33	0.03	0.09	0.67	-0.03
$m_{\text{top}}^{\text{all jets}}$	Weight	-0.04	-0.01	0.30	0.04	0.01	0.71
	Pull	0.71	0.18	0.64	0.05	-0.09	-0.58
$m_{\text{top}}^{(3)}$	Weight		0.17		0.43	0.40	
	Pull		-0.16		0.70	-0.57	
m_{top}	Weight	-0.03	0.16	0.04	0.35	0.37	0.10
	Pull	0.83	-0.30	1.36	0.43	-0.79	0.98

(a) Inputs to the combination

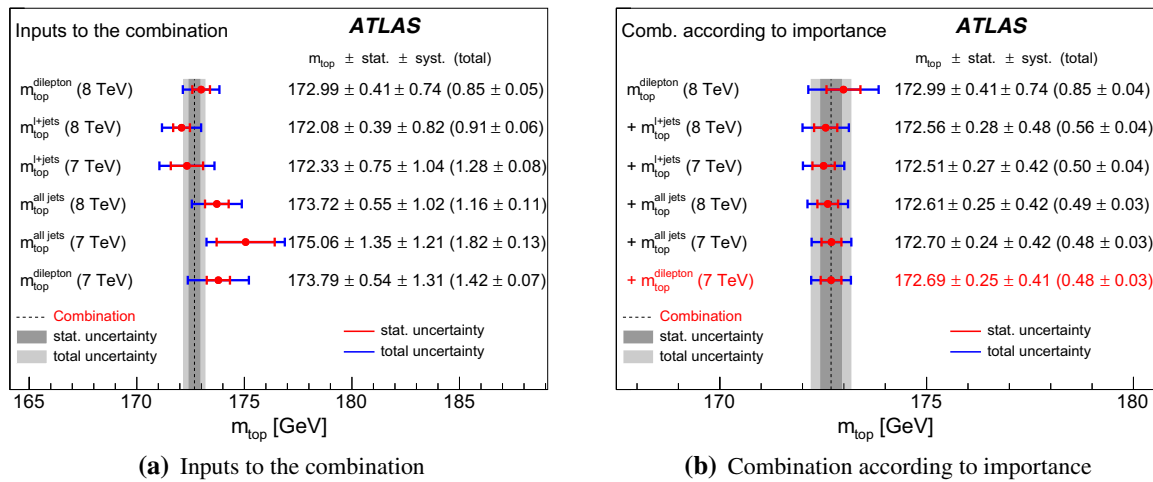**(b)** Combination according to importance

Fig. 10 The combination of the six ATLAS results of m_{top} according to importance Ref. [98]. **a** shows the inputs to the combination. **b** shows results of the combination when successively adding results to the most precise one. The values quoted are the combined value, the statistical uncertainty, the systematic uncertainty, the total uncertainty and

the uncertainty in the total uncertainty. In this figure, each line shows the combined result when adding the result listed to the combination indicated by a '+'. The new ATLAS combination is given in the last line, and shown in both figures as the vertical grey bands

are not Gaussian and are also not exactly centred around the combined value and the combined uncertainty. For $m_{top}^{(3)}$, the root mean square of the distribution of the combined value is 0.03 GeV, and that of the distribution of its uncertainty is 0.04 GeV. The corresponding values for the new ATLAS combination are 0.07 GeV and 0.03 GeV, respectively.

The full breakdown of uncertainties for the new combined ATLAS result for m_{top} is reported in the last column of Table 6. The combined result is

$$m_{top} = 172.69 \pm 0.25 \,(\text{stat}) \pm 0.41 \,(\text{syst}) \text{ GeV}$$

with a total uncertainty of 0.48 ± 0.03 GeV, where the quoted uncertainty in this uncertainty is statistical. This means that the uncertainty in this combined result is only known to this precision, which, given its size, is fully adequate.

The χ^2 probability of $m_{top}^{(3)}$ is 78%. Driven by the larger pulls of the remaining three results listed in Table 7, the χ^2 probability of 64% for the new ATLAS combination of m_{top} is lower but still good. The new ATLAS combined result of m_{top} provides a 44% improvement relative to the most precise single input result, which is the $t\bar{t} \rightarrow$ dilepton analysis at $\sqrt{s} = 8$ TeV. With a relative precision of 0.28%, it improves on the previous combination in Ref. [14] by 31% and supersedes it. As shown in Appendix B, the new ATLAS combined result of m_{top} is more precise than the results from the CDF and D0 experiments, and has a precision similar to the CMS combined result.

In Fig. 11, the 68% and 95% confidence-level contours of the indirect determination of m_W and m_{top} from the global electroweak fit in Ref. [2] are compared with the corresponding confidence-level contours of the direct ATLAS mea-
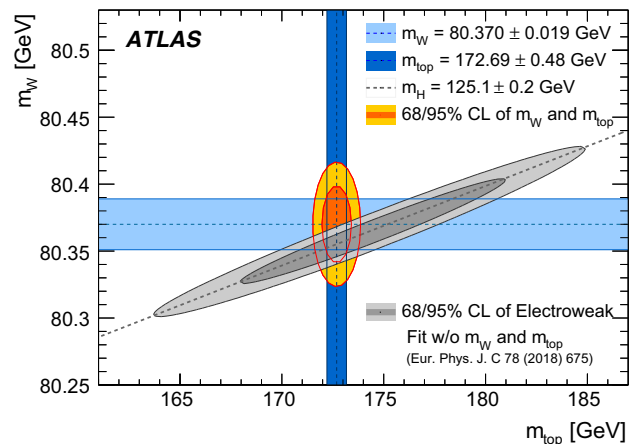

Fig. 11 Comparison of indirect determinations and direct measurements of the top quark and W boson masses. The direct ATLAS measurements of m_W and m_{top} are shown as the horizontal and vertical bands, respectively. Their 68% and 95% confidence-level (CL) contours are compared with the corresponding results from the electroweak fit

surements of the two masses. The top quark mass used in this figure was obtained above, while the W boson mass is taken from Ref. [101]. The electroweak fit uses as input the LHC combined result of the Higgs boson mass of $m_H = 125.09 \pm 0.24$ GeV from Ref. [102]. There is good agreement between the direct ATLAS mass measurements and their indirect determinations by the electroweak fit.

11 Conclusion

The top quark mass is measured via a three-dimensional template method in the $t\bar{t} \rightarrow$ lepton + jets channel and combined with previous ATLAS m_{top} measurements at the LHC.

For the $t\bar{t} \rightarrow$ lepton + jets analysis from $\sqrt{s} = 8$ TeV proton–proton collision data with an integrated luminosity of about 20.2 fb^{-1}, the event selection of the corresponding $\sqrt{s} = 7$ TeV analysis is refined. An optimization employing a BDT selection to efficiently suppress less-well-reconstructed events results in a significant reduction in total uncertainty, driven by a significant decrease in theory-modelling-induced uncertainties. With this approach, the measured value of m_{top} is

$$m_{\text{top}} = 172.08 \pm 0.39\,(\text{stat}) \pm 0.82\,(\text{syst})\text{ GeV}$$

with a total uncertainty of 0.91 ± 0.06 GeV, where the quoted uncertainty in the total uncertainty is statistical. The precision is limited by systematic uncertainties, mostly by uncertainties in the calibration of the jet energy scale, b-tagging and the Monte Carlo modelling of signal events. This result is more precise than the result from the CDF experiment, but less precise than the CMS and D0 results, measured in the same channel.

The correlations of six measurements of m_{top}, performed in the three $t\bar{t}$ decay channels from $\sqrt{s} = 7$ and 8 TeV ATLAS data, are evaluated for all sources of the systematic uncertainty. Using a dedicated mapping of uncertainty categories, combinations are performed, where measurements are added one at a time according to their importance. Treating the pairs of measurements in the three $t\bar{t}$ decay channels as determining potentially different masses, namely $m_{\text{top}}^{\text{dilepton}}, m_{\text{top}}^{\ell+\text{jets}}$ and $m_{\text{top}}^{\text{all jets}}$, yields consistent values within uncertainties, i.e. the data do not show any sign of a decay-channel-dependent m_{top}.

The combined result of m_{top} from the six measurements is

$$m_{\text{top}} = 172.69 \pm 0.25\,(\text{stat}) \pm 0.41\,(\text{syst})\text{ GeV}$$

with a total uncertainty of 0.48 ± 0.03 GeV, where the quoted uncertainty in the total uncertainty is statistical. This combination is dominated by three input measurements: the measurement in the $t\bar{t} \rightarrow$ dilepton channel from $\sqrt{s} = 8$ TeV data and the two measurements in the $t\bar{t} \rightarrow$ lepton + jets channel from $\sqrt{s} = 8$ and 7 TeV data. With a relative precision of 0.28%, this new ATLAS combination of m_{top} is more precise than the result from the CDF and D0 experiments and has a precision similar to the CMS combined result. This result supersedes the previous combined ATLAS result.

With this precision in m_{top} achieved, precise knowledge of the relation between the mass definition of the experimental analysis and the pole mass is becoming relevant. The com-

bined result is mostly limited by the uncertainties in the calibration of the jet energy scales, b-tagging and in the Monte Carlo modelling of signal events.

Data Availability Statement This manuscript has no associated data or the data will not be deposited. [Authors' comment: All ATLAS scientific output is published in journals, and preliminary results are made available in Conference Notes. All are openly available, without restriction on use by external parties beyond copyright law and the standard conditions agreed by CERN. Data associated with journal publications are also made available: tables and data from plots (e.g. cross section values, likelihood profiles, selection efficiencies, cross section limits, …) are stored in appropriate repositories such as HEPDATA (http://hepdata.cedar.ac.uk/). ATLAS also strives to make additional material related to the paper available that allows a reinterpretation of the data in the context of new theoretical models. For example, an extended encapsulation of the analysis is often provided for measurements in the framework of RIVET (http://rivet.hepforge.org/)." This information is taken from the ATLAS Data Access Policy, which is a public document that can be downloaded from http://opendata.cern.ch/record/413 [opendata.cern.ch].]

Appendix A: Results from the BDT optimization and individual sources of systematic uncertainty

This appendix has additional details of the measurement of m_{top} in the $t\bar{t} \rightarrow$ lepton + jets channel from $\sqrt{s} = 8$ TeV data discussed in the main text.

In Fig. 12, the template fit functions of the three observables are compared for the standard and the BDT event selection. The distributions of $m_{\text{top}}^{\text{reco}}$ and m_W^{reco} are narrower for the BDT event selection, which means the resolution in the two masses is improved compared with what is observed for the standard selection. The R_{bq}^{reco} distribution is slightly shifted to lower values for the BDT event selection, but the difference is small.
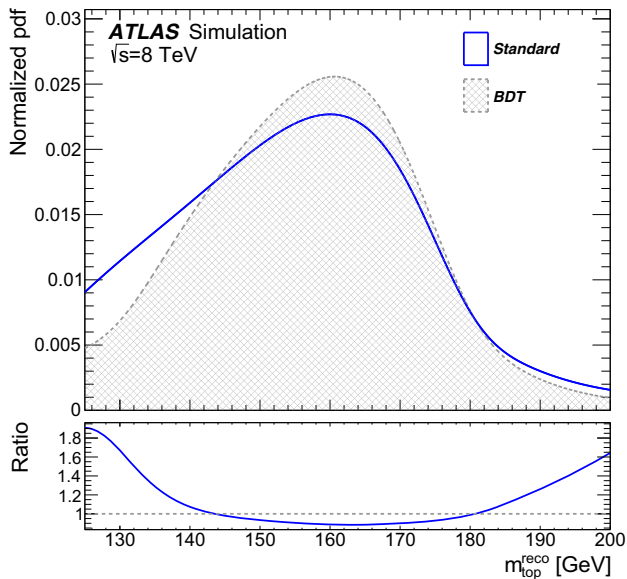
(a) Reconstructed top quark mass
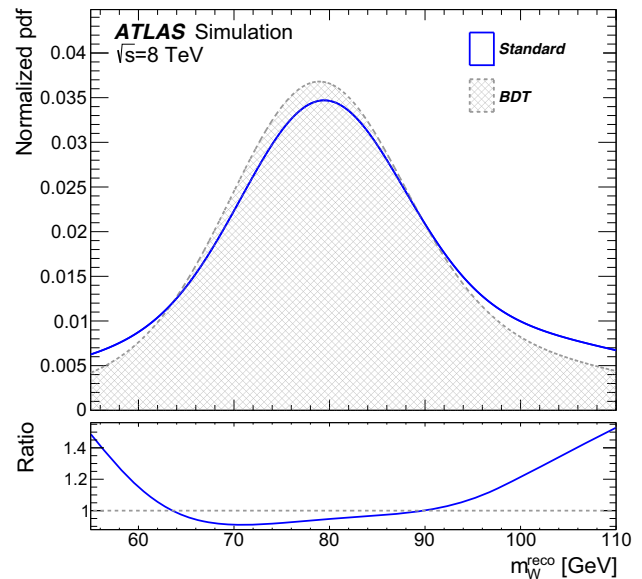
(b) Reconstructed W boson mass
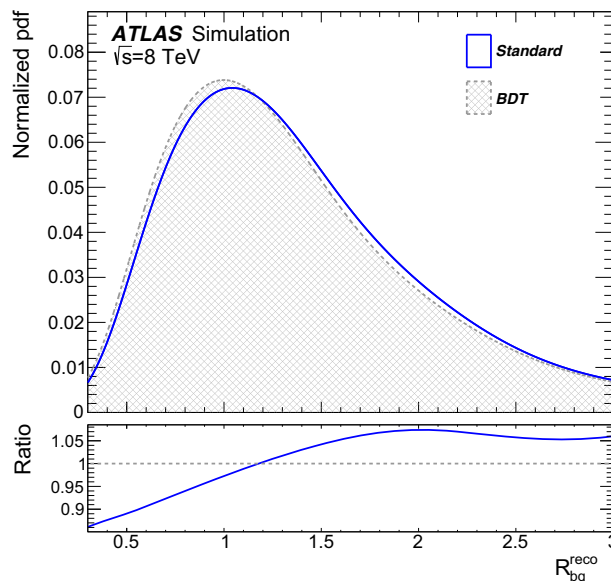
(c) Reconstructed ratio of jet transverse momenta

Fig. 12 Comparison of the template fit functions of the three observables for the standard event selection (solid line) and the BDT event selection (dashed line). The ratios (standard/BDT) of the pairs of functions are also shown. **a** shows the reconstructed top quark mass $m_{\text{top}}^{\text{reco}}$, **b** shows the reconstructed W boson mass m_W^{reco} and **c** shows the reconstructed jet-p_T ratio R_{bq}^{reco}

Table 8 The individual components of the uncertainty sources considered for the $t\bar{t} \rightarrow$ lepton + jets analysis at $\sqrt{s} = 8$ TeV for the sources of uncertainty not documented in Tables 9, 10, 11 and 12. The uncertainties together with their statistical precisions are listed in boldface and given with 0.01 GeV precision. The uncertainty per source is calculated as the sum in quadrature of the subcomponents. Uncertainties quoted as 0.00 (0.000) are smaller than 0.005 (0.0005)

Uncertainty	$\Delta m_{\text{top}}^{\text{up}}$ [GeV]	$\Delta m_{\text{top}}^{\text{dw}}$ [GeV]	Δm_{top} [GeV]
Signal Monte Carlo generator			**0.16 ± 0.17**
Powheg- Box - MC@NLO (Herwig)			-0.161 ± 0.168
Hadronization			**0.15 ± 0.10**
Powheg+Pythia - Powheg+Herwig			$+0.146 \pm 0.098$
Initial- and final-state QCD radiation			**0.08 ± 0.11**
Less I/FSR - more I/FSR	$+0.086$	-0.075	$+0.080 \pm 0.111$
Underlying event			**0.08 ± 0.15**
P2012 - P2012 mpiHi			-0.080 ± 0.153
Colour reconnection			**0.19 ± 0.15**
P2012 - P2012 loCR			$+0.191 \pm 0.154$
Background normalization			**0.08 ± 0.00**
Z+jets norm.	$+0.007$	-0.015	$+0.011 \pm 0.000$
W+jets norm.	-0.017	-0.061	-0.061 ± 0.000
Fake lepton norm.			$+0.046 \pm 0.000$
W/Z+jets shape			**0.11 ± 0.00**
W+jets HF0	-0.001	-0.070	-0.070 ± 0.000
W+jets HF1	-0.005	-0.087	-0.087 ± 0.000
Jet reconstruction efficiency			**0.02 ± 0.01**
Nominal - 0.23% drop			$+0.022 \pm 0.013$
Jet vertex fraction			**0.09 ± 0.01**
	$+0.077$	-0.112	0.095 ± 0.009
Leptons			**0.16 ± 0.01**
Electron energy scale	$+0.025$	-0.006	$+0.016 \pm 0.006$
Electron energy resolution	-0.152	-0.145	-0.152 ± 0.013
Muon resolution (muon spectrometer)			$+0.027 \pm 0.000$
Muon resolution (inner detector)			$+0.023 \pm 0.000$
Muon scale	-0.013	$+0.015$	-0.014 ± 0.000
Lepton trigger SF	-0.005	-0.003	-0.005 ± 0.001
Lepton identification SF	$+0.005$	-0.011	$+0.008 \pm 0.001$
Lepton reconstruction SF	$+0.003$	-0.008	$+0.005 \pm 0.000$
Missing transverse momentum($E_{\text{T}}^{\text{miss}}$)			**0.05 ± 0.01**
$E_{\text{T}}^{\text{miss}}$ (resolution soft term)	$+0.003$	$+0.012$	$+0.012 \pm 0.018$
$E_{\text{T}}^{\text{miss}}$ (scale soft term)	$+0.054$	-0.039	$+0.047 \pm 0.009$

For the BDT selection, a number of systematic uncertainties listed in Table 3 are calculated by performing pseudo-experiments for more than one systematic variation. The individual components are given in Tables 8, 9, 10, 11 and 12 below. Whenever the uncertainty is obtained from just a pair of samples, the shift Δm_{top} is listed together with the definition of the difference evaluated indicating the direction of the shift. For the other cases, the shift in m_{top} is quoted relative to the value measured in the central sample for the upward variation ($\Delta m_{\text{top}}^{\text{up}}$), the downward variation ($\Delta m_{\text{top}}^{\text{dw}}$) and the final shift assigned to this uncertainty component (Δm_{top}). For most of the cases the signs of $\Delta m_{\text{top}}^{\text{up}}$ and $\Delta m_{\text{top}}^{\text{dw}}$ are different, indicating that m_{top} from the central sample is sur-

rounded by the values from the two variations. In this case $|\Delta m_{\text{top}}|$ is $0.5 \cdot |\Delta m_{\text{top}}^{\text{up}} - \Delta m_{\text{top}}^{\text{dw}}|$, otherwise it is the maximum of $|\Delta m_{\text{top}}^{\text{up}}|$ and $|\Delta m_{\text{top}}^{\text{dw}}|$. In both cases, the sign of Δm_{top} is the one from $\Delta m_{\text{top}}^{\text{up}}$.

Appendix B: Additional information about the various combinations

This appendix gives additional information about the various combinations discussed in the main text. For all combinations the values quoted are the combined value, the statistical uncertainty, the systematic uncertainty, the total uncertainty

Table 9 The individual components of the PDF uncertainty considered for the $t\bar{t} \rightarrow$ lepton + jets analysis at $\sqrt{s} = 8$ TeV, the resulting PDF-uncertainty-induced shifts in m_{top} and the final uncertainty in m_{top}. The components [31,39,42] together with their statistical precisions are listed in boldface. The total uncertainty in the CT10 variations is calculated as the sum in quadrature of the CT10 subcomponents. The total uncertainty is given with 0.01 GeV precision. Uncertainties quoted as 0.00 (0.000) are smaller than 0.005 (0.0005). The term *nuisance parameter* is denoted by *NuP*. The last line refers to the sum in quadrature of the PDF subcomponents

PDF uncertainty components	Δm_{top} [GeV]
CT10 variations	**0.09 ± 0.00**
CT10 NuP2 - NuP1	-0.001 ± 0.000
CT10 NuP4 - NuP3	$+0.000 \pm 0.000$
CT10 NuP6 - NuP5	$+0.015 \pm 0.000$
CT10 NuP8 - NuP7	$+0.005 \pm 0.003$
CT10 NuP10 - NuP9	$+0.004 \pm 0.000$
CT10 NuP12 - NuP11	$+0.002 \pm 0.000$
CT10 NuP14 - NuP13	-0.026 ± 0.001
CT10 NuP16 - NuP15	-0.004 ± 0.000
CT10 NuP18 - NuP17	-0.015 ± 0.001
CT10 NuP20 - NuP19	$+0.013 \pm 0.001$
CT10 NuP22 - NuP21	$+0.006 \pm 0.001$
CT10 NuP24 - NuP23	$+0.063 \pm 0.001$
CT10 NuP26 - NuP25	$+0.000 \pm 0.001$
CT10 NuP28 - NuP27	$+0.009 \pm 0.000$
CT10 NuP30 - NuP29	-0.004 ± 0.000
CT10 NuP32 - NuP31	$+0.007 \pm 0.001$
CT10 NuP34 - NuP33	$+0.019 \pm 0.002$
CT10 NuP36 - NuP35	-0.011 ± 0.001
CT10 NuP38 - NuP37	-0.001 ± 0.000
CT10 NuP40 - NuP39	-0.001 ± 0.001
CT10 NuP42 - NuP41	-0.005 ± 0.001
CT10 NuP44 - NuP43	-0.003 ± 0.000
CT10 NuP46 - NuP45	-0.002 ± 0.000
CT10 NuP48 - NuP47	$+0.027 \pm 0.000$
CT10 NuP50 - NuP49	$+0.002 \pm 0.000$
CT10 NuP52 - NuP51	-0.003 ± 0.001
NNPDF - CT10	**-0.034 ± 0.001**
MSTW - CT10	**-0.024 ± 0.002**
Total	0.09 ± 0.00

and the uncertainty in the total uncertainty, which is statistical.

Figure 13a, b shows the independent combinations per centre-of-mass energy. For both centre-of-mass energies, the combination is dominated by the results in the $t\bar{t} \rightarrow$ dilepton and $t\bar{t} \rightarrow$ lepton + jets channels. Using only those in the combinations yields combined results of $m_{\text{top}}^{7\text{TeV}} = 172.99 \pm 0.48\,(\text{stat}) \pm 0.78\,(\text{syst})$ GeV with an uncertainty of 0.91 ± 0.05 GeV at $\sqrt{s} = 7$ TeV and $m_{\text{top}}^{8\text{TeV}} = 172.56 \pm 0.28\,(\text{stat}) \pm 0.48\,(\text{syst})$ GeV with an uncertainty of 0.56 ± 0.04 GeV at $\sqrt{s} = 8$ TeV. At both centre-of-mass energies, the difference between the combined uncertainties of the partial and full combination is much smaller than the respective statistical precision in the total systematic uncertainties. This statistical precision is obtained from varying each systematic uncertainty within its statistical precision and repeating the combination, as explained in the main text.

Figure 13c–e shows the dependent combinations per $t\bar{t}$ decay channel. The combined result of $m_{\text{top}}^{\text{dilepton}}$ based only on the $t\bar{t} \rightarrow$ dilepton measurement from $\sqrt{s} = 8$ TeV data and the measurements in the other decay channels is $m_{\text{top}}^{\text{dilepton}} = 172.94 \pm 0.41\,(\text{stat}) \pm 0.73\,(\text{syst})$ GeV with an uncertainty of 0.84 ± 0.05 GeV. As a consequence of the influence of the measurements in the other decay channels discussed in the main text, this result does not coincide with the $t\bar{t} \rightarrow$ dilepton result at $\sqrt{s} = 8$ TeV.

In Fig. 14, the most precise ATLAS results of m_{top} per decay channel and the new ATLAS combined value of m_{top} are compared with the respective results from the CDF, D0 and CMS experiments.

Table 10 The individual components of the JES uncertainty considered for the $t\bar{t} \to$ lepton + jets analysis at $\sqrt{s} = 8$ TeV, the resulting JES- and bJES-uncertainty-induced shifts in m_{top} and the final uncertainty in m_{top}. The components [63] together with their statistical precisions are listed in boldface and, wherever applicable, calculated as the sum in quadrature of the respective subcomponents. A shift listed as '0' means that the corresponding variation resulted in an unchanged event sample. Uncertainties quoted as 0.00 (0.000) are smaller than 0.005 (0.0005). In the rightmost column, the mapping to the uncertainty components used for $\sqrt{s} = 7$ TeV data is given for the weak and the strong correlation scenarios. The '+' sign indicates corresponding components at the two centre-of-mass energies for the weak and strong scenario, while the '(+)' sign indicates components that only correspond for the strong scenario. Finally, mentioning a name indicates that the mapped sources carry different names at $\sqrt{s} = 7$ and 8 TeV. The uncertainty components and the total uncertainty are given with 0.01 GeV precision. The term *nuisance parameter* is denoted by *NuP*. The last line refers to the sum in quadrature of the JES components

JES uncertainty components	$\Delta m_{\text{top}}^{\text{up}}$ [GeV]	$\Delta m_{\text{top}}^{\text{dw}}$ [GeV]	Δm_{top} [GeV]	Map to $\sqrt{s} = 7$ TeV
Statistical (total)			**0.17 ± 0.01**	
Statistical NuP1	−0.159	+0.151	−0.155 ± 0.013	
Statistical NuP2	−0.008	+0.048	−0.028 ± 0.006	
Statistical NuP3	+0.063	−0.035	+0.049 ± 0.009	
Statistical NuP4	+0.020	+0.022	+0.022 ± 0.018	
η inter-calibration (stat.)	−0.062	+0.020	−0.041 ± 0.011	
Modelling (total)			**0.38 ± 0.02**	
Modelling NuP1	−0.372	+0.389	−0.380 ± 0.020	(+)
Modelling NuP2	+0.029	−0.000	+0.014 ± 0.006	(+)
Modelling NuP3	+0.010	+0.005	+0.010 ± 0.018	(+)
Modelling NuP4	+0.034	−0.026	+0.030 ± 0.006	(+)
η inter-calibration (model)	+0.056	−0.038	+0.047 ± 0.013	+
Detector (total)			**0.11 ± 0.01**	
Detector NuP1	+0.116	−0.103	+0.110 ± 0.011	+
Detector NuP2	−0.015	+0.017	−0.016 ± 0.009	
Detector NuP3	+0.015	−0.014	+0.015 ± 0.006	(+) Detector NuP2
Mixed (total)			**0.09 ± 0.01**	
Mixed NuP1	−0.004	−0.029	−0.029 ± 0.022	(+)
Mixed NuP2	+0.053	−0.054	+0.054 ± 0.009	
Mixed NuP3	−0.044	+0.061	−0.052 ± 0.009	
Mixed NuP4	+0.039	−0.016	+0.028 ± 0.006	(+) Mixed NuP2
Single particle high-$\mathbf{p}_T$			**0.01 ± 0.00**	
Single particle high-$\mathbf{p}_T$	0	+0.005	+0.005 ± 0.000	
Pile-up (total)			**0.18 ± 0.02**	
Pile-up: offset (μ)	+0.041	−0.040	+0.041 ± 0.011	+
Pile-up: offset (n_{vtx})	+0.065	−0.083	+0.074 ± 0.017	+
Pile-up: p_T	+0.042	+0.040	+0.042 ± 0.018	
Pile-up: ρ	−0.173	+0.141	−0.157 ± 0.017	
Punch-through			**0.02 ± 0.01**	
Punch-through	+0.013	+0.017	+0.017 ± 0.013	
Flavour (total)			**0.24 ± 0.02**	
Flavour composition	+0.079	−0.119	+0.099 ± 0.000	+
Flavour response	+0.220	−0.211	+0.215 ± 0.018	+
bJES			**0.03 ± 0.01**	+
bJES	+0.006	−0.047	+0.026 ± 0.013	+
Total (without bJES)			0.54 ± 0.02	

Table 11 The individual components of the JER uncertainty considered for the $t\bar{t} \rightarrow$ lepton + jets analysis at $\sqrt{s} = 8$ TeV, the resulting JER-uncertainty-induced shifts in m_{top} and the final uncertainty in m_{top}. The *data versus simulation difference* and *noise forward region* components are quoted as the difference from the nominal sample. The total uncertainty is calculated as the sum in quadrature of the subcomponents and given with 0.01 GeV precision. The term *nuisance parameter* is denoted by *NuP*

JER uncertainty components	$\Delta m_{\text{top}}^{\text{up}}$ [GeV]	$\Delta m_{\text{top}}^{\text{dw}}$ [GeV]	Δm_{top} [GeV]
JER data versus simulation difference			-0.034 ± 0.018
JER noise forward region			$+0.032 \pm 0.013$
JER NuP1 (only down var.)			-0.111 ± 0.052
JER NuP2	-0.034	$+0.055$	-0.044 ± 0.018
JER NuP3	$+0.025$	-0.084	$+0.054 \pm 0.024$
JER NuP4	-0.074	$+0.090$	-0.082 ± 0.021
JER NuP5	$+0.078$	$+0.016$	$+0.078 \pm 0.037$
JER NuP6	-0.041	$+0.017$	-0.029 ± 0.019
JER NuP7	-0.039	$+0.076$	-0.057 ± 0.016
JER NuP8	-0.053	-0.013	-0.053 ± 0.029
JER NuP9 (only up var.)			$+0.036 \pm 0.018$
Total			0.20 ± 0.04

Table 12 The individual components of the flavour-tagging uncertainty considered for the $t\bar{t} \rightarrow$ lepton + jets analysis at $\sqrt{s} = 8$ TeV, the resulting shifts in m_{top} and the final b-tagging-uncertainty-induced uncertainty in m_{top}. The uncertainty components together with their statistical precisions are listed in boldface and calculated as the sum in quadrature of the respective subcomponents. The uncertainty components and the total uncertainty are given with 0.01 GeV precision. Uncertainties quoted as 0.00 (0.000) are smaller than 0.005 (0.0005). The term *nuisance parameter* is denoted by *NuP*. The last line refers to the sum in quadrature of the components

Flavour-tagging uncertainty components	$\Delta m_{\text{top}}^{\text{up}}$ [GeV]	$\Delta m_{\text{top}}^{\text{dw}}$ [GeV]	Δm_{top} [GeV]
b-tagging scale factor variations			**0.31 ± 0.00**
b-tagging NuP1	$+0.051$	-0.062	$+0.057 \pm 0.000$
b-tagging NuP2	-0.230	$+0.143$	-0.187 ± 0.000
b-tagging NuP3	-0.090	$+0.005$	-0.047 ± 0.001
b-tagging NuP4	$+0.090$	-0.175	$+0.132 \pm 0.000$
b-tagging NuP5	-0.230	$+0.148$	-0.189 ± 0.000
b-tagging NuP6	$+0.023$	-0.105	$+0.064 \pm 0.001$
c/τ-tagging scale factor variations			**0.15 ± 0.00**
c/τ-tagging NuP1	$+0.098$	-0.102	$+0.100 \pm 0.000$
c/τ-tagging NuP2	-0.057	-0.026	-0.057 ± 0.000
c/τ-tagging NuP3	$+0.046$	-0.125	$+0.085 \pm 0.000$
c/τ-tagging NuP4	-0.057	-0.023	-0.057 ± 0.000
Mistagging scale factor variations			**0.16 ± 0.00**
Mistagging NuP1	-0.005	$+0.003$	-0.004 ± 0.000
Mistagging NuP2	-0.042	-0.039	-0.042 ± 0.000
Mistagging NuP3	-0.038	-0.036	-0.038 ± 0.000
Mistagging NuP4	-0.032	-0.040	-0.040 ± 0.000
Mistagging NuP5	-0.037	-0.044	-0.044 ± 0.000
Mistagging NuP6	-0.036	-0.045	-0.045 ± 0.000
Mistagging NuP7	-0.034	-0.040	-0.040 ± 0.000
Mistagging NuP8	-0.041	-0.040	-0.041 ± 0.000
Mistagging NuP9	-0.029	-0.045	-0.045 ± 0.000
Mistagging NuP10	-0.073	-0.001	-0.073 ± 0.000
Mistagging NuP11	-0.026	-0.055	-0.055 ± 0.000
Mistagging NuP12	$+0.007$	-0.095	$+0.051 \pm 0.000$
Total			0.38 ± 0.00

(a) $\sqrt{s} = 7$ TeV

(b) $\sqrt{s} = 8$ TeV

(c) $t\bar{t} \to$ dilepton channel

(d) $t\bar{t} \to$ lepton + jets channel

(e) $t\bar{t} \to$ all jets channel
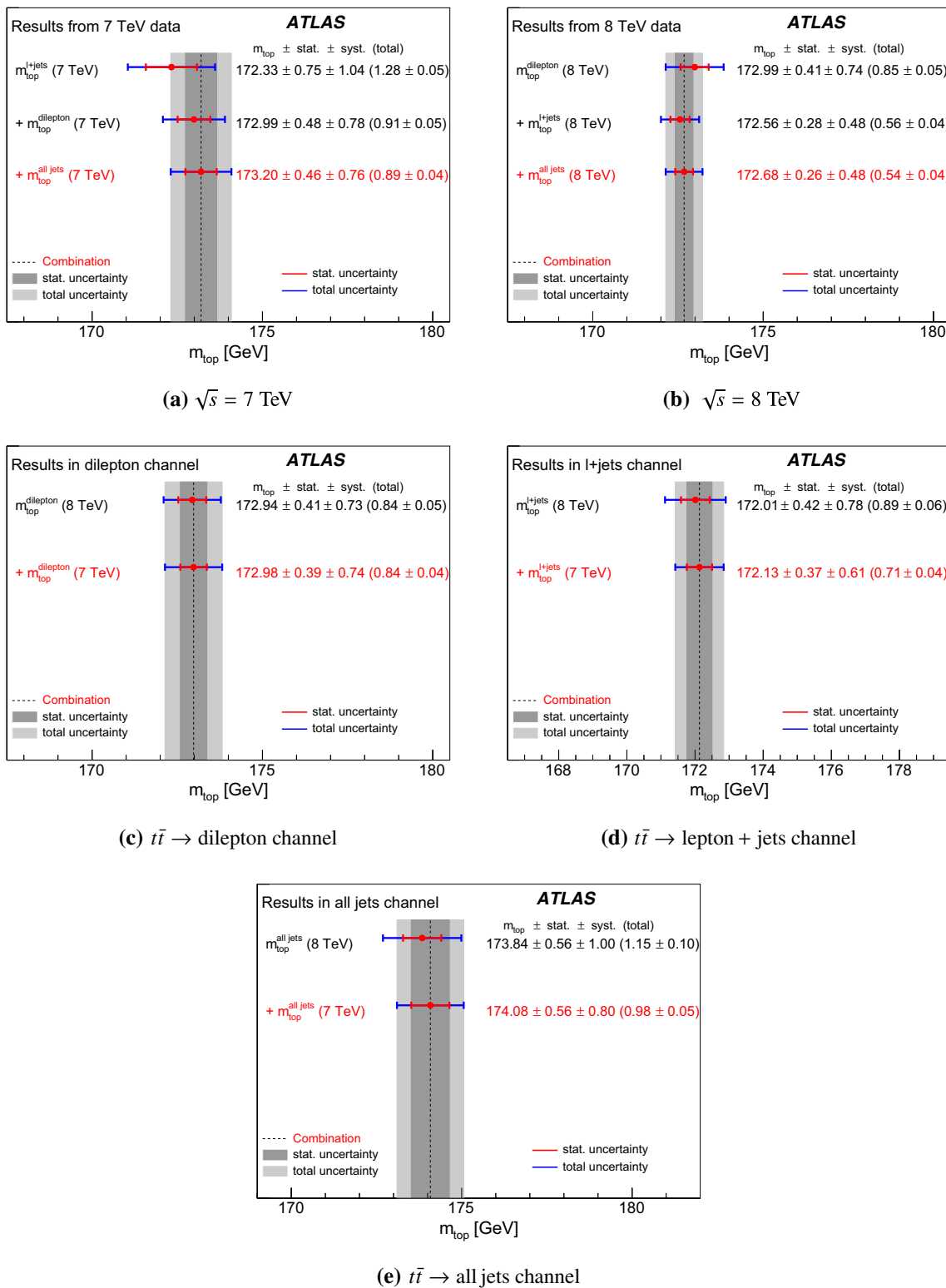
Fig. 13 Selected combinations of the six ATLAS measurements of m_{top} according to importance. The figures show the combined result when successively adding results to the most precise one of a given category. Each line of this figure shows the combined result when adding the result listed to the combination, indicated by a '+'. The values quoted are the combined value, the statistical uncertainty, the systematic uncer-tainty, the total uncertainty and the uncertainty in the total uncertainty, which is statistical. **a** and **b** refer to the independent combinations of the three measurements per centre-of-mass energy resulting in uncor-related results $m_{\text{top}}^{\text{7TeV}}$ and $m_{\text{top}}^{\text{8TeV}}$. **c–e** refer to the combination of the three correlated observables from pairs of measurements per $t\bar{t}$ decay channel, resulting in $m_{\text{top}}^{\text{dilepton}}$, $m_{\text{top}}^{\ell+\text{jets}}$ and $m_{\text{top}}^{\text{all jets}}$

(a) $t\bar{t} \to$ dilepton channel

(b) $t\bar{t} \to$ lepton + jets channel

(c) $t\bar{t} \to$ all jets channel

(d) Combinations

Fig. 14 The most precise result of $m_{\rm top}$ per experiment in the different $t\bar{t}$ decay channels and $m_{\rm top}$ from the latest combinations performed by the individual experiments. **a** shows the measurements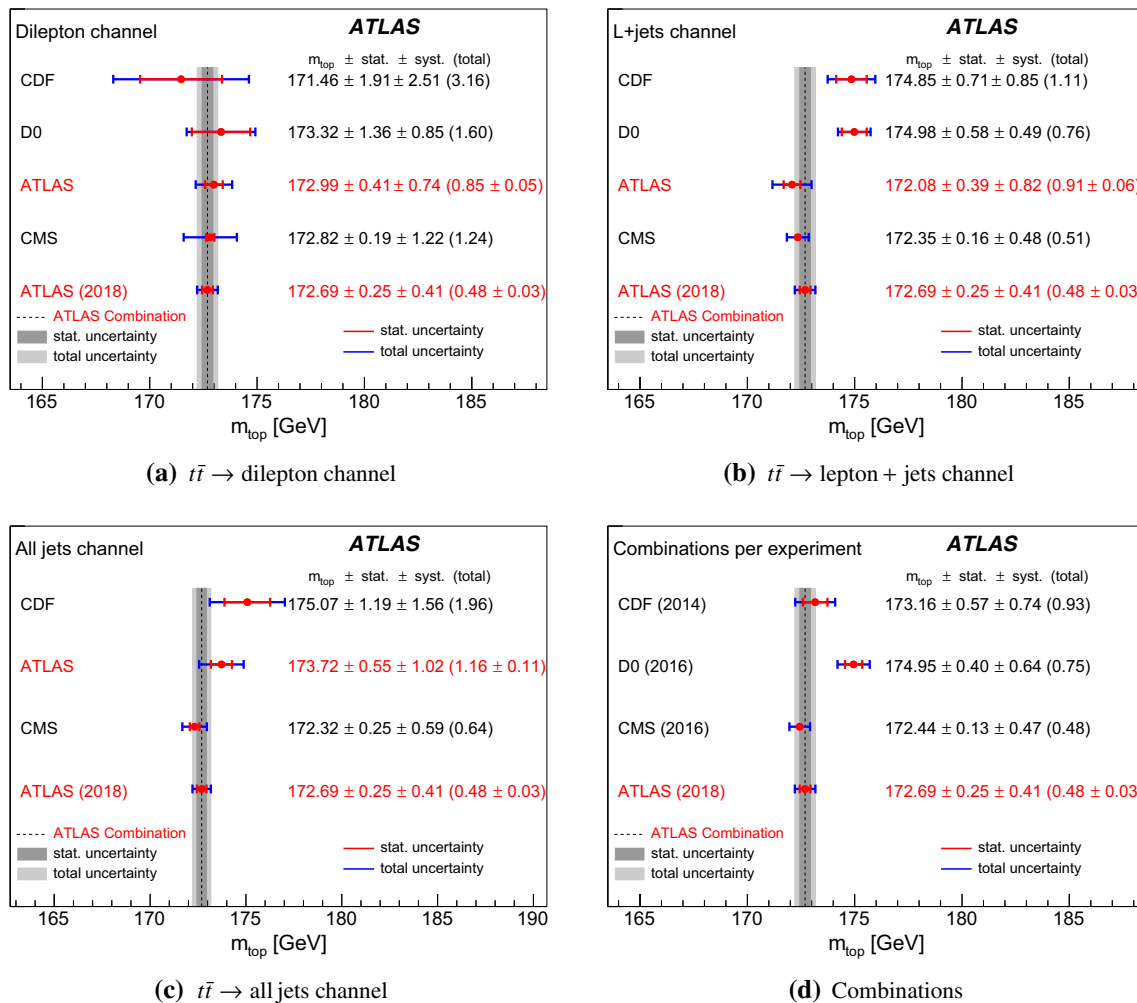 in the $t\bar{t} \to$ dilepton channel, **b** shows those in the $t\bar{t} \to$ lepton + jets and **c** shows the ones in the $t\bar{t} \to$ all jets channel. **d** shows the results of $m_{\rm top}$ from the latest combination per experiment. In all figures the vertical band corresponds to the new ATLAS combined value of $m_{\rm top}$. The values quoted are the combined value, the statistical uncertainty, the

systematic uncertainty, the total uncertainty and for ATLAS results also the uncertainty in the total uncertainty, which is statistical. For CDF, the separation into statistical and systematic uncertainties is different for the result in the $t\bar{t} \to$ lepton + jets channel and the combination. For the former, the statistical component caused by the in situ determination of the jet scale factor is included in the statistical uncertainty, while for the latter, this uncertainty is part of the systematic uncertainty

References

1. ALEPH, CDF, D0, DELPHI, L3, OPAL, SLD Collaborations, The LEP Electroweak Working Group, The Tevatron Electroweak Working Group and The SLD Electroweak and Heavy Flavour Groups, Precision electroweak measurements and constraints on the Standard Model (2010). arXiv: 1012.2367 [hep-ex]
2. M. Baak et al., The global electroweak fit at NNLO and prospects for the LHC and ILC. Eur. Phys. J. C **74**, 3046 (2014). arXiv:1407.3792
3. Particle Data Group, Review of particle physics. Chin. Phys. C **38**, 090001 (2014)
4. G. Degrassi et al., Higgs mass and vacuum stability in the Standard Model at NNLO. JHEP **08**, 98 (2012). arXiv:1205.6497 [hep-ph]
5. F. Bezrukov, M. Shaposhnikov, The Standard Model Higgs boson as the inflaton. Phys. Lett. B **659**, 703 (2008). arXiv:0710.3755 [hep-th]
6. A. De Simone, M.P. Hertzberg, F. Wilczek, Running inflation in the Standard Model. Phys. Lett. B **678**, 1 (2009). arXiv:0812.4946 [hep-ph]
7. CDF Collaboration, Precision top-quark mass measurement at CDF. Phys. Rev. Lett. **109**, 152003 (2012). arXiv:1207.6758 [hep-ex]
8. D0 Collaboration, Precision measurement of the top quark mass in lepton+jets final states. Phys. Rev. Lett. **113**, 032002 (2014). arXiv:1405.1756 [hep-ex]
9. ATLAS Collaboration, Measurement of the top quark mass in the $t\bar{t} \to$ lepton+jets and $t\bar{t} \to$ dilepton channels using $\sqrt{s} = 7$ TeV ATLAS data. Eur. Phys. J. C **75** 330, (2015). arXiv:1503.05427 [hep-ex]

10. CMS Collaboration, Measurement of the top quark mass using proton–proton data at $\sqrt{s} =$ 7 and 8 TeV. Phys. Rev. D **93**, 072004 (2016). arXiv:1509.04044 [hep-ex]

11. ATLAS, CDF, CMS and D0 Collaborations, First combination of Tevatron and LHC measurements of the top-quark mass (2014). arXiv:1403.4427 [hep-ex]

12. CDF Collaboration, Final combination of the CDF results on top-quark mass. CDF note 11080 (2014). https://www-cdf.fnal.gov/physics/new/top/2014/CDFTopCombo

13. D0 Collaboration, Combination of D0 measurements of the top quark mass. Phys. Rev. D **95**, 112004 (2017). arXiv:1703.06994 [hep-ex]

14. ATLAS Collaboration, Measurement of the top quark mass in the $t\bar{t}$ dilepton channel from $\sqrt{s} =$ 8 TeV ATLAS data. Phys. Lett. B **761** 350, (2016). arXiv:1606.02179 [hep-ex]

15. A. Buckley et al., General-purpose event generators for LHC physics. Phys. Rep. **504**, 145 (2011). arXiv:1101.2599 [hep-ph]

16. S. Moch et al., High precision fundamental constants at the TeV scale (2014). arXiv:1405.4781 [hep-ph]

17. M. Butenschoen et al., Top quark mass calibration for Monte Carlo event generators. Phys. Rev. Lett. **117**, 232001 (2016). arXiv:1608.01318 [hep-ph]

18. A.H. Hoang, S. Plätzer, D. Samitz, On the cutoff dependence of the quark mass parameter in angular ordered parton showers. JHEP **1810**, 200 (2018). arXiv:1807.06617 [hep-ph]

19. S. Ravasio, T. Jezo, P. Nason, C. Oleari, A theoretical study of top-mass measurements at the LHC using NLO+PS generators of increasing accuracy. Eur. Phys. J. C **78**, 458 (2018). arXiv:1801.03944

20. ATLAS Collaboration, The ATLAS experiment at the CERN large hadron collider. JINST **3** S08003 (2008)

21. ATLAS Collaboration, Luminosity determination in pp collisions at $\sqrt{s} =$ 8 TeV using the ATLAS detector at the LHC. Eur. Phys. J. C **76** 653, (2016). arXiv:1608.03953 [hep-ex]

22. P. Nason, A new method for combining NLO QCD with shower Monte Carlo algorithms. JHEP **11**, 040 (2004). arXiv:hep-ph/0409146

23. S. Frixione, P. Nason, C. Oleari, Matching NLO QCD computations with parton shower simulations: the POWHEG method. JHEP **11**, 070 (2007). arXiv:0709.2092 [hep-ph]

24. S. Alioli, P. Nason, C. Oleari, E. Re, A general framework for implementing NLO calculations in shower Monte Carlo programs: the POWHEG BOX. JHEP **06**, 043 (2010). arXiv:1002.2581 [hep-ph]

25. S. Frixione, P. Nason, G. Ridolfi, A positive-weight next-to-leading-order Monte Carlo for heavy flavour hadroproduction. JHEP **09**, 126 (2007). arXiv:0707.3088 [hep-ph]

26. S. Alioli, P. Nason, C. Oleari, E. Re, NLO single-top production matched with shower in POWHEG: s- and t-channel contributions. JHEP **09**, 111 (2009). arXiv: 0907.4076 [hep-ph] [Erratum: JHEP **02**, 011 (2010)]

27. E. Re, Single-top Wt-channel production matched with parton showers using the POWHEG method. Eur. Phys. J. C **71**, 1547 (2011). arXiv:1009.2450 [hep-ph]

28. H.-L. Lai et al., New parton distributions for collider physics. Phys. Rev. D **82**, 074024 (2010). arXiv:1007.2241 [hep-ph]

29. T. Sjöstrand, S. Mrenna, P.Z. Skands, PYTHIA 6.4 physics and manual. JHEP **05**, 026 (2006). arXiv:hep-ph/0603175

30. P.Z. Skands, Tuning Monte Carlo generators: the Perugia tunes. Phys. Rev. D **82**, 74018 (2010). arXiv:1005.3457 [hep-ph]

31. J. Pumplin et al., New generation of parton distributions with uncertainties from global QCD analysis. JHEP **07**, 012 (2002). arXiv:hep-ph/0201195

32. M. Cacciari, M. Czakon, M. Mangano, A. Mitov, P. Nason, Top-pair production at hadron colliders with next-to-next-to-leading

33. P. Bärnreuther, M. Czakon, A. Mitov, Percent-level-precision physics at the Tevatron: next-to-next-leading order QCD corrections to $q\bar{q} \rightarrow t\bar{t} +$ X. Phys. Rev. Lett. **109**, 132001 (2012). arXiv:1204.5201 [hep-ph]

34. M. Czakon, A. Mitov, NNLO corrections to top-pair production at hadron colliders: the all-fermionic scattering channels. JHEP **12**, 054 (2012). arXiv:1207.0236 [hep-ph]

35. M. Czakon, A. Mitov, NNLO corrections to top pair production at hadron colliders: the quark–gluon reaction. JHEP **01**, 080 (2013). arXiv:1210.6832 [hep-ph]

36. M. Czakon, P. Fiedler, A. Mitov, The total top-quark pair-production cross section at hadron colliders through $O(\alpha_s^4)$. Phys. Rev. Lett. **110**, 252004 (2013). arXiv:1303.6254 [hep-ph]

37. M. Czakon, A. Mitov, Top++: a program for the calculation of the top-pair cross-section at hadron colliders. Comput. Phys. Commun. **185**, 2930 (2014). arXiv:1112.5675 [hep-ph]

38. M. Botje et al., The PDF4LHC working group interim recommendations (2011). arXiv:1101.0538 [hep-ph]

39. A.D. Martin, W.J. Stirling, R.S. Thorne, G. Watt, Parton distributions for the LHC. Eur. Phys. J. C **63**, 189 (2009). arXiv:0901.0002 [hep-ph]

40. A.D. Martin, W.J. Stirling, R.S. Thorne, G. Watt, Uncertainties on α_s in global PDF analyses and implications for predicted hadronic cross sections. Eur. Phys. J. C **64**, 653 (2009). arXiv:0905.3531 [hep-ph]

41. J. Gao et al., CT10 next-to-next-to-leading order global analysis of QCD. Phys. Rev. D **89**, 033009 (2014). arXiv:1302.6246 [hep-ph]

42. R.D. Ball et al., Parton distributions with LHC data. Nucl. Phys. B **867**, 244 (2013). arXiv:1207.1303 [hep-ph]

43. N. Kidonakis, Next-to-next-to-leading-order collinear and soft gluon corrections for t-channel single top quark production. Phys. Rev. D **83**, 091503 (2011). arXiv:1103.2792 [hep-ph]

44. N. Kidonakis, Two-loop soft anomalous dimensions for single top quark associated production with a W⁻ or H⁻. Phys. Rev. D **82**, 054018 (2010). arXiv:1005.4451 [hep-ph]

45. N. Kidonakis, Next-to-next-to leading logarithm resummation for s-channel single top quark production. Phys. Rev. D **81**, 054028 (2010). arXiv:1001.5034 [hep-ph]

46. M.L. Mangano, M. Moretti, F. Piccinini, R. Pittau, A.D. Polosa, ALPGEN, a generator for hard multiparton processes in hadronic collisions. JHEP **07**, 001 (2003). arXiv:hep-ph/0206293

47. ATLAS Collaboration, New ATLAS event generator tunes to 2010 data. ATL-PHYS-PUB-2011-008 (2011). https://cds.cern.ch/record/1345343

48. K. Melnikov, F. Petriello, Electroweak gauge boson production at hadron colliders through $O(\alpha_s^2)$. Phys. Rev. D **74**, 114017 (2006). arXiv:hep-ph/0609070

49. G. Corcella et al., HERWIG 6: an event generator for hadron emission reactions with interfering gluons (including supersymmetric processes). JHEP **01**, 010 (2001). arXiv:hep-ph/0011363

50. J.M. Butterworth, J.R. Forshaw, M.H. Seymour, Multiparton interactions in photoproduction at HERA. Z. Phys. C **72**, 637 (1996). arXiv:hep-ph/9601371

51. J.M. Campbell, R.K. Ellis, Update on vector boson pair production at hadron colliders. Phys. Rev. D **60**, 113006 (1999). arXiv:hep-ph/9905386

52. T. Sjöstrand, S. Mrenna, P.Z. Skands, A brief introduction to PYTHIA 8.1. Comput. Phys. Commun. **178**, 852 (2008). arXiv:0710.3820 [hep-ph]

53. ATLAS Collaboration, Summary of ATLAS Pythia 8 tunes. ATL-PHYS-PUB-2012-003 (2012). https://cds.cern.ch/record/1474107

54. ATLAS Collaboration, The ATLAS simulation infrastructure. Eur. Phys. J. C **70**, 823 (2010). arXiv:1005.4568 [physics.ins-det]

55. S. Agostinelli et al., GEANT4: a simulation toolkit. Nucl. Instrum. Methods A **506**, 250 (2003)
56. ATLAS Collaboration, The simulation principle and performance of the ATLAS fast calorimeter simulation FastCaloSim. ATL-PHYS-PUB-2010-013 (2010). https://cds.cern.ch/record/1300517
57. ATLAS Collaboration, Electron efficiency measurements with the ATLAS detector using 2012 LHC proton–proton collision data. Eur. Phys. J. C **77**, 195 (2017). arXiv:1612.01456 [hep-ex]
58. ATLAS Collaboration, Measurement of the muon reconstruction performance of the ATLAS detector using 2011 and 2012 LHC proton–proton collision data. Eur. Phys. J. C **74**, 3130 (2014). arXiv:1407.3935 [hep-ex]
59. K. Rehermann, B. Tweedie, Efficient identification of boosted semileptonic top quarks at the LHC. JHEP **03**, 059 (2011). arXiv:1007.2221 [hep-ph]
60. ATLAS Collaboration, Topological cell clustering in the ATLAS calorimeters and its performance in LHC Run 1. Eur. Phys. J. C **77**, 490 (2017). arXiv:1603.02934 [hep-ex]
61. M. Cacciari, G.P. Salam, G. Soyez, The anti-kt jet clustering algorithm. JHEP **04**, 063 (2008). arXiv:0802.1189 [hep-ph]
62. ATLAS Collaboration, Jet energy measurement with the ATLAS detector in proton–proton collisions at $\sqrt{s} = 7$ TeV. Eur. Phys. J. C **73**, 2304 (2013). arXiv:1112.6426 [hep-ex]
63. ATLAS Collaboration, Jet energy measurement and its systematic uncertainty in proton–proton collisions at $\sqrt{s} = 7$ TeV with the ATLAS detector. Eur. Phys. J. C **75**, 17 (2015). arXiv:1406.0076 [hep-ex]
64. ATLAS Collaboration, Monte Carlo calibration and combination of in-situ measurements of jet energy scale, jet energy resolution and jet mass in ATLAS. ATLAS-CONF-2015-037 (2015). https://cds.cern.ch/record/2044941
65. ATLAS Collaboration, Performance of pile-up mitigation techniques for jets in pp collisions at $\sqrt{s} = 8$ TeV using the ATLAS detector. Eur. Phys. J. C **76**, 581 (2016). arXiv:1510.03823 [hep-ex]
66. ATLAS Collaboration, Performance of b-jet identification in the ATLAS experiment. JINST **11**, P04008 (2016). arXiv:1512.01094 [hep-ex]
67. ATLAS Collaboration, Calibration of b-tagging using dileptonic top pair events in a combinatorial likelihood approach with the ATLAS experiment. ATLAS-CONF-2014-004 (2014). https://cds.cern.ch/record/1664335
68. ATLAS Collaboration, Calibration of the performance of b-tagging for c and light-flavour jets in the 2012 ATLAS data. ATLAS-CONF-2014-046 (2014). https://cds.cern.ch/record/1741020
69. ATLAS Collaboration, Performance of algorithms that reconstruct missing transverse momentum in $\sqrt{s} = 8$ TeV proton–proton collisions in the ATLAS detector. Eur. Phys. J. C **77**, 241 (2017). arXiv:1609.09324 [hep-ex]
70. ATLAS Collaboration, Estimation of non-prompt and fake lepton backgrounds in final states with top quarks produced in proton–proton collisions at $\sqrt{s} = 8$ TeV with the ATLAS detector. ATLAS-CONF-2014-058 (2014). https://cds.cern.ch/record/1951336
71. ATLAS Collaboration, Measurement of the top quark-pair production cross section with ATLAS in pp collisions at $\sqrt{s}$ 7 TeV. Eur. Phys. J. C **71**, 1577 (2011). arXiv:1012.1792 [hep-ex]
72. ATLAS Collaboration, Measurement of the charge asymmetry in top quark pair production in pp collisions at $\sqrt{s} = 7$ TeV using the ATLAS detector. Eur. Phys. J. C **72**, 2039 (2012). arXiv:1203.4211 [hep-ex]
73. ATLAS Collaboration, A search for tt resonances using lepton-plus-jets events in proton–proton collisions at $\sqrt{s} = 8$ TeV with the ATLAS detector. JHEP **08**, 148 (2015). arXiv:1505.07018 [hep-ex]
74. ATLAS Collaboration, Top-quark mass measurement in the all-hadronic $t\bar{t}$ decay channel at $\sqrt{s} = 8$ TeV with the ATLAS detector. JHEP **09**, 118 (2017). arXiv:1702.07546 [hep-ex]
75. F.A. Berends, H. Kuijf, B. Tausk, W.T. Giele, On the production of a W and jets at hadron colliders. Nucl. Phys. B **357**, 32 (1991)
76. J. Erdmann et al., A likelihood-based reconstruction algorithm for top-quark pairs and the KLFitter framework. Nucl. Instrum. Methods A **748**, 18 (2014). arXiv:1312.5595 [hep-ex]
77. ATLAS Collaboration, Measurement of the top quark mass with the template method in the $t\bar{t} \rightarrow$ lepton + jets channel using ATLAS data. Eur. Phys. J. C **72**, 2046 (2012). arXiv:1203.5755 [hep-ex]
78. ATLAS Collaboration, Measurements of top-quark pair differential cross-sections in the lepton+jets channel in pp collisions at $\sqrt{s} = 8$ TeV using the ATLAS detector. Eur. Phys. J. C **76**, 538 (2016). arXiv:1511.04716 [hep-ex]
79. A. Höcker et al., TMVA—toolkit for multivariate data analysis (2007). arXiv:physics/0703039
80. R. Barlow, SLUO lectures on statistics and numerical methods in HEP, lecture 6: resampling and the bootstrap (2000). http://www-group.slac.stanford.edu/sluo/Lectures/stat_lecture_files/sluolec6.pdf
81. R. Barlow, Systematic errors: facts and fictions (2002). arXiv:hep-ex/0207026
82. S. Frixione, B.R. Webber, Matching NLO QCD computations and parton shower simulations. JHEP **06**, 029 (2002). arXiv:hep-ph/0204244
83. S. Frixione, P. Nason, B.R. Webber, Matching NLO QCD and parton showers in heavy flavour production. JHEP **08**, 007 (2003). arXiv:hep-ph/0305252
84. B. Andersson, G. Gustafson, G. Ingelman, T. Sjöstrand, Parton fragmentation and string dynamics. Phys. Rep. **97**, 31 (1983)
85. B. Andersson, *The Lund model* (Cambridge University Press, Cambridge, 1997). ISBN:9780521017343
86. B. Webber, A QCD model for jet fragmentation including soft gluon interference. Nucl. Phys. B **238**, 492 (1984)
87. ATLAS Collaboration, Impact of fragmentation modelling on the jet energy and the top-quark mass measurement using the ATLAS detector. ATL-PHYS-PUB-2015-042 (2015). https://cds.cern.ch/record/2054420
88. ATLAS Collaboration, Measurement of $t\bar{t}$ production with a veto on additional central jet activity in pp collisions at $\sqrt{s} = 7$ TeV using the ATLAS detector. Eur. Phys. J. C **72**, 2043 (2012). arXiv:1203.5015 [hep-ex]
89. ATLAS Collaboration, Measurement of the $t\bar{t}$ production cross-section as a function of jet multiplicity and jet transverse momentum in 7 TeV proton–proton collisions with the ATLAS detector. JHEP **01**, 020 (2015). arXiv:1407.0891 [hep-ex]
90. ATLAS Collaboration, Comparison of Monte Carlo generator predictions to ATLAS measurements of top pair production at 7 TeV. ATL-PHYS-PUB-2015-002 (2015). https://cds.cern.ch/record/1981319
91. ATLAS Collaboration, Comparison of Monte Carlo generator predictions for gap fraction and jet multiplicity observables in $t\bar{t}$ events. ATL-PHYS-PUB-2014-005 (2014). https://cds.cern.ch/record/1703034
92. H.L. Lai et al., Global QCD analysis of parton structure of the nucleon: CTEQ5 parton distributions. Eur. Phys. J. C **12**, 375 (2000). arXiv:hep-ph/9903282
93. ATLAS Collaboration, Determination of the jet energy scale and resolution at ATLAS using Z/γ-jet events in data at $\sqrt{s} = 8$ TeV. ATLAS-CONF-2015-057 (2015). https://cds.cern.ch/record/2059846

94. ATLAS Collaboration, Data-driven determination of the energy scale and resolution of jets reconstructed in the ATLAS calorimeters using dijet and multijet events at $\sqrt{s}$ = 8 TeV. ATLAS-CONF-2015-017 (2015). https://cds.cern.ch/record/2008678
95. ATLAS Collaboration, Electron and photon energy calibration with the ATLAS detector using LHC Run 1 data. Eur. Phys. J. C **74**, 3071 (2014). arXiv:1407.5063 [hep-ex]
96. ATLAS Collaboration, Measurement of the top-quark mass in the fully hadronic decay channel from ATLAS data at $\sqrt{s}$ = 7 TeV. Eur. Phys. J. C **75**, 158 (2015). arXiv:1409.0832 [hep-ex]
97. L. Lyons et al., How to combine correlated estimates of a single physical quantity. Nucl. Instrum. Methods A **270**, 110 (1988)
98. R. Nisius, On the combination of correlated estimates of a physics observable. Eur. Phys. J. C **74**, 3004 (2014). arXiv:1402.4016 [physics.data-an]
99. R. Nisius, A ROOT class to combine a number of correlated estimates of one or more observables using the Best Linear Unbiased Estimate method (2015). http://blue.hepforge.org/Bluemanual.pdf
100. A. Valassi, Combining correlated measurements of several different physical quantities. Nucl. Instrum. Methods A **500**, 391 (2003)
101. ATLAS Collaboration, Measurement of the W-boson mass in pp collisions at $\sqrt{s}$ = 7 TeV with the ATLAS detector. Eur. Phys. J. C **78** 110 (2018). arXiv:1701.07240 [hep-ex]
102. ATLAS and CMS Collaborations, Combined measurement of the Higgs boson mass in pp collisions at $\sqrt{s}$ = 7 and 8 TeV with the ATLAS and CMS experiments. Phys. Rev. Lett. **114**, 191803 (2015). arXiv:1503.07589 [hep-ex]
103. ATLAS Collaboration, ATLAS computing acknowledgements. ATL-GEN-PUB-2016-002. https://cds.cern.ch/record/2202407

ATLAS Collaboration

M. Aaboud[34d], G. Aad[99], B. Abbott[124], O. Abdinov[13,*], B. Abeloos[128], D. K. Abhayasinghe[91], S. H. Abidi[164], O. S. AbouZeid[39], N. L. Abraham[153], H. Abramowicz[158], H. Abreu[157], Y. Abulaiti[6], B. S. Acharya[64a,64b,o], S. Adachi[160], L. Adam[97], L. Adamczyk[81a], J. Adelman[119], M. Adersberger[112], A. Adiguzel[12c,ag], T. Adye[141], A. A. Affolder[143], Y. Afik[157], C. Agheorghiesei[27c], J. A. Aguilar-Saavedra[136a,136f], F. Ahmadov[77,ae], G. Aielli[71a,71b], S. Akatsuka[83], T. P. A. Åkesson[94], E. Akilli[52], A. V. Akimov[108], G. L. Alberghi[23a,23b], J. Albert[173], P. Albicocco[49], M. J. Alconada Verzini[86], S. Alderweireldt[117], M. Aleksa[35], I. N. Aleksandrov[77], C. Alexa[27b], T. Alexopoulos[10], M. Alhroob[124], B. Ali[138], G. Alimonti[66a], J. Alison[36], S. P. Alkire[145], C. Allaire[128], B. M. M. Allbrooke[153], B. W. Allen[127], P. P. Allport[21], A. Aloisio[67a,67b], A. Alonso[39], F. Alonso[86], C. Alpigiani[145], A. A. Alshehri[55], M. I. Alstaty[99], B. Alvarez Gonzalez[35], D. Álvarez Piqueras[171], M. G. Alviggi[67a,67b], B. T. Amadio[18], Y. Amaral Coutinho[78b], A. Ambler[101], L. Ambroz[131], C. Amelung[26], D. Amidei[103], S. P. Amor Dos Santos[136a,136c], S. Amoroso[44], C. S. Amrouche[52], F. An[76], C. Anastopoulos[146], L. S. Ancu[52], N. Andari[142], T. Andeen[11], C. F. Anders[59b], J. K. Anders[20], K. J. Anderson[36], A. Andreazza[66a,66b], V. Andrei[59a], C. R. Anelli[173], S. Angelidakis[37], I. Angelozzi[118], A. Angerami[38], A. V. Anisenkov[120a,120b], A. Annovi[69a], C. Antel[59a], M. T. Anthony[146], M. Antonelli[49], D. J. A. Antrim[168], F. Anulli[70a], M. Aoki[79], J. A. Aparisi Pozo[171], L. Aperio Bella[35], G. Arabidze[104], J. P. Araque[136a], V. Araujo Ferraz[78b], R. Araujo Pereira[78b], A. T. H. Arce[47], R. E. Ardell[91], F. A. Arduh[86], J-F. Arguin[107], S. Argyropoulos[75], A. J. Armbruster[35], L. J. Armitage[90], A Armstrong[168], O. Arnaez[164], H. Arnold[118], M. Arratia[31], O. Arslan[24], A. Artamonov[109,*], G. Artoni[131], S. Artz[97], S. Asai[160], N. Asbah[57], E. M. Asimakopoulou[169], L. Asquith[153], K. Assamagan[29], R. Astalos[28a], R. J. Atkin[32a], M. Atkinson[170], N. B. Atlay[148], K. Augsten[138], G. Avolio[35], R. Avramidou[58a], M. K. Ayoub[15a], A. M. Azoulay[165b], G. Azuelos[107,as], A. E. Baas[59a], M. J. Baca[21], H. Bachacou[142], K. Bachas[65a,65b], M. Backes[131], P. Bagnaia[70a,70b], M. Bahmani[82], H. Bahrasemani[149], A. J. Bailey[171], J. T. Baines[141], M. Bajic[39], C. Bakalis[10], O. K. Baker[180], P. J. Bakker[118], D. Bakshi Gupta[8], S. Balaji[154], E. M. Baldin[120a,120b], P. Balek[177], F. Balli[142], W. K. Balunas[133], J. Balz[97], E. Banas[82], A. Bandyopadhyay[24], S. Banerjee[178,k], A. A. Bannoura[179], L. Barak[158], W. M. Barbe[37], E. L. Barberio[102], D. Barberis[53a,53b], M. Barbero[99], T. Barillari[113], M-S. Barisits[35], J. Barkeloo[127], T. Barklow[150], R. Barnea[157], S. L. Barnes[58c], B. M. Barnett[141], R. M. Barnett[18], Z. Barnovska-Blenessy[58a], A. Baroncelli[72a], G. Barone[29], A. J. Barr[131], L. Barranco Navarro[171], F. Barreiro[96], J. Barreiro Guimarães da Costa[15a], R. Bartoldus[150], A. E. Barton[87], P. Bartos[28a], A. Basalaev[134], A. Bassalat[128], R. L. Bates[55], S. J. Batista[164], S. Batlamous[34e], J. R. Batley[31], M. Battaglia[143], M. Bauce[70a,70b], F. Bauer[142], K. T. Bauer[168], H. S. Bawa[150,m], J. B. Beacham[122], T. Beau[132], P. H. Beauchemin[167], P. Bechtle[24], H. C. Beck[51], H. P. Beck[20,r], K. Becker[50], M. Becker[97], C. Becot[44], A. Beddall[12d], A. J. Beddall[12a], V. A. Bednyakov[77], M. Bedognetti[118], C. P. Bee[152], T. A. Beermann[74], M. Begalli[78b], M. Begel[29], A. Behera[152], J. K. Behr[44], A. S. Bell[92], G. Bella[158], L. Bellagamba[23b], A. Bellerive[33], M. Bellomo[157], P. Bellos[9], K. Belotskiy[110], N. L. Belyaev[110], O. Benary[158,*], D. Benchekroun[34a], M. Bender[112], N. Benekos[10], Y. Benhammou[158], E. Benhar Noccioli[180], J. Benitez[75], D. P. Benjamin[47], M. Benoit[52], J. R. Bensinger[26], S. Bentvelsen[118], L. Beresford[131], M. Beretta[49], D. Berge[44], E. Bergeaas Kuutmann[169], N. Berger[5], L. J. Bergsten[26], J. Beringer[18], S. Berlendis[7], N. R. Bernard[100], G. Bernardi[132], C. Bernius[150], F. U. Bernlochner[24], T. Berry[91], P. Berta[97], C. Bertella[15a], G. Bertoli[43a,43b], I. A. Bertram[87], G. J. Besjes[39], O. Bessidskaia Bylund[179], M. Bessner[44], N. Besson[142], A. Bethani[98], S. Bethke[113], A. Betti[24], A. J. Bevan[90], J. Beyer[113], R. Bi[135], R. M. Bianchi[135], O. Biebel[112], D. Biedermann[19],

R. Bielski[35], K. Bierwagen[97], N. V. Biesuz[69a,69b], M. Biglietti[72a], T. R. V. Billoud[107], M. Bindi[51], A. Bingul[12d], C. Bini[70a,70b], S. Biondi[23a,23b], M. Birman[177], T. Bisanz[51], J. P. Biswal[158], C. Bittrich[46], D. M. Bjergaard[47], J. E. Black[150], K. M. Black[25], T. Blazek[28a], I. Bloch[44], C. Blocker[26], A. Blue[55], U. Blumenschein[90], Dr. Blunier[144a], G. J. Bobbink[118], V. S. Bobrovnikov[120a,120b], S. S. Bocchetta[94], A. Bocci[47], D. Boerner[179], D. Bogavac[112], A. G. Bogdanchikov[120a,120b], C. Bohm[43a], V. Boisvert[91], P. Bokan[169], T. Bold[81a], A. S. Boldyrev[111], A. E. Bolz[59b], M. Bomben[132], M. Bona[90], J. S. Bonilla[127], M. Boonekamp[142], A. Borisov[140], G. Borissov[87], J. Bortfeldt[35], D. Bortoletto[131], V. Bortolotto[71a,71b], D. Boscherini[23b], M. Bosman[14], J. D. Bossio Sola[30], K. Bouaouda[34a], J. Boudreau[135], E. V. Bouhova-Thacker[87], D. Boumediene[37], C. Bourdarios[128], S. K. Boutle[55], A. Boveia[122], J. Boyd[35], D. Boye[32b], I. R. Boyko[77], A. J. Bozson[91], J. Bracinik[21], N. Brahimi[99], A. Brandt[8], G. Brandt[179], O. Brandt[59a], F. Braren[44], U. Bratzler[161], B. Brau[100], J. E. Brau[127], W. D. Breaden Madden[55], K. Brendlinger[44], L. Brenner[44], R. Brenner[169], S. Bressler[177], B. Brickwedde[97], D. L. Briglin[21], D. Britton[55], D. Britzger[113], I. Brock[24], R. Brock[104], G. Brooijmans[38], T. Brooks[91], W. K. Brooks[144b], E. Brost[119], J. H Broughton[21], P. A. Bruckman de Renstrom[82], D. Bruncko[28b], A. Bruni[23b], G. Bruni[23b], L. S. Bruni[118], S. Bruno[71a,71b], B.H. Brunt[31], M. Bruschi[23b], N. Bruscino[135], P. Bryant[36], L. Bryngemark[44], T. Buanes[17], Q. Buat[35], P. Buchholz[148], A. G. Buckley[55], I. A. Budagov[77], M. K. Bugge[130], F. Bührer[50], O. Bulekov[110], D. Bullock[8], T. J. Burch[119], S. Burdin[88], C. D. Burgard[118], A. M. Burger[5], B. Burghgrave[119], K. Burka[82], S. Burke[141], I. Burmeister[45], J. T. P. Burr[131], V. Büscher[97], E. Buschmann[51], P. Bussey[55], J. M. Butler[25], C. M. Buttar[55], J. M. Butterworth[92], P. Butti[35], W. Buttinger[35], A. Buzatu[155], A. R. Buzykaev[120a,120b], G. Cabras[23a,23b], S. Cabrera Urbán[171], D. Caforio[138], H. Cai[170], V. M. M. Cairo[2], O. Cakir[4a], N. Calace[52], P. Calafiura[18], A. Calandri[99], G. Calderini[132], P. Calfayan[63], G. Callea[55], L. P. Caloba[78b], S. Calvente Lopez[96], D. Calvet[37], S. Calvet[37], T. P. Calvet[152], M. Calvetti[69a,69b], R. Camacho Toro[132], S. Camarda[35], D. Camarero Munoz[96], P. Camarri[71a,71b], D. Cameron[130], R. Caminal Armadans[100], C. Camincher[35], S. Campana[35], M. Campanelli[92], A. Camplani[39], A. Campoverde[148], V. Canale[67a,67b], M. Cano Bret[58c], J. Cantero[125], T. Cao[158], Y. Cao[170], M. D. M. Capeans Garrido[35], I. Caprini[27b], M. Caprini[27b], M. Capua[40a,40b], R. M. Carbone[38], R. Cardarelli[71a], F. C. Cardillo[146], I. Carli[139], T. Carli[35], G. Carlino[67a], B. T. Carlson[135], L. Carminati[66a,66b], R. M. D. Carney[43a,43b], S. Caron[117], E. Carquin[144b], S. Carrá[66a,66b], G. D. Carrillo-Montoya[35], D. Casadei[32b], M. P. Casado[14,g], A. F. Casha[164], D. W. Casper[168], R. Castelijn[118], F. L. Castillo[171], V. Castillo Gimenez[171], N. F. Castro[136a,136e], A. Catinaccio[35], J. R. Catmore[130], A. Cattai[35], J. Caudron[24], V. Cavaliere[29], E. Cavallaro[14], D. Cavalli[66a], M. Cavalli-Sforza[14], V. Cavasinni[69a,69b], E. Celebi[12b], F. Ceradini[72a,72b], L. Cerda Alberich[171], A. S. Cerqueira[78a], A. Cerri[153], L. Cerrito[71a,71b], F. Cerutti[18], A. Cervelli[23a,23b], S. A. Cetin[12b], A. Chafaq[34a], D Chakraborty[119], S. K. Chan[57], W. S. Chan[118], Y. L. Chan[61a], J. D. Chapman[31], B. Chargeishvili[156b], D. G. Charlton[21], C. C. Chau[33], C. A. Chavez Barajas[153], S. Che[122], A. Chegwidden[104], S. Chekanov[6], S. V. Chekulaev[165a], G. A. Chelkov[77,ar], M. A. Chelstowska[35], C. Chen[58a], C. H. Chen[76], H. Chen[29], J. Chen[58a], J. Chen[38], S. Chen[133], S. J. Chen[15c], X. Chen[15b,aq], Y. Chen[80], Y-H. Chen[44], H. C. Cheng[103], H. J. Cheng[15d], A. Cheplakov[77], E. Cheremushkina[140], R. Cherkaoui El Moursli[34e], E. Cheu[7], K. Cheung[62], T. J. A. Chevalérias[142], L. Chevalier[142], V. Chiarella[49], G. Chiarelli[69a], G. Chiodini[65a], A. S. Chisholm[35,21], A. Chitan[27b], I. Chiu[160], Y. H. Chiu[173], M. V. Chizhov[77], K. Choi[63], A. R. Chomont[128], S. Chouridou[159], Y. S. Chow[118], V. Christodoulou[92], M. C. Chu[61a], J. Chudoba[137], A. J. Chuinard[101], J. J. Chwastowski[82], L. Chytka[126], D. Cinca[45], V. Cindro[89], I. A. Cioară[24], A. Ciocio[18], F. Cirotto[67a,67b], Z. H. Citron[177], M. Citterio[66a], A. Clark[52], M. R. Clark[38], P. J. Clark[48], C. Clement[43a,43b], Y. Coadou[99], M. Cobal[64a,64c], A. Coccaro[53a,53b], J. Cochran[76], H. Cohen[158], A. E. C. Coimbra[177], L. Colasurdo[117], B. Cole[38], A. P. Colijn[118], J. Collot[56], P. Conde Muiño[136a,136b], E. Coniavitis[50], S. H. Connell[32b], I. A. Connelly[98], S. Constantinescu[27b], F. Conventi[67a,at], A. M. Cooper-Sarkar[131], F. Cormier[172], K. J. R. Cormier[164], L. D. Corpe[92], M. Corradi[70a,70b], E. E. Corrigan[94], F. Corriveau[101,ac], A. Cortes-Gonzalez[35], M. J. Costa[171], F. Costanza[5], D. Costanzo[146], G. Cottin[31], G. Cowan[91], B. E. Cox[98], J. Crane[98], K. Cranmer[121], S. J. Crawley[55], R. A. Creager[133], G. Cree[33], S. Crépé-Renaudin[56], F. Crescioli[132], M. Cristinziani[24], V. Croft[121], G. Crosetti[40a,40b], A. Cueto[96], T. Cuhadar Donszelmann[146], A. R. Cukierman[150], S. Czekierda[82], P. Czodrowski[35], M. J. Da Cunha Sargedas De Sousa[58b], C. Da Via[98], W. Dabrowski[81a], T. Dado[28a,x], S. Dahbi[34e], T. Dai[103], F. Dallaire[107], C. Dallapiccola[100], M. Dam[39], G. D'amen[23a,23b], J. Damp[97], J. R. Dandoy[133], M. F. Daneri[30], N. P. Dang[178,k], N. D Dann[98], M. Danninger[172], V. Dao[35], G. Darbo[53b], S. Darmora[8], O. Dartsi[5], A. Dattagupta[127], T. Daubney[44], S. D'Auria[66a,66b], W. Davey[24], C. David[44], T. Davidek[139], D. R. Davis[47], E. Dawe[102], I. Dawson[146], K. De[8], R. De Asmundis[67a], A. De Benedetti[124], M. De Beurs[118], S. De Castro[23a,23b], S. De Cecco[70a,70b], N. De Groot[117], P. de Jong[118], H. De la Torre[104], F. De Lorenzi[76], A. De Maria[69a,69b], D. De Pedis[70a], A. De Salvo[70a], U. De Sanctis[71a,71b], M. De Santis[71a,71b], A. De Santo[153], K. De Vasconcelos Corga[99], J. B. De Vivie De Regie[128], C. Debenedetti[143], D. V. Dedovich[77], N. Dehghanian[3], M. Del Gaudio[40a,40b], J. Del Peso[96], Y. Delabat Diaz[44], D. Delgove[128], F. Deliot[142], C. M. Delitzsch[7], M. Della Pietra[67a,67b], D. Della Volpe[52], A. Dell'Acqua[35], L. Dell'Asta[25], M. Delmastro[5], C. Delporte[128], P. A. Delsart[56], D. A. DeMarco[164], S. Demers[180], M. Demichev[77], S. P. Denisov[140], D. Denysiuk[118],

L. D'Eramo[132], D. Derendarz[82], J. E. Derkaoui[34d], F. Derue[132], P. Dervan[88], K. Desch[24], C. Deterre[44], K. Dette[164], M. R. Devesa[30], P. O. Deviveiros[35], A. Dewhurst[141], S. Dhaliwal[26], F. A. Di Bello[52], A. Di Ciaccio[71a,71b], L. Di Ciaccio[5], W. K. Di Clemente[133], C. Di Donato[67a,67b], A. Di Girolamo[35], G. Di Gregorio[69a,69b], B. Di Micco[72a,72b], R. Di Nardo[100], K. F. Di Petrillo[57], R. Di Sipio[164], D. Di Valentino[33], C. Diaconu[99], M. Diamond[164], F. A. Dias[39], T. Dias Do Vale[136a], M. A. Diaz[144a], J. Dickinson[18], E. B. Diehl[103], J. Dietrich[19], S. Díez Cornell[44], A. Dimitrievska[18], J. Dingfelder[24], F. Dittus[35], F. Djama[99], T. Djobava[156b], J. I. Djuvsland[59a], M. A. B. Do Vale[78c], M. Dobre[27b], D. Dodsworth[26], C. Doglioni[94], J. Dolejsi[139], Z. Dolezal[139], M. Donadelli[78d], J. Donini[37], A. D'onofrio[90], M. D'Onofrio[88], J. Dopke[141], A. Doria[67a], M. T. Dova[86], A. T. Doyle[55], E. Drechsler[51], E. Dreyer[149], T. Dreyer[51], Y. Du[58b], F. Dubinin[108], M. Dubovsky[28a], A. Dubreuil[52], E. Duchovni[177], G. Duckeck[112], A. Ducourthial[132], O. A. Ducu[107,w], D. Duda[113], A. Dudarev[35], A. C. Dudder[97], E. M. Duffield[18], L. Duflot[128], M. Dührssen[35], C. Dülsen[179], M. Dumancic[177], A. E. Dumitriu[27b,e], A. K. Duncan[55], M. Dunford[59a], A. Duperrin[99], H. Duran Yildiz[4a], M. Düren[54], A. Durglishvili[156b], D. Duschinger[46], B. Dutta[44], D. Duvnjak[1], M. Dyndal[44], S. Dysch[98], B. S. Dziedzic[82], C. Eckardt[44], K. M. Ecker[113], R. C. Edgar[103], T. Eifert[35], G. Eigen[17], K. Einsweiler[18], T. Ekelof[169], M. El Kacimi[34c], R. El Kosseifi[99], V. Ellajosyula[99], M. Ellert[169], F. Ellinghaus[179], A. A. Elliot[90], N. Ellis[35], J. Elmsheuser[29], M. Elsing[35], D. Emeliyanov[141], A. Emerman[38], Y. Enari[160], J. S. Ennis[175], M. B. Epland[47], J. Erdmann[45], A. Ereditato[20], S. Errede[170], M. Escalier[128], C. Escobar[171], O. Estrada Pastor[171], A. I. Etienvre[142], E. Etzion[158], H. Evans[63], A. Ezhilov[134], M. Ezzi[34e], F. Fabbri[55], L. Fabbri[23a,23b], V. Fabiani[117], G. Facini[92], R. M. Faisca Rodrigues Pereira[136a], R. M. Fakhrutdinov[140], S. Falciano[70a], P. J. Falke[5], S. Falke[5], J. Faltova[139], Y. Fang[15a], M. Fanti[66a,66b], A. Farbin[8], A. Farilla[72a], E. M. Farina[68a,68b], T. Farooque[104], S. Farrell[18], S. M. Farrington[175], P. Farthouat[35], F. Fassi[34e], P. Fassnacht[35], D. Fassouliotis[9], M. Faucci Giannelli[48], A. Favareto[53a,53b], W. J. Fawcett[31], L. Fayard[128], O. L. Fedin[134,p], W. Fedorko[172], M. Feickert[41], S. Feigl[130], L. Feligioni[99], C. Feng[58b], E. J. Feng[35], M. Feng[47], M. J. Fenton[55], A. B. Fenyuk[140], L. Feremenga[8], J. Ferrando[44], A. Ferrari[169], P. Ferrari[118], R. Ferrari[68a], D. E. Ferreira de Lima[59b], A. Ferrer[171], D. Ferrere[52], C. Ferretti[103], F. Fiedler[97], A. Filipčič[89], F. Filthaut[117], K. D. Finelli[25], M. C. N. Fiolhais[136a,136c,a], L. Fiorini[171], C. Fischer[14], W. C. Fisher[104], N. Flaschel[44], I. Fleck[148], P. Fleischmann[103], R. R. M. Fletcher[133], T. Flick[179], B. M. Flierl[112], L. M. Flores[133], L. R. Flores Castillo[61a], F. M. Follega[73a,73b], N. Fomin[17], G. T. Forcolin[73a,73b], A. Formica[142], F. A. Förster[14], A. C. Forti[98], A. G. Foster[21], D. Fournier[128], H. Fox[87], S. Fracchia[146], P. Francavilla[69a,69b], M. Franchini[23a,23b], S. Franchino[59a], D. Francis[35], L. Franconi[143], M. Franklin[57], M. Frate[168], M. Fraternali[68a,68b], A. N. Fray[90], D. Freeborn[92], S. M. Fressard-Batraneanu[35], B. Freund[107], W. S. Freund[78b], E. M. Freundlich[45], D. C. Frizzell[124], D. Froidevaux[35], J. A. Frost[131], C. Fukunaga[161], E. Fullana Torregrosa[171], T. Fusayasu[114], J. Fuster[171], O. Gabizon[157], A. Gabrielli[23a,23b], A. Gabrielli[18], G. P. Gach[81a], S. Gadatsch[52], P. Gadow[113], G. Gagliardi[53a,53b], L. G. Gagnon[107], C. Galea[27b], B. Galhardo[136a,136c], E. J. Gallas[131], B. J. Gallop[141], P. Gallus[138], G. Galster[39], R. Gamboa Goni[90], K. K. Gan[122], S. Ganguly[177], J. Gao[58a], Y. Gao[88], Y. S. Gao[150,m], C. García[171], J. E. García Navarro[171], J. A. García Pascual[15a], M. Garcia-Sciveres[18], R. W. Gardner[36], N. Garelli[150], S. Gargiulo[50], V. Garonne[130], K. Gasnikova[44], A. Gaudiello[53a,53b], G. Gaudio[68a], I. L. Gavrilenko[108], A. Gavrilyuk[109], C. Gay[172], G. Gaycken[24], E. N. Gazis[10], C. N. P. Gee[141], J. Geisen[51], M. Geisen[97], M. P. Geisler[59a], K. Gellerstedt[43a,43b], C. Gemme[53b], M. H. Genest[56], C. Geng[103], S. Gentile[70a,70b], S. George[91], D. Gerbaudo[14], G. Gessner[45], S. Ghasemi[148], M. Ghasemi Bostanabad[173], M. Ghneimat[24], B. Giacobbe[23b], S. Giagu[70a,70b], N. Giangiacomi[23a,23b], P. Giannetti[69a], A. Giannini[67a,67b], S. M. Gibson[91], M. Gignac[143], D. Gillberg[33], G. Gilles[179], D. M. Gingrich[3,as], M. P. Giordani[64a,64c], F. M. Giorgi[23b], P. F. Giraud[142], P. Giromini[57], G. Giugliarelli[64a,64c], D. Giugni[66a], F. Giuli[131], M. Giulini[59b], S. Gkaitatzis[159], I. Gkialas[9,j], E. L. Gkougkousis[14], P. Gkountoumis[10], L. K. Gladilin[111], C. Glasman[96], J. Glatzer[14], P. C. F. Glaysher[44], A. Glazov[44], M. Goblirsch-Kolb[26], J. Godlewski[82], S. Goldfarb[102], T. Golling[52], D. Golubkov[140], A. Gomes[136a,136b,136d], R. Goncalves Gama[78a], R. Gonçalo[136a], G. Gonella[50], L. Gonella[21], A. Gongadze[77], F. Gonnella[21], J. L. Gonski[57], S. González de la Hoz[171], S. Gonzalez-Sevilla[52], L. Goossens[35], P. A. Gorbounov[109], H. A. Gordon[29], B. Gorini[35], E. Gorini[65a,65b], A. Gorišek[89], A. T. Goshaw[47], C. Gössling[45], M. I. Gostkin[77], C. A. Gottardo[24], C. R. Goudet[128], D. Goujdami[34c], A. G. Goussiou[145], N. Govender[32b,c], C. Goy[5], E. Gozani[157], I. Grabowska-Bold[81a], P. O. J. Gradin[169], E. C. Graham[88], J. Gramling[168], E. Gramstad[130], S. Grancagnolo[19], V. Gratchev[134], P. M. Gravila[27f], F. G. Gravili[65a,65b], C. Gray[55], H. M. Gray[18], Z. D. Greenwood[93,ai], C. Grefe[24], K. Gregersen[94], I. M. Gregor[44], P. Grenier[150], K. Grevtsov[44], N. A. Grieser[124], J. Griffiths[8], A. A. Grillo[143], K. Grimm[150,b], S. Grinstein[14,y], Ph. Gris[37], J.-F. Grivaz[128], S. Groh[97], E. Gross[177], J. Grosse-Knetter[51], G. C. Grossi[93], Z. J. Grout[92], C. Grud[103], A. Grummer[116], L. Guan[103], W. Guan[178], J. Guenther[35], A. Guerguichon[128], F. Guescini[165a], D. Guest[168], R. Gugel[50], B. Gui[122], T. Guillemin[5], S. Guindon[35], U. Gul[55], C. Gumpert[35], J. Guo[58c], W. Guo[103], Y. Guo[58a,s], Z. Guo[99], R. Gupta[44], S. Gurbuz[12c], G. Gustavino[124], B. J. Gutelman[157], P. Gutierrez[124], C. Gutschow[92], C. Guyot[142], M. P. Guzik[81a], C. Gwenlan[131], C. B. Gwilliam[88], A. Haas[121], C. Haber[18], H. K. Hadavand[8], N. Haddad[34e], A. Hadef[58a], S. Hageböck[24], M. Hagihara[166], H. Hakobyan[181,*], M. Haleem[174], J. Haley[125], G. Halladjian[104], G. D. Hallewell[99], K. Hamacher[179],

P. Hamal[126], K. Hamano[173], A. Hamilton[32a], G. N. Hamity[146], K. Han[58a,ah], L. Han[58a], S. Han[15d], K. Hanagaki[79,u], M. Hance[143], D. M. Handl[112], B. Haney[133], R. Hankache[132], P. Hanke[59a], E. Hansen[94], J. B. Hansen[39], J. D. Hansen[39], M. C. Hansen[24], P. H. Hansen[39], K. Hara[166], A. S. Hard[178], T. Harenberg[179], S. Harkusha[105], P. F. Harrison[175], N. M. Hartmann[112], Y. Hasegawa[147], A. Hasib[48], S. Hassani[142], S. Haug[20], R. Hauser[104], L. Hauswald[46], L. B. Havener[38], M. Havranek[138], C. M. Hawkes[21], R. J. Hawkings[35], D. Hayden[104], C. Hayes[152], C. P. Hays[131], J. M. Hays[90], H. S. Hayward[88], S. J. Haywood[141], M. P. Heath[48], V. Hedberg[94], L. Heelan[8], S. Heer[24], K. K. Heidegger[50], J. Heilman[33], S. Heim[44], T. Heim[18], B. Heinemann[44,an], J. J. Heinrich[112], L. Heinrich[121], C. Heinz[54], J. Hejbal[137], L. Helary[35], A. Held[172], S. Hellesund[130], C. M. Helling[143], S. Hellman[43a,43b], C. Helsens[35], R. C. W. Henderson[87], Y. Heng[178], S. Henkelmann[172], A. M. Henriques Correia[35], G. H. Herbert[19], H. Herde[26], V. Herget[174], Y. Hernández Jiménez[32c], H. Herr[97], M. G. Herrmann[112], T. Herrmann[46], G. Herten[50], R. Hertenberger[112], L. Hervas[35], T. C. Herwig[133], G. G. Hesketh[92], N. P. Hessey[165a], A. Higashida[160], S. Higashino[79], E. Higón-Rodriguez[171], K. Hildebrand[36], E. Hill[173], J. C. Hill[31], K. K. Hill[29], K. H. Hiller[44], S. J. Hillier[21], M. Hils[46], I. Hinchliffe[18], M. Hirose[129], D. Hirschbuehl[179], B. Hiti[89], O. Hladik[137], D. R. Hlaluku[32c], X. Hoad[48], J. Hobbs[152], N. Hod[165a], M. C. Hodgkinson[146], A. Hoecker[35], M. R. Hoeferkamp[116], F. Hoenig[112], D. Hohn[24], D. Hohov[128], T. R. Holmes[36], M. Holzbock[112], M. Homann[45], B. H. Hommels[31], S. Honda[166], T. Honda[79], T. M. Hong[135], A. Hönle[113], B. H. Hooberman[170], W. H. Hopkins[127], Y. Horii[115], P. Horn[46], A. J. Horton[149], L. A. Horyn[36], J-Y. Hostachy[56], A. Hostiuc[145], S. Hou[155], A. Hoummada[34a], J. Howarth[98], J. Hoya[86], M. Hrabovsky[126], I. Hristova[19], J. Hrivnac[128], A. Hrynevich[106], T. Hryn'ova[5], P. J. Hsu[62], S.-C. Hsu[145], Q. Hu[29], S. Hu[58c], Y. Huang[15a], Z. Hubacek[138], F. Hubaut[99], M. Huebner[24], F. Huegging[24], T. B. Huffman[131], M. Huhtinen[35], R. F. H. Hunter[33], P. Huo[152], A. M. Hupe[33], N. Huseynov[77,ae], J. Huston[104], J. Huth[57], R. Hyneman[103], G. Iacobucci[52], G. Iakovidis[29], I. Ibragimov[148], L. Iconomidou-Fayard[128], Z. Idrissi[34e], P. Iengo[35], R. Ignazzi[39], O. Igonkina[118,aa], R. Iguchi[160], T. Iizawa[52], Y. Ikegami[79], M. Ikeno[79], D. Iliadis[159], N. Ilic[150], F. Iltzsche[46], G. Introzzi[68a,68b], M. Iodice[72a], K. Iordanidou[38], V. Ippolito[70a,70b], M. F. Isacson[169], N. Ishijima[129], M. Ishino[160], M. Ishitsuka[162], W. Islam[125], C. Issever[131], S. Istin[157], F. Ito[166], J. M. Iturbe Ponce[61a], R. Iuppa[73a,73b], A. Ivina[177], H. Iwasaki[79], J. M. Izen[42], V. Izzo[67a], P. Jacka[137], P. Jackson[1], R. M. Jacobs[24], V. Jain[2], G. Jäkel[179], K. B. Jakobi[97], K. Jakobs[50], S. Jakobsen[74], T. Jakoubek[137], D. O. Jamin[125], R. Jansky[52], J. Janssen[24], M. Janus[51], P. A. Janus[81a], G. Jarlskog[94], N. Javadov[77,ae], T. Javůrek[35], M. Javurkova[50], F. Jeanneau[142], L. Jeanty[18], J. Jejelava[156a,af], A. Jelinskas[175], P. Jenni[50,d], J. Jeong[44], N. Jeong[44], S. Jézéquel[5], H. Ji[178], J. Jia[152], H. Jiang[76], Y. Jiang[58a], Z. Jiang[150,q], S. Jiggins[50], F. A. Jimenez Morales[37], J. Jimenez Pena[171], S. Jin[15c], A. Jinaru[27b], O. Jinnouchi[162], H. Jivan[32c], P. Johansson[146], K. A. Johns[7], C. A. Johnson[63], W. J. Johnson[145], K. Jon-And[43a,43b], R. W. L. Jones[87], S. D. Jones[153], S. Jones[7], T. J. Jones[88], J. Jongmanns[59a], P. M. Jorge[136a,136b], J. Jovicevic[165a], X. Ju[18], J. J. Junggeburth[113], A. Juste Rozas[14,y], A. Kaczmarska[82], M. Kado[128], H. Kagan[122], M. Kagan[150], T. Kaji[176], E. Kajomovitz[157], C. W. Kalderon[94], A. Kaluza[97], S. Kama[41], A. Kamenshchikov[140], L. Kanjir[89], Y. Kano[160], V. A. Kantserov[110], J. Kanzaki[79], B. Kaplan[121], L. S. Kaplan[178], D. Kar[32c], M. J. Kareem[165b], E. Karentzos[10], S. N. Karpov[77], Z. M. Karpova[77], V. Kartvelishvili[87], A. N. Karyukhin[140], L. Kashif[178], R. D. Kass[122], A. Kastanas[43a,43b], Y. Kataoka[160], C. Kato[58c,58d], J. Katzy[44], K. Kawade[80], K. Kawagoe[85], T. Kawamoto[160], G. Kawamura[51], E. F. Kay[88], V. F. Kazanin[120a,120b], R. Keeler[173], R. Kehoe[41], J. S. Keller[33], E. Kellermann[94], J. J. Kempster[21], J. Kendrick[21], O. Kepka[137], S. Kersten[179], B. P. Kerševan[89], S. Ketabchi Haghighat[164], R. A. Keyes[101], M. Khader[170], F. Khalil-Zada[13], A. Khanov[125], A. G. Kharlamov[120a,120b], T. Kharlamova[120a,120b], E. E. Khoda[172], A. Khodinov[163], T. J. Khoo[52], E. Khramov[77], J. Khubua[156b], S. Kido[80], M. Kiehn[52], C. R. Kilby[91], Y. K. Kim[36], N. Kimura[64a,64c], O. M. Kind[19], B. T. King[88], D. Kirchmeier[46], J. Kirk[141], A. E. Kiryunin[113], T. Kishimoto[160], D. Kisielewska[81a], V. Kitali[44], O. Kivernyk[5], E. Kladiva[28b,*], T. Klapdor-Kleingrothaus[50], M. H. Klein[103], M. Klein[88], U. Klein[88], K. Kleinknecht[97], P. Klimek[119], A. Klimentov[29], T. Klingl[24], T. Klioutchnikova[35], F. F. Klitzner[112], P. Kluit[118], S. Kluth[113], E. Kneringer[74], E. B. F. G. Knoops[99], A. Knue[50], A. Kobayashi[160], D. Kobayashi[85], T. Kobayashi[160], M. Kobel[46], M. Kocian[150], P. Kodys[139], P. T. Koenig[24], T. Koffas[33], E. Koffeman[118], N. M. Köhler[113], T. Koi[150], M. Kolb[59b], I. Koletsou[5], T. Kondo[79], N. Kondrashova[58c], K. Köneke[50], A. C. König[117], T. Kono[79], R. Konoplich[121,ak], V. Konstantinides[92], N. Konstantinidis[92], B. Konya[94], R. Kopeliansky[63], S. Koperny[81a], K. Korcyl[82], K. Kordas[159], G. Koren[158], A. Korn[92], I. Korolkov[14], E. V. Korolkova[146], N. Korotkova[111], O. Kortner[113], S. Kortner[113], T. Kosek[139], V. V. Kostyukhin[24], A. Kotwal[47], A. Koulouris[10], A. Kourkoumeli-Charalampidi[68a,68b], C. Kourkoumelis[9], E. Kourlitis[146], V. Kouskoura[29], A. B. Kowalewska[82], R. Kowalewski[173], T. Z. Kowalski[81a], C. Kozakai[160], W. Kozanecki[142], A. S. Kozhin[140], V. A. Kramarenko[111], G. Kramberger[89], D. Krasnopevtsev[58a], M. W. Krasny[132], A. Krasznahorkay[35], D. Krauss[113], J. A. Kremer[81a], J. Kretzschmar[88], P. Krieger[164], K. Krizka[18], K. Kroeninger[45], H. Kroha[113], J. Kroll[137], J. Kroll[133], J. Krstic[16], U. Kruchonak[77], H. Krüger[24], N. Krumnack[76], M. C. Kruse[47], T. Kubota[102], S. Kuday[4b], J. T. Kuechler[179], S. Kuehn[35], A. Kugel[59a], F. Kuger[174], T. Kuhl[44], V. Kukhtin[77], R. Kukla[99], Y. Kulchitsky[105], S. Kuleshov[144b], Y. P. Kulinich[170], M. Kuna[56], T. Kunigo[83], A. Kupco[137], T. Kupfer[45], O. Kuprash[158], H. Kurashige[80],

L. L. Kurchaninov[165a], Y. A. Kurochkin[105], A. Kurova[110], M. G. Kurth[15d], E. S. Kuwertz[35], M. Kuze[162], J. Kvita[126], T. Kwan[101], A. La Rosa[113], J. L. La Rosa Navarro[78d], L. La Rotonda[40a,40b], F. La Ruffa[40a,40b], C. Lacasta[171], F. Lacava[70a,70b], J. Lacey[44], D. P. J. Lack[98], H. Lacker[19], D. Lacour[132], E. Ladygin[77], R. Lafaye[5], B. Laforge[132], T. Lagouri[32c], S. Lai[51], S. Lammers[63], W. Lampl[7], E. Lançon[29], U. Landgraf[50], M. P. J. Landon[90], M. C. Lanfermann[52], V. S. Lang[44], J. C. Lange[51], R. J. Langenberg[35], A. J. Lankford[168], F. Lanni[29], K. Lantzsch[24], A. Lanza[68a], A. Lapertosa[53a,53b], S. Laplace[132], J. F. Laporte[142], T. Lari[66a], F. Lasagni Manghi[23a,23b], M. Lassnig[35], T. S. Lau[61a], A. Laudrain[128], M. Lavorgna[67a,67b], M. Lazzaroni[66a,66b], B. Le[102], O. Le Dortz[132], E. Le Guirriec[99], E. P. Le Quilleuc[142], M. LeBlanc[7], T. LeCompte[6], F. Ledroit-Guillon[56], C. A. Lee[29], G. R. Lee[144a], L. Lee[57], S. C. Lee[155], B. Lefebvre[101], M. Lefebvre[173], F. Legger[112], C. Leggett[18], K. Lehmann[149], N. Lehmann[179], G. Lehmann Miotto[35], W. A. Leight[44], A. Leisos[159,v], M. A. L. Leite[78d], R. Leitner[139], D. Lellouch[177], K. J. C. Leney[92], T. Lenz[24], B. Lenzi[35], R. Leone[7], S. Leone[69a], C. Leonidopoulos[48], G. Lerner[153], C. Leroy[107], R. Les[164], A. A. J. Lesage[142], C. G. Lester[31], M. Levchenko[134], J. Levêque[5], D. Levin[103], L. J. Levinson[177], D. Lewis[90], B. Li[15b], B. Li[103], C-Q. Li[58a,aj], H. Li[58a], H. Li[58b], L. Li[58c], M. Li[15a], Q. Li[15d], Q. Y. Li[58a], S. Li[58c,58d], X. Li[58c], Y. Li[148], Z. Liang[15a], B. Liberti[71a], A. Liblong[164], K. Lie[61c], S. Liem[118], A. Limosani[154], C. Y. Lin[31], K. Lin[104], T. H. Lin[97], R. A. Linck[63], J. H. Lindon[21], B. E. Lindquist[152], A. L. Lionti[52], E. Lipeles[133], A. Lipniacka[17], M. Lisovyi[59b], T. M. Liss[170,ap], A. Lister[172], A. M. Litke[143], J. D. Little[8], B. Liu[76], B. L Liu[6], H. B. Liu[29], H. Liu[103], J. B. Liu[58a], J. K. K. Liu[131], K. Liu[132], M. Liu[58a], P. Liu[18], Y. Liu[15a], Y. L. Liu[58a], Y. W. Liu[58a], M. Livan[68a,68b], A. Lleres[56], J. Llorente Merino[15a], S. L. Lloyd[90], C. Y. Lo[61b], F. Lo Sterzo[41], E. M. Lobodzinska[44], P. Loch[7], T. Lohse[19], K. Lohwasser[146], M. Lokajicek[137], J. D. Long[170], R. E. Long[87], L. Longo[65a,65b], K. A. Looper[122], J. A. Lopez[144b], I. Lopez Paz[98], A. Lopez Solis[146], J. Lorenz[112], N. Lorenzo Martinez[5], M. Losada[22], P. J. Lösel[112], A. Lösle[50], X. Lou[44], X. Lou[15a], A. Lounis[128], J. Love[6], P. A. Love[87], J. J. Lozano Bahilo[171], H. Lu[61a], M. Lu[58a], Y. J. Lu[62], H. J. Lubatti[145], C. Luci[70a,70b], A. Lucotte[56], C. Luedtke[50], F. Luehring[63], I. Luise[132], L. Luminari[70a], B. Lund-Jensen[151], M. S. Lutz[100], P. M. Luzi[132], D. Lynn[29], R. Lysak[137], E. Lytken[94], F. Lyu[15a], V. Lyubushkin[77], T. Lyubushkina[77], H. Ma[29], L. L. Ma[58b], Y. Ma[58b], G. Maccarrone[49], A. Macchiolo[113], C. M. Macdonald[146], J. Machado Miguens[133,136b], D. Madaffari[171], R. Madar[37], W. F. Mader[46], A. Madsen[44], N. Madysa[46], J. Maeda[80], K. Maekawa[160], S. Maeland[17], T. Maeno[29], M. Maerker[46], A. S. Maevskiy[111], V. Magerl[50], D. J. Mahon[38], C. Maidantchik[78b], T. Maier[112], A. Maio[136a,136b,136d], O. Majersky[28a], S. Majewski[127], Y. Makida[79], N. Makovec[128], B. Malaescu[132], Pa. Malecki[82], V. P. Maleev[134], F. Malek[56], U. Mallik[75], D. Malon[6], C. Malone[31], S. Maltezos[10], S. Malyukov[35], J. Mamuzic[171], G. Mancini[49], I. Mandić[89], J. Maneira[136a], L. Manhaes de Andrade Filho[78a], J. Manjarres Ramos[46], K. H. Mankinen[94], A. Mann[112], A. Manousos[74], B. Mansoulie[142], J. D. Mansour[15a], M. Mantoani[51], S. Manzoni[66a,66b], A. Marantis[159], G. Marceca[30], L. March[52], L. Marchese[131], G. Marchiori[132], M. Marcisovsky[137], C. Marcon[94], C. A. Marin Tobon[35], M. Marjanovic[37], D. E. Marley[103], F. Marroquim[78b], Z. Marshall[18], M. U. F Martensson[169], S. Marti-Garcia[171], C. B. Martin[122], T. A. Martin[175], V. J. Martin[48], B. Martin dit Latour[17], M. Martinez[14,y], V. I. Martinez Outschoorn[100], S. Martin-Haugh[141], V. S. Martoiu[27b], A. C. Martyniuk[92], A. Marzin[35], L. Masetti[97], T. Mashimo[160], R. Mashinistov[108], J. Masik[98], A. L. Maslennikov[120a,120b], L. H. Mason[102], L. Massa[71a,71b], P. Massarotti[67a,67b], P. Mastrandrea[5], A. Mastroberardino[40a,40b], T. Masubuchi[160], P. Mättig[179], J. Maurer[27b], B. Maček[89], S. J. Maxfield[88], D. A. Maximov[120a,120b], R. Mazini[155], I. Maznas[159], S. M. Mazza[143], G. Mc Goldrick[164], S. P. Mc Kee[103], A. McCarn[103], T. G. McCarthy[113], L. I. McClymont[92], W. P. McCormack[18], E. F. McDonald[102], J. A. Mcfayden[35], G. Mchedlidze[51], M. A. McKay[41], K. D. McLean[173], S. J. McMahon[141], P. C. McNamara[102], C. J. McNicol[175], R. A. McPherson[173,ac], J. E. Mdhluli[32c], Z. A. Meadows[100], S. Meehan[145], T. M. Megy[50], S. Mehlhase[112], A. Mehta[88], T. Meideck[56], B. Meirose[42], D. Melini[171,h], B. R. Mellado Garcia[32c], J. D. Mellenthin[51], M. Melo[28a], F. Meloni[44], A. Melzer[24], S. B. Menary[98], E. D. Mendes Gouveia[136a], L. Meng[88], X. T. Meng[103], A. Mengarelli[23a,23b], S. Menke[113], E. Meoni[40a,40b], S. Mergelmeyer[19], S. A. M. Merkt[135], C. Merlassino[20], P. Mermod[52], L. Merola[67a,67b], C. Meroni[66a], F. S. Merritt[36], A. Messina[70a,70b], J. Metcalfe[6], A. S. Mete[168], C. Meyer[133], J. Meyer[157], J-P. Meyer[142], H. Meyer Zu Theenhausen[59a], F. Miano[153], R. P. Middleton[141], L. Mijović[48], G. Mikenberg[177], M. Mikestikova[137], M. Mikuž[89], M. Milesi[102], A. Milic[164], D. A. Millar[90], D. W. Miller[36], A. Milov[177], D. A. Milstead[43a,43b], A. A. Minaenko[140], M. Miñano Moya[171], I. A. Minashvili[156b], A. I. Mincer[121], B. Mindur[81a], M. Mineev[77], Y. Minegishi[160], Y. Ming[178], L. M. Mir[14], A. Mirto[65a,65b], K. P. Mistry[133], T. Mitani[176], J. Mitrevski[112], V. A. Mitsou[171], M. Mittal[58c], A. Miucci[20], P. S. Miyagawa[146], A. Mizukami[79], J. U. Mjörnmark[94], T. Mkrtchyan[181], M. Mlynarikova[139], T. Moa[43a,43b], K. Mochizuki[107], P. Mogg[50], S. Mohapatra[38], S. Molander[43a,43b], R. Moles-Valls[24], M. C. Mondragon[104], K. Mönig[44], J. Monk[39], E. Monnier[99], A. Montalbano[149], J. Montejo Berlingen[35], F. Monticelli[86], S. Monzani[66a], N. Morange[128], D. Moreno[22], M. Moreno Llácer[35], P. Morettini[53b], M. Morgenstern[118], S. Morgenstern[46], D. Mori[149], M. Morii[57], M. Morinaga[176], V. Morisbak[130], A. K. Morley[35], G. Mornacchi[35], A. P. Morris[92], J. D. Morris[90], L. Morvaj[152], P. Moschovakos[10], M. Mosidze[156b], H. J. Moss[146], J. Moss[150,n],

K. Motohashi[162], R. Mount[150], E. Mountricha[35], E. J. W. Moyse[100], S. Muanza[99], F. Mueller[113], J. Mueller[135], R. S. P. Mueller[112], D. Muenstermann[87], G. A. Mullier[94], F. J. Munoz Sanchez[98], P. Murin[28b], W. J. Murray[175,141], A. Murrone[66a,66b], M. Muškinja[89], C. Mwewa[32a], A. G. Myagkov[140,al], J. Myers[127], M. Myska[138], B. P. Nachman[18], O. Nackenhorst[45], K. Nagai[131], K. Nagano[79], Y. Nagasaka[60], M. Nagel[50], E. Nagy[99], A. M. Nairz[35], Y. Nakahama[115], K. Nakamura[79], T. Nakamura[160], I. Nakano[123], H. Nanjo[129], F. Napolitano[59a], R. F. Naranjo Garcia[44], R. Narayan[11], D. I. Narrias Villar[59a], I. Naryshkin[134], T. Naumann[44], G. Navarro[22], R. Nayyar[7], H. A. Neal[103,*], P. Y. Nechaeva[108], T. J. Neep[142], A. Negri[68a,68b], M. Negrini[23b], S. Nektarijevic[117], C. Nellist[51], M. E. Nelson[131], S. Nemecek[137], P. Nemethy[121], M. Nessi[35,f], M. S. Neubauer[170], M. Neumann[179], P. R. Newman[21], T. Y. Ng[61c], Y. S. Ng[19], H. D. N. Nguyen[99], T. Nguyen Manh[107], E. Nibigira[37], R. B. Nickerson[131], R. Nicolaidou[142], D. S. Nielsen[39], J. Nielsen[143], N. Nikiforou[11], V. Nikolaenko[140,al], I. Nikolic-Audit[132], K. Nikolopoulos[21], P. Nilsson[29], Y. Ninomiya[79], A. Nisati[70a], N. Nishu[58c], R. Nisius[113], I. Nitsche[45], T. Nitta[176], T. Nobe[160], Y. Noguchi[83], M. Nomachi[129], I. Nomidis[132], M. A. Nomura[29], T. Nooney[90], M. Nordberg[35], N. Norjoharuddeen[131], T. Novak[89], O. Novgorodova[46], R. Novotny[138], L. Nozka[126], K. Ntekas[168], E. Nurse[92], F. Nuti[102], F. G. Oakham[33,as], H. Oberlack[113], J. Ocariz[132], A. Ochi[80], I. Ochoa[38], J. P. Ochoa-Ricoux[144a], K. O'Connor[26], S. Oda[85], S. Odaka[79], S. Oerdek[51], A. Oh[98], S. H. Oh[47], C. C. Ohm[151], H. Oide[53a,53b], M. L. Ojeda[164], H. Okawa[166], Y. Okazaki[83], Y. Okumura[160], T. Okuyama[79], A. Olariu[27b], L. F. Oleiro Seabra[136a], S. A. Olivares Pino[144a], D. Oliveira Damazio[29], J. L. Oliver[1], M. J. R. Olsson[36], A. Olszewski[82], J. Olszowska[82], D. C. O'Neil[149], A. Onofre[136a,136e], K. Onogi[115], P. U. E. Onyisi[11], H. Oppen[130], M. J. Oreglia[36], G. E. Orellana[86], Y. Oren[158], D. Orestano[72a,72b], E. C. Orgill[98], N. Orlando[61b], A. A. O'Rourke[44], R. S. Orr[164], B. Osculati[53a,53b,*], V. O'Shea[55], R. Ospanov[58a], G. Otero y Garzon[30], H. Otono[85], M. Ouchrif[34d], F. Ould-Saada[130], A. Ouraou[142], Q. Ouyang[15a], M. Owen[55], R. E. Owen[21], V. E. Ozcan[12c], N. Ozturk[8], J. Pacalt[126], H. A. Pacey[31], K. Pachal[149], A. Pacheco Pages[14], L. Pacheco Rodriguez[142], C. Padilla Aranda[14], S. Pagan Griso[18], M. Paganini[180], G. Palacino[63], S. Palazzo[48], S. Palestini[35], M. Palka[81b], D. Pallin[37], I. Panagoulias[10], C. E. Pandini[35], J. G. Panduro Vazquez[91], P. Pani[35], G. Panizzo[64a,64c], L. Paolozzi[52], T. D. Papadopoulou[10], K. Papageorgiou[9,j], A. Paramonov[6], D. Paredes Hernandez[61b], S. R. Paredes Saenz[131], B. Parida[163], T. H. Park[33], A. J. Parker[87], K. A. Parker[44], M. A. Parker[31], F. Parodi[53a,53b], J. A. Parsons[38], U. Parzefall[50], V. R. Pascuzzi[164], J. M. P. Pasner[143], E. Pasqualucci[70a], S. Passaggio[53b], F. Pastore[91], P. Pasuwan[43a,43b], S. Pataraia[97], J. R. Pater[98], A. Pathak[178,k], T. Pauly[35], B. Pearson[113], M. Pedersen[130], L. Pedraza Diaz[117], R. Pedro[136a,136b], S. V. Peleganchuk[120a,120b], O. Penc[137], C. Peng[15d], H. Peng[58a], B. S. Peralva[78a], M. M. Perego[128], A. P. Pereira Peixoto[136a], D. V. Perepelitsa[29], F. Peri[19], L. Perini[66a,66b], H. Pernegger[35], S. Perrella[67a,67b], V. D. Peshekhonov[77,*], K. Peters[44], R. F. Y. Peters[98], B. A. Petersen[35], T. C. Petersen[39], E. Petit[56], A. Petridis[1], C. Petridou[159], P. Petroff[128], M. Petrov[131], F. Petrucci[72a,72b], M. Pettee[180], N. E. Pettersson[100], A. Peyaud[142], R. Pezoa[144b], T. Pham[102], F. H. Phillips[104], P. W. Phillips[141], M. W. Phipps[170], G. Piacquadio[152], E. Pianori[18], A. Picazio[100], M. A. Pickering[131], R. H. Pickles[98], R. Piegaia[30], J. E. Pilcher[36], A. D. Pilkington[98], M. Pinamonti[71a,71b], J. L. Pinfold[3], M. Pitt[177], L. Pizzimento[71a,71b], M.-A. Pleier[29], V. Pleskot[139], E. Plotnikova[77], D. Pluth[76], P. Podberezko[120a,120b], R. Poettgen[94], R. Poggi[52], L. Poggioli[128], I. Pogrebnyak[104], D. Pohl[24], I. Pokharel[51], G. Polesello[68a], A. Poley[18], A. Policicchio[70a,70b], R. Polifka[35], A. Polini[23b], C. S. Pollard[44], V. Polychronakos[29], D. Ponomarenko[110], L. Pontecorvo[35], G. A. Popeneciu[27d], D. M. Portillo Quintero[132], S. Pospisil[138], K. Potamianos[44], I. N. Potrap[77], C. J. Potter[31], H. Potti[11], T. Poulsen[94], J. Poveda[35], T. D. Powell[146], M. E. Pozo Astigarraga[35], P. Pralavorio[99], S. Prell[76], D. Price[98], M. Primavera[65a], S. Prince[101], N. Proklova[110], K. Prokofiev[61c], F. Prokoshin[144b], S. Protopopescu[29], J. Proudfoot[6], M. Przybycien[81a], A. Puri[170], P. Puzo[128], J. Qian[103], Y. Qin[98], A. Quadt[51], M. Queitsch-Maitland[44], A. Qureshi[1], P. Rados[102], F. Ragusa[66a,66b], G. Rahal[95], J. A. Raine[52], S. Rajagopalan[29], A. Ramirez Morales[90], T. Rashid[128], S. Raspopov[5], M. G. Ratti[66a,66b], D. M. Rauch[44], F. Rauscher[112], S. Rave[97], B. Ravina[146], I. Ravinovich[177], J. H. Rawling[98], M. Raymond[35], A. L. Read[130], N. P. Readioff[56], M. Reale[65a,65b], D. M. Rebuzzi[68a,68b], A. Redelbach[174], G. Redlinger[29], R. Reece[143], R. G. Reed[32c], K. Reeves[42], L. Rehnisch[19], J. Reichert[133], D. Reikher[158], A. Reiss[97], C. Rembser[35], H. Ren[15d], M. Rescigno[70a], S. Resconi[66a], E. D. Resseguie[133], S. Rettie[172], E. Reynolds[21], O. L. Rezanova[120a,120b], P. Reznicek[139], E. Ricci[73a,73b], R. Richter[113], S. Richter[44], E. Richter-Was[81b], O. Ricken[24], M. Ridel[132], P. Rieck[113], C. J. Riegel[179], O. Rifki[44], M. Rijssenbeek[152], A. Rimoldi[68a,68b], M. Rimoldi[20], L. Rinaldi[23b], G. Ripellino[151], B. Ristić[87], E. Ritsch[35], I. Riu[14], J. C. Rivera Vergara[144a], F. Rizatdinova[125], E. Rizvi[90], C. Rizzi[14], R. T. Roberts[98], S. H. Robertson[101,ac], D. Robinson[31], J. E. M. Robinson[44], A. Robson[55], E. Rocco[97], C. Roda[69a,69b], Y. Rodina[99], S. Rodriguez Bosca[171], A. Rodriguez Perez[14], D. Rodriguez Rodriguez[171], A. M. Rodríguez Vera[165b], S. Roe[35], C. S. Rogan[57], O. Røhne[130], R. Röhrig[113], C. P. A. Roland[63], J. Roloff[57], A. Romaniouk[110], M. Romano[23a,23b], N. Rompotis[88], M. Ronzani[121], L. Roos[132], S. Rosati[70a], K. Rosbach[50], N-A. Rosien[51], B. J. Rosser[133], E. Rossi[44], E. Rossi[72a,72b], E. Rossi[67a,67b], L. P. Rossi[53b], L. Rossini[66a,66b], J. H. N. Rosten[31], R. Rosten[14], M. Rotaru[27b], J. Rothberg[145], D. Rousseau[128], D. Roy[32c], A. Rozanov[99], Y. Rozen[157], X. Ruan[32c], F. Rubbo[150], F. Rühr[50], A. Ruiz-Martinez[171], Z. Rurikova[50], N. A. Rusakovich[77],

H. L. Russell[101],   J. P. Rutherfoord[7],   E. M. Rüttinger[44,l],   Y. F. Ryabov[134],   M. Rybar[170],   G. Rybkin[128],   S. Ryu[6],
A. Ryzhov[140],   G. F. Rzehorz[51],   P. Sabatini[51],   G. Sabato[118],   S. Sacerdoti[128],   H. F-W. Sadrozinski[143],   R. Sadykov[77],
F. Safai Tehrani[70a],   P. Saha[119],   M. Sahinsoy[59a],   A. Sahu[179],   M. Saimpert[44],   M. Saito[160],   T. Saito[160],   H. Sakamoto[160],
A. Sakharov[121,ak],   D. Salamani[52],   G. Salamanna[72a,72b],   J. E. Salazar Loyola[144b],   P. H. Sales De Bruin[169],   D. Salihagic[113],
A. Salnikov[150],   J. Salt[171],   D. Salvatore[40a,40b],   F. Salvatore[153],   A. Salvucci[61a,61b,61c],   A. Salzburger[35],   J. Samarati[35],
D. Sammel[50],   D. Sampsonidis[159],   D. Sampsonidou[159],   J. Sánchez[171],   A. Sanchez Pineda[64a,64c],   H. Sandaker[130],
C. O. Sander[44],   M. Sandhoff[179],   C. Sandoval[22],   D. P. C. Sankey[141],   M. Sannino[53a,53b],   Y. Sano[115],   A. Sansoni[49],
C. Santoni[37],   H. Santos[136a],   I. Santoyo Castillo[153],   A. Santra[171],   A. Sapronov[77],   J. G. Saraiva[136a,136d],   O. Sasaki[79],
K. Sato[166],   E. Sauvan[5],   P. Savard[164,as],   N. Savic[113],   R. Sawada[160],   C. Sawyer[141],   L. Sawyer[93,ai],   C. Sbarra[23b],
A. Sbrizzi[23b,23a],   T. Scanlon[92],   J. Schaarschmidt[145],   P. Schacht[113],   B. M. Schachtner[112],   D. Schaefer[36],   L. Schaefer[133],
J. Schaeffer[97],   S. Schaepe[35],   U. Schäfer[97],   A. C. Schaffer[128],   D. Schaile[112],   R. D. Schamberger[152],   N. Scharmberg[98],
V. A. Schegelsky[134],   D. Scheirich[139],   F. Schenck[19],   M. Schernau[168],   C. Schiavi[53a,53b],   S. Schier[143],   L. K. Schildgen[24],
Z. M. Schillaci[26],   E. J. Schioppa[35],   M. Schioppa[40a,40b],   K. E. Schleicher[50],   S. Schlenker[35],   K. R. Schmidt-Sommerfeld[113],
K. Schmieden[35],   C. Schmitt[97],   S. Schmitt[44],   S. Schmitz[97],   J. C. Schmoeckel[44],   U. Schnoor[50],   L. Schoeffel[142],
A. Schoening[59b],   E. Schopf[131],   M. Schott[97],   J. F. P. Schouwenberg[117],   J. Schovancova[35],   S. Schramm[52],   A. Schulte[97],
H-C. Schultz-Coulon[59a],   M. Schumacher[50],   B. A. Schumm[143],   Ph. Schune[142],   A. Schwartzman[150],   T. A. Schwarz[103],
Ph. Schwemling[142],   R. Schwienhorst[104],   A. Sciandra[24],   G. Sciolla[26],   M. Scornajenghi[40a,40b],   F. Scuri[69a],   F. Scutti[102],
L. M. Scyboz[113],   C. D. Sebastiani[70a,70b],   P. Seema[19],   S. C. Seidel[116],   A. Seiden[143],   T. Seiss[36],   J. M. Seixas[78b],
G. Sekhniaidze[67a],   K. Sekhon[103],   S. J. Sekula[41],   N. Semprini-Cesari[23a,23b],   S. Sen[47],   S. Senkin[37],   C. Serfon[130],
L. Serin[128],   L. Serkin[64a,64b],   M. Sessa[58a],   H. Severini[124],   F. Sforza[167],   A. Sfyrla[52],   E. Shabalina[51],   J. D. Shahinian[143],
N. W. Shaikh[43a,43b],   L. Y. Shan[15a],   R. Shang[170],   J. T. Shank[25],   M. Shapiro[18],   A. S. Sharma[1],   A. Sharma[131],
P. B. Shatalov[109],   K. Shaw[153],   S. M. Shaw[98],   A. Shcherbakova[134],   Y. Shen[124],   N. Sherafati[33],   A. D. Sherman[25],
P. Sherwood[92],   L. Shi[155,ao],   S. Shimizu[79],   C. O. Shimmin[180],   Y. Shimogama[176],   M. Shimojima[114],   I. P. J. Shipsey[131],
S. Shirabe[85],   M. Shiyakova[77],   J. Shlomi[177],   A. Shmeleva[108],   D. Shoaleh Saadi[107],   M. J. Shochet[36],   S. Shojaii[102],
D. R. Shope[124],   S. Shrestha[122],   E. Shulga[110],   P. Sicho[137],   A. M. Sickles[170],   P. E. Sidebo[151],   E. Sideras Haddad[32c],
O. Sidiropoulou[35],   A. Sidoti[23a,23b],   F. Siegert[46],   Dj. Sijacki[16],   J. Silva[136a],   M. Silva Jr.[178],   M. V. Silva Oliveira[78a],
S. B. Silverstein[43a],   S. Simion[128],   E. Simioni[97],   M. Simon[97],   R. Simoniello[97],   P. Sinervo[164],   N. B. Sinev[127],   M. Sioli[23a,23b],
G. Siragusa[174],   I. Siral[103],   S. Yu. Sivoklokov[111],   J. Sjölin[43a,43b],   P. Skubic[124],   M. Slater[21],   T. Slavicek[138],   M. Slawinska[82],
K. Sliwa[167],   R. Slovak[139],   V. Smakhtin[177],   B. H. Smart[5],   J. Smiesko[28a],   N. Smirnov[110],   S. Yu. Smirnov[110],   Y. Smirnov[110],
L. N. Smirnova[111],   O. Smirnova[94],   J. W. Smith[51],   M. Smizanska[87],   K. Smolek[138],   A. Smykiewicz[82],   A. A. Snesarev[108],
I. M. Snyder[127],   S. Snyder[29],   R. Sobie[173,ac],   A. M. Soffa[168],   A. Soffer[158],   A. Søgaard[48],   D. A. Soh[155],   G. Sokhrannyi[89],
C. A. Solans Sanchez[35],   M. Solar[138],   E. Yu. Soldatov[110],   U. Soldevila[171],   A. A. Solodkov[140],   A. Soloshenko[77],
O. V. Solovyanov[140],   V. Solovyev[134],   P. Sommer[146],   H. Son[167],   W. Song[141],   W. Y. Song[165b],   A. Sopczak[138],   F. Sopkova[28b],
C. L. Sotiropoulou[69a,69b],   S. Sottocornola[68a,68b],   R. Soualah[64a,64c,i],   A. M. Soukharev[120a,120b],   D. South[44],   B. C. Sowden[91],
S. Spagnolo[65a,65b],   M. Spalla[113],   M. Spangenberg[175],   F. Spanò[91],   D. Sperlich[19],   T. M. Spieker[59a],   R. Spighi[23b],   G. Spigo[35],
L. A. Spiller[102],   D. P. Spiteri[55],   M. Spousta[139],   A. Stabile[66a,66b],   R. Stamen[59a],   S. Stamm[19],   E. Stanecka[82],   R. W. Stanek[6],
C. Stanescu[72a],   B. Stanislaus[131],   M. M. Stanitzki[44],   B. Stapf[118],   S. Stapnes[130],   E. A. Starchenko[140],   G. H. Stark[36],
J. Stark[56],   S. H Stark[39],   P. Staroba[137],   P. Starovoitov[59a],   S. Stärz[35],   R. Staszewski[82],   M. Stegler[44],   P. Steinberg[29],
B. Stelzer[149],   H. J. Stelzer[35],   O. Stelzer-Chilton[165a],   H. Stenzel[54],   T. J. Stevenson[90],   G. A. Stewart[55],   M. C. Stockton[35],
G. Stoicea[27b],   P. Stolte[51],   S. Stonjek[113],   A. Straessner[46],   J. Strandberg[151],   S. Strandberg[43a,43b],   M. Strauss[124],
P. Strizenec[28b],   R. Ströhmer[174],   D. M. Strom[127],   R. Stroynowski[41],   A. Strubig[48],   S. A. Stucci[29],   B. Stugu[17],   J. Stupak[124],
N. A. Styles[44],   D. Su[150],   J. Su[135],   S. Suchek[59a],   Y. Sugaya[129],   M. Suk[138],   V. V. Sulin[108],   M. J. Sullivan[88],   D. M. S. Sultan[52],
S. Sultansoy[4c],   T. Sumida[83],   S. Sun[103],   X. Sun[3],   K. Suruliz[153],   C. J. E. Suster[154],   M. R. Sutton[153],   S. Suzuki[79],
M. Svatos[137],   M. Swiatlowski[36],   S. P. Swift[2],   A. Sydorenko[97],   I. Sykora[28a],   T. Sykora[139],   D. Ta[97],   K. Tackmann[44,z],
J. Taenzer[158],   A. Taffard[168],   R. Tafirout[165a],   E. Tahirovic[90],   N. Taiblum[158],   H. Takai[29],   R. Takashima[84],   E. H. Takasugi[113],
K. Takeda[80],   T. Takeshita[147],   Y. Takubo[79],   M. Talby[99],   A. A. Talyshev[120a,120b],   J. Tanaka[160],   M. Tanaka[162],   R. Tanaka[128],
B. B. Tannenwald[122],   S. Tapia Araya[144b],   S. Tapprogge[97],   A. Tarek Abouelfadl Mohamed[132],   S. Tarem[157],   G. Tarna[27b,e],
G. F. Tartarelli[66a],   P. Tas[139],   M. Tasevsky[137],   T. Tashiro[83],   E. Tassi[40a,40b],   A. Tavares Delgado[136a,136b],   Y. Tayalati[34e],
A. C. Taylor[116],   A. J. Taylor[48],   G. N. Taylor[102],   P. T. E. Taylor[102],   W. Taylor[165b],   A. S. Tee[87],   P. Teixeira-Dias[91],
H. Ten Kate[35],   J. J. Teoh[118],   S. Terada[79],   K. Terashi[160],   J. Terron[96],   S. Terzo[14],   M. Testa[49],   R. J. Teuscher[164,ac],
S. J. Thais[180],   T. Theveneaux-Pelzer[44],   F. Thiele[39],   D. W. Thomas[91],   J. P. Thomas[21],   A. S. Thompson[55],   P. D. Thompson[21],
L. A. Thomsen[180],   E. Thomson[133],   Y. Tian[38],   R. E. Ticse Torres[51],   V. O. Tikhomirov[108,am],   Yu. A. Tikhonov[120a,120b],
S. Timoshenko[110],   P. Tipton[180],   S. Tisserant[99],   K. Todome[162],   S. Todorova-Nova[5],   S. Todt[46],   J. Tojo[85],   S. Tokár[28a],

K. Tokushuku[79], E. Tolley[122], K. G. Tomiwa[32c], M. Tomoto[115], L. Tompkins[150,q], K. Toms[116], B. Tong[57], P. Tornambe[50], E. Torrence[127], H. Torres[46], E. Torró Pastor[145], C. Tosciri[131], J. Toth[99,ab], F. Touchard[99], D. R. Tovey[146], C. J. Treado[121], T. Trefzger[174], F. Tresoldi[153], A. Tricoli[29], I. M. Trigger[165a], S. Trincaz-Duvoid[132], M. F. Tripiana[14], W. Trischuk[164], B. Trocmé[56], A. Trofymov[128], C. Troncon[66a], M. Trovatelli[173], F. Trovato[153], L. Truong[32b], M. Trzebinski[82], A. Trzupek[82], F. Tsai[44], J. C-L. Tseng[131], P. V. Tsiareshka[105], A. Tsirigotis[159], N. Tsirintanis[9], V. Tsiskaridze[152], E. G. Tskhadadze[156a], I. I. Tsukerman[109], V. Tsulaia[18], S. Tsuno[79], D. Tsybychev[152,163], Y. Tu[61b], A. Tudorache[27b], V. Tudorache[27b], T. T. Tulbure[27a], A. N. Tuna[57], S. Turchikhin[77], D. Turgeman[177], I. Turk Cakir[4b,t], R. Turra[66a], P. M. Tuts[38], E. Tzovara[97], G. Ucchielli[23a,23b], I. Ueda[79], M. Ughetto[43a,43b], F. Ukegawa[166], G. Unal[35], A. Undrus[29], G. Unel[168], F. C. Ungaro[102], Y. Unno[79], K. Uno[160], J. Urban[28b], P. Urquijo[102], P. Urrejola[97], G. Usai[8], J. Usui[79], L. Vacavant[99], V. Vacek[138], B. Vachon[101], K. O. H. Vadla[130], A. Vaidya[92], C. Valderanis[112], E. Valdes Santurio[43a,43b], M. Valente[52], S. Valentinetti[23a,23b], A. Valero[171], L. Valéry[44], R. A. Vallance[21], A. Vallier[5], J. A. Valls Ferrer[171], T. R. Van Daalen[14], H. Van der Graaf[118], P. Van Gemmeren[6], J. Van Nieuwkoop[149], I. Van Vulpen[118], M. Vanadia[71a,71b], W. Vandelli[35], A. Vaniachine[163], P. Vankov[118], R. Vari[70a], E. W. Varnes[7], C. Varni[53a,53b], T. Varol[41], D. Varouchas[128], K. E. Varvell[154], G. A. Vasquez[144b], J. G. Vasquez[180], F. Vazeille[37], D. Vazquez Furelos[14], T. Vazquez Schroeder[35], J. Veatch[51], V. Vecchio[72a,72b], L. M. Veloce[164], F. Veloso[136a,136c], S. Veneziano[70a], A. Ventura[65a,65b], M. Venturi[173], N. Venturi[35], V. Vercesi[68a], M. Verducci[72a,72b], C. M. Vergel Infante[76], C. Vergis[24], W. Verkerke[118], A. T. Vermeulen[118], J. C. Vermeulen[118], M. C. Vetterli[149,as], N. Viaux Maira[144b], M. Vicente Barreto Pinto[52], I. Vichou[170,*], T. Vickey[146], O. E. Vickey Boeriu[146], G. H. A. Viehhauser[131], S. Viel[18], L. Vigani[131], M. Villa[23a,23b], M. Villaplana Perez[66a,66b], E. Vilucchi[49], M. G. Vincter[33], V. B. Vinogradov[77], A. Vishwakarma[44], C. Vittori[23a,23b], I. Vivarelli[153], S. Vlachos[10], M. Vogel[179], P. Vokac[138], G. Volpi[14], S. E. Von Buddenbrock[32c], E. von Toerne[24], V. Vorobel[139], K. Vorobev[110], M. Vos[171], J. H. Vossebeld[88], N. Vranjes[16], M. Vranjes Milosavljevic[16], V. Vrba[138], M. Vreeswijk[118], T. Šfiligoj[89], R. Vuillermet[35], I. Vukotic[36], T. Ženiš[28a], L. Živković[16], P. Wagner[24], W. Wagner[179], J. Wagner-Kuhr[112], H. Wahlberg[86], S. Wahrmund[46], K. Wakamiya[80], V. M. Walbrecht[113], J. Walder[87], R. Walker[112], S. D. Walker[91], W. Walkowiak[148], V. Wallangen[43a,43b], A. M. Wang[57], C. Wang[58b,e], F. Wang[178], H. Wang[18], H. Wang[3], J. Wang[154], J. Wang[59b], P. Wang[41], Q. Wang[124], R.-J. Wang[132], R. Wang[58a], R. Wang[6], S. M. Wang[155], W. T. Wang[58a], W. Wang[15c,ad], W. X. Wang[58a,ad], Y. Wang[58a,aj], Z. Wang[58c], C. Wanotayaroj[44], A. Warburton[101], C. P. Ward[31], D. R. Wardrope[92], A. Washbrook[48], P. M. Watkins[21], A. T. Watson[21], M. F. Watson[21], G. Watts[145], S. Watts[98], B. M. Waugh[92], A. F. Webb[11], S. Webb[97], C. Weber[180], M. S. Weber[20], S. A. Weber[33], S. M. Weber[59a], A. R. Weidberg[131], B. Weinert[63], J. Weingarten[45], M. Weirich[97], C. Weiser[50], P. S. Wells[35], T. Wenaus[29], T. Wengler[35], S. Wenig[35], N. Wermes[24], M. D. Werner[76], P. Werner[35], M. Wessels[59a], T. D. Weston[20], K. Whalen[127], N. L. Whallon[145], A. M. Wharton[87], A. S. White[103], A. White[8], M. J. White[1], R. White[144b], D. Whiteson[168], B. W. Whitmore[87], F. J. Wickens[141], W. Wiedenmann[178], M. Wielers[141], C. Wiglesworth[39], L. A. M. Wiik-Fuchs[50], F. Wilk[98], H. G. Wilkens[35], L. J. Wilkins[91], H. H. Williams[133], S. Williams[31], C. Willis[104], S. Willocq[100], J. A. Wilson[21], I. Wingerter-Seez[5], E. Winkels[153], F. Winklmeier[127], O. J. Winston[153], B. T. Winter[50], M. Wittgen[150], M. Wobisch[93], A. Wolf[97], T. M. H. Wolf[118], R. Wolff[99], M. W. Wolter[82], H. Wolters[136a,136c], V. W. S. Wong[172], N. L. Woods[143], S. D. Worm[21], B. K. Wosiek[82], K. W. Woźniak[82], K. Wraight[55], M. Wu[36], S. L. Wu[178], X. Wu[52], Y. Wu[58a], T. R. Wyatt[98], B. M. Wynne[48], S. Xella[39], Z. Xi[103], L. Xia[175], D. Xu[15a], H. Xu[58a,e], L. Xu[29], T. Xu[142], W. Xu[103], B. Yabsley[154], S. Yacoob[32a], K. Yajima[129], D. P. Yallup[92], D. Yamaguchi[162], Y. Yamaguchi[162], A. Yamamoto[79], T. Yamanaka[160], F. Yamane[80], M. Yamatani[160], T. Yamazaki[160], Y. Yamazaki[80], Z. Yan[25], H. J. Yang[58c,58d], H. T. Yang[18], S. Yang[75], Y. Yang[160], Z. Yang[17], W-M. Yao[18], Y. C. Yap[44], Y. Yasu[79], E. Yatsenko[58c,58d], J. Ye[41], S. Ye[29], I. Yeletskikh[77], E. Yigitbasi[25], E. Yildirim[97], K. Yorita[176], K. Yoshihara[133], C. J. S. Young[35], C. Young[150], J. Yu[8], J. Yu[76], X. Yue[59a], S. P. Y. Yuen[24], B. Zabinski[82], G. Zacharis[10], E. Zaffaroni[52], R. Zaidan[14], A. M. Zaitsev[140,al], T. Zakareishvili[156b], N. Zakharchuk[33], J. Zalieckas[17], S. Zambito[57], D. Zanzi[35], D. R. Zaripovas[55], S. V. Zeißner[45], C. Zeitnitz[179], G. Zemaityte[131], J. C. Zeng[170], Q. Zeng[150], O. Zenin[140], D. Zerwas[128], M. Zgubič[131], D. F. Zhang[58b], D. Zhang[103], F. Zhang[178], G. Zhang[58a], G. Zhang[15b], H. Zhang[15c], J. Zhang[6], L. Zhang[15c], L. Zhang[58a], M. Zhang[170], P. Zhang[15c], R. Zhang[58a], R. Zhang[24], X. Zhang[58b], Y. Zhang[15d], Z. Zhang[128], P. Zhao[47], Y. Zhao[58b,128,ah], Z. Zhao[58a], A. Zhemchugov[77], Z. Zheng[103], D. Zhong[170], B. Zhou[103], C. Zhou[178], L. Zhou[41], M. S. Zhou[15d], M. Zhou[152], N. Zhou[58c], Y. Zhou[7], C. G. Zhu[58b], H. L. Zhu[58a], H. Zhu[15a], J. Zhu[103], Y. Zhu[58a], X. Zhuang[15a], K. Zhukov[108], V. Zhulanov[120a,120b], A. Zibell[174], D. Zieminska[63], N. I. Zimine[77], S. Zimmermann[50], Z. Zinonos[113], M. Zinser[97], M. Ziolkowski[148], G. Zobernig[178], A. Zoccoli[23a,23b], K. Zoch[51], T. G. Zorbas[146], R. Zou[36], M. Zur Nedden[19], L. Zwalinski[35]

[1] Department of Physics, University of Adelaide, Adelaide, Australia
[2] Physics Department, SUNY Albany, Albany, NY, USA
[3] Department of Physics, University of Alberta, Edmonton, AB, Canada

[4] [a]Department of Physics, Ankara University, Ankara, Turkey; [b]Istanbul Aydin University, Istanbul, Turkey; [c]Division of Physics, TOBB University of Economics and Technology, Ankara, Turkey

[5] LAPP, Université Grenoble Alpes, Université Savoie Mont Blanc, CNRS/IN2P3, Annecy, France

[6] High Energy Physics Division, Argonne National Laboratory, Argonne, IL, USA

[7] Department of Physics, University of Arizona, Tucson, AZ, USA

[8] Department of Physics, University of Texas at Arlington, Arlington, TX, USA

[9] Physics Department, National and Kapodistrian University of Athens, Athens, Greece

[10] Physics Department, National Technical University of Athens, Zografou, Greece

[11] Department of Physics, University of Texas at Austin, Austin, TX, USA

[12] [a]Faculty of Engineering and Natural Sciences, Bahcesehir University, Istanbul, Turkey; [b]Faculty of Engineering and Natural Sciences, Istanbul Bilgi University, Istanbul, Turkey; [c]Department of Physics, Bogazici University, Istanbul, Turkey; [d]Department of Physics Engineering, Gaziantep University, Gaziantep, Turkey

[13] Institute of Physics, Azerbaijan Academy of Sciences, Baku, Azerbaijan

[14] Institut de Física d'Altes Energies (IFAE), Barcelona Institute of Science and Technology, Barcelona, Spain

[15] [a]Institute of High Energy Physics, Chinese Academy of Sciences, Beijing, China; [b]Physics Department, Tsinghua University, Beijing, China; [c]Department of Physics, Nanjing University, Nanjing, China; [d]University of Chinese Academy of Science (UCAS), Beijing, China

[16] Institute of Physics, University of Belgrade, Belgrade, Serbia

[17] Department for Physics and Technology, University of Bergen, Bergen, Norway

[18] Physics Division, Lawrence Berkeley National Laboratory and University of California, Berkeley, CA, USA

[19] Institut für Physik, Humboldt Universität zu Berlin, Berlin, Germany

[20] Albert Einstein Center for Fundamental Physics and Laboratory for High Energy Physics, University of Bern, Bern, Switzerland

[21] School of Physics and Astronomy, University of Birmingham, Birmingham, UK

[22] Centro de Investigaciónes, Universidad Antonio Nariño, Bogotá, Colombia

[23] [a]Dipartimento di Fisica e Astronomia, Università di Bologna, Bologna, Italy; [b]INFN Sezione di Bologna, Bologna, Italy

[24] Physikalisches Institut, Universität Bonn, Bonn, Germany

[25] Department of Physics, Boston University, Boston, MA, USA

[26] Department of Physics, Brandeis University, Waltham, MA, USA

[27] [a]Transilvania University of Brasov, Brasov, Romania; [b]Horia Hulubei National Institute of Physics and Nuclear Engineering, Bucharest, Romania; [c]Department of Physics, Alexandru Ioan Cuza University of Iasi, Iasi, Romania; [d]Physics Department, National Institute for Research and Development of Isotopic and Molecular Technologies, Cluj-Napoca, Romania; [e]University Politehnica Bucharest, Bucharest, Romania; [f]West University in Timisoara, Timisoara, Romania

[28] [a]Faculty of Mathematics, Physics and Informatics, Comenius University, Bratislava, Slovakia; [b]Department of Subnuclear Physics, Institute of Experimental Physics of the Slovak Academy of Sciences, Kosice, Slovak Republic

[29] Physics Department, Brookhaven National Laboratory, Upton, NY, USA

[30] Departamento de Física, Universidad de Buenos Aires, Buenos Aires, Argentina

[31] Cavendish Laboratory, University of Cambridge, Cambridge, UK

[32] [a]Department of Physics, University of Cape Town, Cape Town, South Africa; [b]Department of Mechanical Engineering Science, University of Johannesburg, Johannesburg, South Africa; [c]School of Physics, University of the Witwatersrand, Johannesburg, South Africa

[33] Department of Physics, Carleton University, Ottawa, ON, Canada

[34] [a]Faculté des Sciences Ain Chock, Réseau Universitaire de Physique des Hautes Energies-Université Hassan II, Casablanca, Morocco; [b]Centre National de l'Energie des Sciences Techniques Nucleaires (CNESTEN), Rabat, Morocco; [c]Faculté des Sciences Semlalia, Université Cadi Ayyad, LPHEA-Marrakech, Marrakech, Morocco; [d]Faculté des Sciences, Université Mohamed Premier and LPTPM, Oujda, Morocco; [e]Faculté des sciences, Université Mohammed V, Rabat, Morocco

[35] CERN, Geneva, Switzerland

[36] Enrico Fermi Institute, University of Chicago, Chicago, IL, USA

[37] LPC, Université Clermont Auvergne, CNRS/IN2P3, Clermont-Ferrand, France

[38] Nevis Laboratory, Columbia University, Irvington, NY, USA

[39] Niels Bohr Institute, University of Copenhagen, Copenhagen, Denmark

[40] (a)Dipartimento di Fisica, Università della Calabria, Rende, Italy; (b)INFN Gruppo Collegato di Cosenza, Laboratori Nazionali di Frascati, Frascati, Italy

[41] Physics Department, Southern Methodist University, Dallas, TX, USA

[42] Physics Department, University of Texas at Dallas, Richardson, TX, USA

[43] (a)Department of Physics, Stockholm University, Stockholm, Sweden; (b)Oskar Klein Centre, Stockholm, Sweden

[44] Deutsches Elektronen-Synchrotron DESY, Hamburg and Zeuthen, Germany

[45] Lehrstuhl für Experimentelle Physik IV, Technische Universität Dortmund, Dortmund, Germany

[46] Institut für Kern- und Teilchenphysik, Technische Universität Dresden, Dresden, Germany

[47] Department of Physics, Duke University, Durham, NC, USA

[48] SUPA-School of Physics and Astronomy, University of Edinburgh, Edinburgh, UK

[49] INFN e Laboratori Nazionali di Frascati, Frascati, Italy

[50] Physikalisches Institut, Albert-Ludwigs-Universität Freiburg, Freiburg, Germany

[51] II. Physikalisches Institut, Georg-August-Universität Göttingen, Göttingen, Germany

[52] Département de Physique Nucléaire et Corpusculaire, Université de Genève, Geneva, Switzerland

[53] (a)Dipartimento di Fisica, Università di Genova, Genoa, Italy; (b)INFN Sezione di Genova, Genoa, Italy

[54] II. Physikalisches Institut, Justus-Liebig-Universität Giessen, Giessen, Germany

[55] SUPA-School of Physics and Astronomy, University of Glasgow, Glasgow, UK

[56] LPSC, Université Grenoble Alpes, CNRS/IN2P3, Grenoble INP, Grenoble, France

[57] Laboratory for Particle Physics and Cosmology, Harvard University, Cambridge, MA, USA

[58] (a)Department of Modern Physics and State Key Laboratory of Particle Detection and Electronics, University of Science and Technology of China, Hefei, China; (b)Institute of Frontier and Interdisciplinary Science and Key Laboratory of Particle Physics and Particle Irradiation (MOE), Shandong University, Qingdao, China; (c)School of Physics and Astronomy, Shanghai Jiao Tong University, KLPPAC-MoE, SKLPPC, Shanghai, China; (d)Tsung-Dao Lee Institute, Shanghai, China

[59] (a)Kirchhoff-Institut für Physik, Ruprecht-Karls-Universität Heidelberg, Heidelberg, Germany; (b)Physikalisches Institut, Ruprecht-Karls-Universität Heidelberg, Heidelberg, Germany

[60] Faculty of Applied Information Science, Hiroshima Institute of Technology, Hiroshima, Japan

[61] (a)Department of Physics, Chinese University of Hong Kong, Shatin, NT, Hong Kong; (b)Department of Physics, University of Hong Kong, Hong Kong, China; (c)Department of Physics and Institute for Advanced Study, Hong Kong University of Science and Technology, Clear Water Bay, Kowloon, Hong Kong, China

[62] Department of Physics, National Tsing Hua University, Hsinchu, Taiwan

[63] Department of Physics, Indiana University, Bloomington, IN, USA

[64] (a)INFN Gruppo Collegato di Udine, Sezione di Trieste, Udine, Italy; (b)ICTP, Trieste, Italy; (c)Dipartimento di Chimica, Fisica e Ambiente, Università di Udine, Udine, Italy

[65] (a)INFN Sezione di Lecce, Lecce, Italy; (b)Dipartimento di Matematica e Fisica, Università del Salento, Lecce, Italy

[66] (a)INFN Sezione di Milano, Milan, Italy; (b)Dipartimento di Fisica, Università di Milano, Milan, Italy

[67] (a)INFN Sezione di Napoli, Naples, Italy; (b)Dipartimento di Fisica, Università di Napoli, Naples, Italy

[68] (a)INFN Sezione di Pavia, Pavia, Italy; (b)Dipartimento di Fisica, Università di Pavia, Pavia, Italy

[69] (a)INFN Sezione di Pisa, Pisa, Italy; (b)Dipartimento di Fisica E. Fermi, Università di Pisa, Pisa, Italy

[70] (a)INFN Sezione di Roma, Rome, Italy; (b)Dipartimento di Fisica, Sapienza Università di Roma, Rome, Italy

[71] (a)INFN Sezione di Roma Tor Vergata, Rome, Italy; (b)Dipartimento di Fisica, Università di Roma Tor Vergata, Rome, Italy

[72] (a)INFN Sezione di Roma Tre, Rome, Italy; (b)Dipartimento di Matematica e Fisica, Università Roma Tre, Rome, Italy

[73] (a)INFN-TIFPA, Povo, Italy; (b)Università degli Studi di Trento, Trento, Italy

[74] Institut für Astro- und Teilchenphysik, Leopold-Franzens-Universität, Innsbruck, Austria

[75] University of Iowa, Iowa City, IA, USA

[76] Department of Physics and Astronomy, Iowa State University, Ames, IA, USA

[77] Joint Institute for Nuclear Research, Dubna, Russia

[78] (a)Departamento de Engenharia Elétrica, Universidade Federal de Juiz de Fora (UFJF), Juiz de Fora, Brazil; (b)Universidade Federal do Rio De Janeiro COPPE/EE/IF, Rio de Janeiro, Brazil; (c)Universidade Federal de São João del Rei (UFSJ), São João del Rei, Brazil; (d)Instituto de Física, Universidade de São Paulo, São Paulo, Brazil

[79] KEK, High Energy Accelerator Research Organization, Tsukuba, Japan

[80] Graduate School of Science, Kobe University, Kobe, Japan

[81] [a]Faculty of Physics and Applied Computer Science, AGH University of Science and Technology, Kraków, Poland; [b]Marian Smoluchowski Institute of Physics, Jagiellonian University, Kraków, Poland

[82] Institute of Nuclear Physics Polish Academy of Sciences, Kraków, Poland

[83] Faculty of Science, Kyoto University, Kyoto, Japan

[84] Kyoto University of Education, Kyoto, Japan

[85] Research Center for Advanced Particle Physics and Department of Physics, Kyushu University, Fukuoka, Japan

[86] Instituto de Física La Plata, Universidad Nacional de La Plata and CONICET, La Plata, Argentina

[87] Physics Department, Lancaster University, Lancaster, UK

[88] Oliver Lodge Laboratory, University of Liverpool, Liverpool, UK

[89] Department of Experimental Particle Physics, Jožef Stefan Institute and Department of Physics, University of Ljubljana, Ljubljana, Slovenia

[90] School of Physics and Astronomy, Queen Mary University of London, London, UK

[91] Department of Physics, Royal Holloway University of London, Egham, UK

[92] Department of Physics and Astronomy, University College London, London, UK

[93] Louisiana Tech University, Ruston, LA, USA

[94] Fysiska institutionen, Lunds universitet, Lund, Sweden

[95] Centre de Calcul de l'Institut National de Physique Nucléaire et de Physique des Particules (IN2P3), Villeurbanne, France

[96] Departamento de Física Teorica C-15 and CIAFF, Universidad Autónoma de Madrid, Madrid, Spain

[97] Institut für Physik, Universität Mainz, Mainz, Germany

[98] School of Physics and Astronomy, University of Manchester, Manchester, UK

[99] CPPM, Aix-Marseille Université, CNRS/IN2P3, Marseille, France

[100] Department of Physics, University of Massachusetts, Amherst, MA, USA

[101] Department of Physics, McGill University, Montreal, QC, Canada

[102] School of Physics, University of Melbourne, Melbourne, VIC, Australia

[103] Department of Physics, University of Michigan, Ann Arbor, MI, USA

[104] Department of Physics and Astronomy, Michigan State University, East Lansing, MI, USA

[105] B.I. Stepanov Institute of Physics, National Academy of Sciences of Belarus, Minsk, Belarus

[106] Research Institute for Nuclear Problems of Byelorussian State University, Minsk, Belarus

[107] Group of Particle Physics, University of Montreal, Montreal, QC, Canada

[108] P.N. Lebedev Physical Institute of the Russian Academy of Sciences, Moscow, Russia

[109] Institute for Theoretical and Experimental Physics (ITEP), Moscow, Russia

[110] National Research Nuclear University MEPhI, Moscow, Russia

[111] D.V. Skobeltsyn Institute of Nuclear Physics, M.V. Lomonosov Moscow State University, Moscow, Russia

[112] Fakultät für Physik, Ludwig-Maximilians-Universität München, Munich, Germany

[113] Max-Planck-Institut für Physik (Werner-Heisenberg-Institut), Munich, Germany

[114] Nagasaki Institute of Applied Science, Nagasaki, Japan

[115] Graduate School of Science and Kobayashi-Maskawa Institute, Nagoya University, Nagoya, Japan

[116] Department of Physics and Astronomy, University of New Mexico, Albuquerque, NM, USA

[117] Institute for Mathematics, Astrophysics and Particle Physics, Radboud University Nijmegen/Nikhef, Nijmegen, The Netherlands

[118] Nikhef National Institute for Subatomic Physics and University of Amsterdam, Amsterdam, The Netherlands

[119] Department of Physics, Northern Illinois University, De Kalb, IL, USA

[120] [a]Budker Institute of Nuclear Physics, SB RAS, Novosibirsk, Russia; [b]Novosibirsk State University, Novosibirsk, Russia

[121] Department of Physics, New York University, New York, NY, USA

[122] Ohio State University, Columbus, OH, USA

[123] Faculty of Science, Okayama University, Okayama, Japan

[124] Homer L. Dodge Department of Physics and Astronomy, University of Oklahoma, Norman, OK, USA

[125] Department of Physics, Oklahoma State University, Stillwater, OK, USA

[126] Palacký University, RCPTM, Joint Laboratory of Optics, Olomouc, Czech Republic

[127] Center for High Energy Physics, University of Oregon, Eugene, OR, USA

[128] LAL, Université Paris-Sud, CNRS/IN2P3, Université Paris-Saclay, Orsay, France

[129] Graduate School of Science, Osaka University, Osaka, Japan

[130] Department of Physics, University of Oslo, Oslo, Norway

[131] Department of Physics, Oxford University, Oxford, UK

[132] LPNHE, Sorbonne Université, Paris Diderot Sorbonne Paris Cité, CNRS/IN2P3, Paris, France

[133] Department of Physics, University of Pennsylvania, Philadelphia, PA, USA

[134] Konstantinov Nuclear Physics Institute of National Research Centre "Kurchatov Institute", PNPI, St. Petersburg, Russia

[135] Department of Physics and Astronomy, University of Pittsburgh, Pittsburgh, PA, USA

[136] [a]Laboratório de Instrumentação e Física Experimental de Partículas-LIP, Lisbon, Portugal; [b]Departamento de Física, Faculdade de Ciências, Universidade de Lisboa, Lisbon, Portugal; [c]Departamento de Física, Universidade de Coimbra, Coimbra, Portugal; [d]Centro de Física Nuclear da Universidade de Lisboa, Lisbon, Portugal; [e]Departamento de Física, Universidade do Minho, Braga, Portugal; [f]Departamento de Física Teorica y del Cosmos, Universidad de Granada, Granada, Spain; [g]Dep Física and CEFITEC of Faculdade de Ciências e Tecnologia, Universidade Nova de Lisboa, Caparica, Portugal

[137] Institute of Physics, Academy of Sciences of the Czech Republic, Prague, Czech Republic

[138] Czech Technical University in Prague, Prague, Czech Republic

[139] Faculty of Mathematics and Physics, Charles University, Prague, Czech Republic

[140] State Research Center Institute for High Energy Physics, NRC KI, Protvino, Russia

[141] Particle Physics Department, Rutherford Appleton Laboratory, Didcot, UK

[142] IRFU, CEA, Université Paris-Saclay, Gif-sur-Yvette, France

[143] Santa Cruz Institute for Particle Physics, University of California Santa Cruz, Santa Cruz, CA, USA

[144] [a]Departamento de Física, Pontificia Universidad Católica de Chile, Santiago, Chile; [b]Departamento de Física, Universidad Técnica Federico Santa María, Valparaiso, Chile

[145] Department of Physics, University of Washington, Seattle, WA, USA

[146] Department of Physics and Astronomy, University of Sheffield, Sheffield, UK

[147] Department of Physics, Shinshu University, Nagano, Japan

[148] Department Physik, Universität Siegen, Siegen, Germany

[149] Department of Physics, Simon Fraser University, Burnaby, BC, Canada

[150] SLAC National Accelerator Laboratory, Stanford, CA, USA

[151] Physics Department, Royal Institute of Technology, Stockholm, Sweden

[152] Departments of Physics and Astronomy, Stony Brook University, Stony Brook, NY, USA

[153] Department of Physics and Astronomy, University of Sussex, Brighton, UK

[154] School of Physics, University of Sydney, Sydney, Australia

[155] Institute of Physics, Academia Sinica, Taipei, Taiwan

[156] [a]E. Andronikashvili Institute of Physics, Iv. Javakhishvili Tbilisi State University, Tbilisi, Georgia; [b]High Energy Physics Institute, Tbilisi State University, Tbilisi, Georgia

[157] Department of Physics, Technion, Israel Institute of Technology, Haifa, Israel

[158] Raymond and Beverly Sackler School of Physics and Astronomy, Tel Aviv University, Tel Aviv, Israel

[159] Department of Physics, Aristotle University of Thessaloniki, Thessaloníki, Greece

[160] International Center for Elementary Particle Physics and Department of Physics, University of Tokyo, Tokyo, Japan

[161] Graduate School of Science and Technology, Tokyo Metropolitan University, Tokyo, Japan

[162] Department of Physics, Tokyo Institute of Technology, Tokyo, Japan

[163] Tomsk State University, Tomsk, Russia

[164] Department of Physics, University of Toronto, Toronto, ON, Canada

[165] [a]TRIUMF, Vancouver, BC, Canada; [b]Department of Physics and Astronomy, York University, Toronto, ON, Canada

[166] Division of Physics and Tomonaga Center for the History of the Universe, Faculty of Pure and Applied Sciences, University of Tsukuba, Tsukuba, Japan

[167] Department of Physics and Astronomy, Tufts University, Medford, MA, USA

[168] Department of Physics and Astronomy, University of California Irvine, Irvine, CA, USA

[169] Department of Physics and Astronomy, University of Uppsala, Uppsala, Sweden

[170] Department of Physics, University of Illinois, Urbana, IL, USA

[171] Instituto de Física Corpuscular (IFIC), Centro Mixto Universidad de Valencia - CSIC, Valencia, Spain

[172] Department of Physics, University of British Columbia, Vancouver, BC, Canada

173 Department of Physics and Astronomy, University of Victoria, Victoria, BC, Canada

174 Fakultät für Physik und Astronomie, Julius-Maximilians-Universität Würzburg, Würzburg, Germany

175 Department of Physics, University of Warwick, Coventry, UK

176 Waseda University, Tokyo, Japan

177 Department of Particle Physics, Weizmann Institute of Science, Rehovot, Israel

178 Department of Physics, University of Wisconsin, Madison, WI, USA

179 Fakultät für Mathematik und Naturwissenschaften, Fachgruppe Physik, Bergische Universität Wuppertal, Wuppertal, Germany

180 Department of Physics, Yale University, New Haven, CT, USA

181 Yerevan Physics Institute, Yerevan, Armenia

a Also at Borough of Manhattan Community College, City University of New York, NY, USA

b Also at California State University, East Bay, USA

c Also at Centre for High Performance Computing, CSIR Campus, Rosebank, Cape Town, South Africa

d Also at CERN, Geneva, Switzerland

e Also at CPPM, Aix-Marseille Université, CNRS/IN2P3, Marseille, France

f Also at Département de Physique Nucléaire et Corpusculaire, Université de Genève, Genève, Switzerland

g Also at Departament de Fisica de la Universitat Autonoma de Barcelona, Barcelona, Spain

h Also at Departamento de Física Teorica y del Cosmos, Universidad de Granada, Granada, Spain

i Also at Department of Applied Physics and Astronomy, University of Sharjah, Sharjah, United Arab Emirates

j Also at Department of Financial and Management Engineering, University of the Aegean, Chios, Greece

k Also at Department of Physics and Astronomy, University of Louisville, Louisville, KY, USA

l Also at Department of Physics and Astronomy, University of Sheffield, Sheffield, UK

m Also at Department of Physics, California State University, Fresno, CA, USA

n Also at Department of Physics, California State University, Sacramento, CA, USA

o Also at Department of Physics, King's College London, London, UK

p Also at Department of Physics, St. Petersburg State Polytechnical University, St. Petersburg, Russia

q Also at Department of Physics, Stanford University, Stanford, USA

r Also at Department of Physics, University of Fribourg, Fribourg, Switzerland

s Also at Department of Physics, University of Michigan, Ann Arbor, MI, USA

t Also at Giresun University, Faculty of Engineering, Giresun, Turkey

u Also at Graduate School of Science, Osaka University, Osaka, Japan

v Also at Hellenic Open University, Patras, Greece

w Also at Horia Hulubei National Institute of Physics and Nuclear Engineering, Bucharest, Romania

x Also at II Physikalisches Institut, Georg-August-Universität Göttingen, Göttingen, Germany

y Also at Institucio Catalana de Recerca i Estudis Avancats, ICREA, Barcelona, Spain

z Also at Institut für Experimentalphysik, Universität Hamburg, Hamburg, Germany

aa Also at Institute for Mathematics, Astrophysics and Particle Physics, Radboud University Nijmegen/Nikhef, Nijmegen, The Netherlands

ab Also at Institute for Particle and Nuclear Physics, Wigner Research Centre for Physics, Budapest, Hungary

ac Also at Institute of Particle Physics (IPP), Canada

ad Also at Institute of Physics, Academia Sinica, Taipei, Taiwan

ae Also at Institute of Physics, Azerbaijan Academy of Sciences, Baku, Azerbaijan

af Also at Institute of Theoretical Physics, Ilia State University, Tbilisi, Georgia

ag Also at Istanbul University, Dept. of Physics, Istanbul; Turkey

ah Also at LAL, Université Paris-Sud, CNRS/IN2P3, Université Paris-Saclay, Orsay, France

ai Also at Louisiana Tech University, Ruston, LA, USA

aj Also at LPNHE, Sorbonne Université, Paris Diderot Sorbonne Paris Cité, CNRS/IN2P3, Paris, France

ak Also at Manhattan College, New York, NY, USA

al Also at Moscow Institute of Physics and Technology State University, Dolgoprudny, Russia

am Also at National Research Nuclear University MEPhI, Moscow, Russia

an Also at Physikalisches Institut, Albert-Ludwigs-Universität Freiburg, Freiburg, Germany

ao Also at School of Physics, Sun Yat-sen University, Guangzhou, China

[ap] Also at The City College of New York, New York, NY, USA

[aq] Also at The Collaborative Innovation Center of Quantum Matter (CICQM), Beijing, China

[ar] Also at Tomsk State University, Tomsk, and Moscow Institute of Physics and Technology State University, Dolgoprudny, Russia

[as] Also at TRIUMF, Vancouver, BC, Canada

[at] Also at Universita di Napoli Parthenope, Naples, Italy

[*] Deceased